University of Alberta
Department of Civil &
Environmental Engineering

Structural Engineering Report No. 205

Shear Strengthening of Concrete Girders Using Carbon Fibre Reinforced Plastic

by

E.H. Drimoussis

and

J.J.R. Cheng

October, 1994

Shear Strengthening of Concrete Girders Using Carbon Fibre Reinforced Plastic Sheets

by

E.H. Drimoussis

and

J.J.R. Cheng

Structural Engineering Report 205

Department of Civil and Environmental Engineering

University of Alberta

Edmonton, Alberta

October 1994

Abstract

The rehabilitation or upgrading of structures has become an increasingly important aspect of structural engineering and different structures and materials present a variety of challenges for engineers. In particular, given the age of the infrastructure, various types of structural deficiencies have been found in reinforced and prestressed concrete bridges. This thesis is based on research undertaken to investigate the strengthening of shear deficient concrete bridge girders using carbon fibre reinforced plastic (CFRP) sheets bonded to the webs of the members. Three precast reinforced concrete girders were salvaged from a demolished bridge, strengthened for shear, and tested to failure. The sheets were bonded to the web faces of the members in various arrangements. By testing each girder more than once, it was possible to carry out five shear and three flexural tests. One shear span of one girder was left unstrengthened and served as the control to which the strengthened sections were compared. The increase in shear capacity resulting from the use of the CFRP sheets was calculated. The behaviour of the strengthened specimens was described and analyzed. Based on test observations, two possible mechanisms were proposed by which the CFRP sheets may contribute to shear capacity. Based on test results, a model was proposed to describe and predict the CFRP shear contribution.

Acknowledgements

The research presented in this thesis was undertaken for the Structural Group of the Department of Civil Engineering at the University of Alberta under the supervision of Dr. J.J. Roger Cheng.

I would first like to thank Dr. Cheng for his guidance, encouragement and interest. I appreciate his approach to research and education which emphasize not only technical proficiency but also other qualities important to an engineer and individual. His suggestions and comments were always welcome and helped clarify many issues and confusing points.

As all students working in the I.F. Morrison Structures Laboratory well know, the efforts and expertise of the technical staff, Larry Burden and Richard Helfrich, play a vital role in the success of our experimental work. I learnt a great deal from them as well and appreciate their assistance and cooperation.

I would like to also thank all of my fellow students in the Structures graduate program and particularly in the lab. The atmosphere was always one of camaraderie, support and keen interest in one another's work. Helping hands were often and enthusiastically proffered.

The financial assistance provided by NSERC during the course of the Master's program is gratefully acknowledged.

Although not directly related to th research work, the encouragement and moral support of my parents and sisters has mea... a great deal to me over the years. This has contributed significantly to the completion of this work and my education in general.

Last, but most of all, I must thank my fiance, John, for his love, encouragement and perpetually optimistic outlook on life. He emotionally supported and believed in me making it easier to survive the inevitable frustrating moments of producing this thesis.

Table of Contents

List of Tables

List of Figures

List of Notation

A_{CFRP}	cross-sectional area of CFRP sheets
AFRP	aramid fibre reinforced plastic
A_s	cross-sectional area of tension reinforcement
A_{sf}	cross-sectional area of reinforcement to develop compressive strength of overhanging flanges of I- and T- sections
A_v	area of shear reinforcement within a distance s
a	shear span; depth of equivalent rectangular stress block
b_w	width of the web of the cross-section; for tapered webs, the average width or 1.2 times the minimum width, whichever is smaller
CFRP	carbon fibre reinforced plastic
d	distance from extreme compression fibre to centroid of tension reinforcement
E	modulus of elasticity of steel
f'_c	specified compressive strength of concrete
fu	ultimate tensile strength of steel reinforcement
Fu	ultimate tensile breaking strength of FRP
f_y	specified yield stress of reinforcement
GFRP	glass fibre reinforced plastic
h	overall depth of member
h_f	compression flange thickness of I- and T-sections
jd	moment arm between the internal tension and compression forces in in a reinforced concrete section; typically, j ≈ 0.875 for beams
l	length of vertical CFRP sheets
l_a	minimum anchorage length of vertical CFRP sheets
l_{bf}	length of non-vertical fibres
l_{eff}	effective length of verticals CFRP sheets
M	moment at a section due to applied loads
M_n	nominal moment resistance of a section
$M_{O.W.}$	moment due to the girder's own weight
M_{G1T2}	maximum moment reached in test G1-T2
P	load applied during testing
Pmax	load at failure during testing
Pservice	maximum service load due to standard truck loading
Pu	peak load reached during testing

P_y	load during testing at which slope of the load-deflection curves loses its linearity
s	shear reinforcement spacing in a direction parallel to the longitudinal reinforcement
v_b	permissible shear stress carried by the concrete (notation used in S6-88)
v_c	allowable shear stress in the concrete
V	shear force at a section due to applied loads
V_c	shear resistance provided by the concrete
V_{CFRP}	shear resistance provided by CFRP sheets
V_{GITI}	shear carried by the control section
V_n	nominal shear resistance of a section
V_{PRED}	total predicted shear capacity of a section
V_s	shear resistance provided by the shear reinforcement
V_{TEST}	maximum shear carried by a leg of a girder at failure
α	coefficient of thermal expansion
Δu	deflection at the end of the post-elastic range
Δy	deflection at yield
Θ	angle of the compression strut
ε	strain
ε_c	strain in concrete
ε_s	strain in steel reinforcement
μ	ductility of a member or structure ($=\Delta u/\Delta y$)
ρ_w	$=A_s/b_w d$, reinforcement ratio used in S6-88 formula for shear resistance, v_b
σ_{CFRP}	specified ultimate breaking strength of CFRP sheets
σ_{eff}	design stress level used for CFRP sheets
σ_s	stress level in steel reinforcement
σ_y	yield stress level of steel reinforcement

1.0 Introduction

1.1 Statement of Problem

Increasingly, a substantial proportion of structural engineering work is in the rehabilitation or upgrading of existing structures. This may be necessary for various reasons. Loading conditions may have changed since the original design, damage may have occurred, omissions may inadvertently been made in the original design and/or construction phases, or design requirements may have changed. Whatever the reason, a large and increasing number of structures fall into this category, representing a sizeable cost for either replacement or rehabilitation.

As replacement costs are a significant capital expenditure, extensive research has been conducted to find improved methods of both structural evaluation and rehabilitation, and this trend is likely to increase. It is also a more sensible approach to maintain the current superstructure (either for historic/cultural or for economic reasons) than to simply demolish and rebuild.

Bridges are often of prime concern in this respect. There is a higher degree of safety associated with the design and maintenance of bridges. In addition, there is an extremely high initial capital cost paid by the public which has justifiably high expectations for safety and serviceability.

Many creative and innovative solutions have been generated and implemented over the years to strengthen concrete, steel, timber or masonry structures. Different structures and materials present different problems, and there are several special concerns associated with the strengthening of existing concrete bridges. The environmentally exposed structure is vulnerable to potential corrosion problems. The primary live loads, traffic loads, are continually increasing in magnitude and may introduce potentially serious fatigue problems. Serviceability demands are high, as is the necessity of maintaining service during any repair work/construction. The repair should ideally minimize the amount of material added to the structure in order to avoid increasing the dead load or decreasing the clearance requirements above, beneath or around the bridge. Finally, the repair work should minimize disruption to the structure and its use. These issues must be addressed when repair work is being designed and implemented.

Steel in the form of rods, bars or plates, or structural shapes, has been the most commonly used repair material on concrete bridges, as well as in other types of structures. In the last 10 years or so, a new family of materials has gained increased exposure in civil engineering -- the so-called advanced composite materials (ACM). These ACM's originally developed by and applied in the aerospace and other high-tech industries, possess certain properties which make them superior to steel in some respects. Amongst the most important properties are an extremely high strength to weight ratio and non-corrosiveness. These new materials may have a valuable role in retrofitting work, particularly if most of the problems described above can be addressed.

1.2 Objectives and Scope

The primary objective of this research program was to strengthen existing concrete girders using a carbon fibre reinforced-plastic (CFRP) material in order to increase the shear capacity of the members. The girders tested had been removed from a demolished concrete highway bridge and were considered shear deficient. A total of eight tests were carried out on three specimens on which CFRP sheets were applied to the sides of the webs in different arrangements in order to determine the optimum means of strengthening this type of girder. In order to determine the additional benefit provided by this material, unstrengthened sections were tested first to determine the in situ shear and moment capacities. The effect of the CFRP strengthening method on stiffness, ductility and ultimate strength and on the behaviour of the members was investigated and observed. Based on the test results, a mechanism was proposed to model the behaviour of the strengthened girders and to determine the shear capacity contributed by the CFRP sheets.

1.3 Organization of Thesis

The background and literature review in Chapter 2 covers several topics. The basis for the shear deficiencies of the girders is investigated and the means of shear evaluation of concrete members is described. Methods which have been used for strengthening concrete beams are reviewed and compared. Advanced composite materials are defined and described and a review of their possible applicability in strengthening work is presented. Chapter 3 outlines the experimental program for the testing of the girders. The results of the testing program and observations of the progression of failure are presented in Chapter

4. Chapter 5 includes a discussion of these results as well as a proposed mechanism for the behaviour of the CFRP strengthened girders.

2.0 Background and Literature Review

2.1 Introduction

Some causes of shear deficiencies in concrete bridge members are discussed in Section 2.2, with specific reference to the girders tested in this program. The prediction and evaluation of shear capacity in existing members is presented in Section 2.3, based on different approaches or codes. Section 2.4 summarizes some methods of strengthening concrete girders for shear and discusses their relative merits. Advanced composite materials (ACM) and their various properties which are relevant to structural engineering are described in Section 2.5 and their possible application in the repair of concrete members is discussed in Section 2.6.

2.2 Shear Deficiencies of Existing Girders and Bridges

Shear failure of concrete members is, in general, sudden and brittle. Ductility of a structure is one of its most important characteristics especially in, though not limited to, situations where seismic loads must be resisted. In order to ensure ductile behaviour of the member and structure, it is necessary that the design ensures that the flexural capacity is reached before shear failure occurs.

Although the flexural behaviour of reinforced concrete has been well understood and experimentally verified for many years , shear behaviour has been less well understood and much of the research is relatively recent. Until cracks develop, an elastic theory approach can give good strength predictions. However, in the post-cracked range, behaviour is far more complex. The situation is complicated by the fact that shear never acts alone, but exists in conjunction with bending moment and perhaps also with torsion and/or axial load. This gives rise to an interaction which decreases the ability of the member to develop its full shear or flexural capacity.

Historically, research has primarily been aimed at developing shear transfer mechanisms after cracking in order to predict the behaviour at service and ultimate loads. This has been well-documented although perhaps is not, as yet, conclusive (Regan, 1993; Park and Paulay, 1975; ACI-ASCE Committee 426, 1974). It is not an objective of this thesis to present the theory of shear behaviour of reinforced concrete. However,

important points are discussed as they arise and are pertinent to the discussion of the particular members tested.

There are approximately 14,000 highway bridges in operation in the Province of Alberta, most of which are reinforced or prestressed concrete structures. Many of these concrete bridges were designed and built more than thirty years ago in accordance with standards that are now obsolete. An extensive inspection and assessment program has identified many of these bridges as being shear deficient. Shear problems have been found in both reinforced and prestressed concrete bridges, simply supported and continuous structures, of many structural types (e.g., I-girder, T-girder, hat-shaped girder). Although the problems and their potential solutions are applicable to many other types of concrete bridges, this thesis is limited to discussion of the Type 'E' girder which forms the superstructure of about 50 highway bridges around the province. Thorough field inspections have been carried out on all Type 'E' girder bridges and, along with various other problems, diagonal shear cracks have been observed in the webs of more than 60% of them, which may be an indication of shear deficiencies. Analysis and evaluation of the original design in accordance with current design standards (CAN/CSA-S6-88, 1988) also indicate shear deficiencies.

A typical bridge composed of these members is shown in Figures 2.1 and 2.2. The Type 'E' stringer is a simply supported pre-cast reinforced concrete member designed in the late 1950's in accordance with AASHO-57 (1957) and used in bridge construction for several years. It is hat-shaped in section and varies between 9.1 m and 12.8 m in length. Placed side-by-side, the girders are transversely connected by means of a reinforced grouted shear key which is intended to aid lateral distribution of traffic loads. All girders are identical, except that the longer ones have heavier flexural reinforcement. All are reinforced identically for shear. Schematic views of the cross-section and elevation, based on the original design drawings, are shown in Figure 2.3

In the years since the original design of the Type 'E' girder, the situation has changed on both the load and resistance sides of the design equation. First, traffic loads have increased considerably and current rules governing live loads are generally more severe than they used to be. Second, research since the publication of AASHO-57 has resulted in changes not only in code shear requirements, but also in the general understanding of shear behaviour in reinforced concrete members.

The design truck loading originally specified was the H20-S16 truck loading, as defined in AASHO-57. This loading is shown in Figure 2.4 and amounts to a total weight of 320 kN (72 kips). Currently, three standard design truck loadings are used in Alberta (Figure 2.5) (Alberta Transportation and Utilities, 1993). The largest of these has a total weight of 647 kN, more than twice the weight of the 1957 truck. The dynamic load allowance has also been re-defined and can now be a greater value, depending on the bridge type. Wheel loads, rather than total loads, are more significant for shear loading. One 1957 wheel load is 71 kN whereas now the maximum single wheel load is 103 kN. Although this has not doubled, it is still a substantial increase. The longitudinal axle spacing was actually slightly more onerous for shear in AASHO-57 than it is currently; this probably is not as significant a difference as the load applied. Rules for lateral distribution of wheel loads for shear have changed and are now more severe, at least for this particular type of bridge (AASHO-57, S6-88).

The second critical change in the codes is in the requirements for shear design. The shear resistance of a concrete member is defined as:

$$V_n = V_c + V_s \tag{2.1}$$

where V_c is the shear resistance provided by the concrete and V_s is the shear resistance provided by the web reinforcement, if any is present. There are two fundamental differences between the original AASHO-57 shear provisions and those in common use today, such as in S6-88. Changes have been made both to the way in which the allowable shear stress in the concrete is calculated and in the provisions for transverse reinforcement.

In AASHO-57, the allowable shear stress for beams without web reinforcement (longitudinal bars anchored) was (Article 1.4.11.(2)):

$$v_c = 0.03\, f'_c \leq 0.62 \text{ MPa} \tag{2.2}$$

If the allowable stress in the concrete was exceeded, transverse reinforcement had to be provided. If reinforcement was used, the concrete was assumed to carry shear stress as specified by Equation (2.2). In addition, regardless of the size, strength or spacing of the stirrups, the allowable shear on a section with stirrups was specified by :

$$V = 0.075\, f'_c b_w jd \qquad (2.3)$$

where f'_c is the compressive strength of the concrete, b_w is the width of the web and jd is the moment arm between the internal tension and compression forces in steel and concrete.

In the current S6-88 code the permissible shear stress in the concrete (Clause 8.6.6.2.1) is:

$$v_h = (0.07 + 10.0\,\rho_w)\sqrt{f'_c} \;\geq\; 0.08\sqrt{f'_c} \qquad (2.4)$$
$$\leq\; 0.19\sqrt{f'_c}$$

where $\rho_w = A_s/b_w d$ is the web reinforcement ratio and A_s is the cross-sectional area of the tensile reinforcing steel. The code specifies that stirrups are required if shear due to the factored loads, V_f, exceeds one half of ϕV_c, the factored shear resistance, where:

$$\phi V_c = \phi v_h b_w d \qquad (2.5)$$

where ϕ=0.75 for shear (Clause 8.6.1), d is the distance from the extreme fibre in compression to the centroid of the tensile reinforcing steel.

In order to compare the current limit states code specifications to the working stress AASHO-57 code, the S6-88 requirements must be adjusted to eliminate the effect of the load and resistance factors. The factored shear may include one or more load factors depending on the type of loading. For simplicity and comparison purposes, an average of the dead and live load resistance factors will be assumed:

$$\alpha = \frac{\alpha_D + \alpha_L}{2} = \frac{1.25 + 1.5}{2} = 1.375$$

If the upper limit of Equation (2.4) is adjusted to eliminate the effect of the load and resistance factors, the permissible shear stress becomes:

$$v_c = \frac{\phi\, 0.19\sqrt{f'_c}}{\alpha} = 0.10\sqrt{f'_c}$$

If, for example, f'_c = 20 MPa, then the two codes give the following permissible shear stresses in the concrete:

AASHO-57: $v_c = 0.03f'_c = 0.60$ MPa

S6-88: $v_c = 0.10\sqrt{f'_c} = 0.45$ MPa

This comparison shows that the older codes assumed the concrete to carry more shear than is currently permitted; therefore, they were less conservative than current codes.

The second basic change in code shear requirements affects the amount of transverse reinforcement required. In AASHO-57 (Clause 1.7.7(c)) the spacing limits were:

(a) Where stirrups were required to carry shear:

$$s_{max} = \tfrac{1}{2}\, h \qquad (2.6)$$

(b) Where stirrups were not required to carry shear:

$$s_{max} = \tfrac{3}{4}\, h \qquad (2.7)$$

where h is the overall depth of the beam. The current S6-88 requirements (Clause 8.2.7.3) are expressed in terms of effective depth, d:

$$s_{max} = 0.50d \leq 600 \text{ mm} \qquad (2.8)$$

with the further restriction (Clause 8.6.6.3.4) that when the shear resistance provided by the transverse reinforcement, V_s, exceeds $0.33b_w d\sqrt{f'_c}$, the maximum spacing given in Equation (2.8) must be reduced by one-half. The essential difference is that, according to AASHO-57, stirrups did need not have to be provided until the allowable unit shearing stress for concrete, v_c, was exceeded (Article 1.7.7(a), AASHO-57), with the exception of the webs of T-girders and box sections which had to be reinforced with stirrups in all cases, in which case Equation (2.7) applied.

In S6-88, if one-half the permissible shear resistance provided by the concrete, V_c, is exceeded, a minimum number of stirrups must be provided such that a minimum area requirement is satisfied (Clause 8.2.7.1.2):

$$A_v > \frac{0.35 b_w s}{f_y} \qquad (2.9)$$

where A_v is the area of shear reinforcement, f_y is the specified yield stress of the reinforcement and $s \leq s_{max}$. This requirement exists because shear strength is, by nature, more unpredictable than flexural strength and shear failure loads can vary considerably from those calculated by design equations. This area calculation is equivalent to providing enough web reinforcement to transmit a shear stress of 0.35 MPa (MacGregor, 1992). There was no such provision in the original code.

According to the original drawings (as shown in Figure 2.3), the maximum spacing between stirrups was specified as 508 mm (20") in the middle third of the girder length. The overall depth of the member, h, is 610 mm (24"); the effective depth, d, is 525 mm (21") in this region. According to the original AASHO-57 requirements:

$$s_{max} = \tfrac{3}{4}\, h = \tfrac{3}{4}\,(610 \text{ mm}) = 457 \text{ mm } (18")$$

if not required to carry shear and:

$$s_{max} = \tfrac{1}{2}\, h = 305 \text{ mm}$$

if required to carry shear.

According to S6-88:

$$s_{max} = 0.50d = 0.50*525 = 263 \text{ mm}$$

The specified maximum stirrup spacing of 508 mm provided exceeds the AASHO-57 requirements by 11% and the current S6-88 requirements by 93%. Since this hat-shaped girder is analogous to T-beam construction (i.e. wide compression flange, narrower webs) the ¾h rule should apply. The stirrup design is insufficient by both

current standards and contemporary standards. A peculiarity of this bridge type is that, over most of the girder's length, the stirrups alternate from leg to leg (single loop stirrups). This means that the maximum spacing is actually twice this distance if considering only one leg. The specified distances between stirrups from original drawings are shown in Figure 2.3. In the elevation, a solid vertical line indicates a single loop stirrup in the near leg while a dashed line indicates a stirrup in the far leg. Double loop stirrups, i.e. a loop in each leg at the same cross-section, occur only near the ends of the girder.

2.3 Evaluation of Girders - Shear and Moment

In order to predict the shear capacity of the Type 'E' girders, it is important to estimate both components (V_c, V_s) as accurately as possible. Because there are so few stirrups over much of the girder's length, this is particularly critical for V_c. Aside from the S6-88 equation presented above as a comparison to the original AASHO-57 requirements, there are other expressions which have been proposed for calculating the concrete contribution. The S6-88 equation, Equation (2.4), is equivalent to that proposed by ACI-ASCE Committee 426 in 1974. This equation is not found in the current AASHTO code (AASHTO, 1989) which, since 1974, has used the same expression as was introduced into the ACI code in 1963 (ACI-ASCE Committee 426, 1974):

$$v_c = 0.16\sqrt{f'_c} + 17\rho_w Vd/M \leq 0.29\sqrt{f'_c} \qquad (2.10)$$

where V and M are the co-incident shear and moment at a given section. It is generally used in its simplified form:

$$v_c = 0.17\sqrt{f'_c} \qquad (2.11)$$

This value is also given in the simplified shear calculations of CAN/CSA-A23.3 (1984). Subsequent research has shown that Equations (2.10) and (2.11) are unconservative for beams have web reinforcement ratios ρ_w less than 1% and overconservative for beams with ρ_w greater than 1% and that it does not correctly take into account the a/d (Vd/M) ratio, where a is the shear span. For the Type 'E' girder, since it may be argued that the sparse stirrups are almost like no stirrups, and since ρ_w is greater than 1%, these equations may be too conservative. An alternative to the above equations is the

expression derived by Zsutty (1968) based on statistical studies of beams without web reinforcement:

$$v_c = 2.137 (f'_c \rho_w d/a)^{1/3} \qquad (2.12)$$

This formulation is not included in any of the codes, but it may give better estimates of the concrete contribution.

Although the V_c calculation may be the most critical, the contribution of the stirrups to V_n cannot be neglected, even if they are sparsely provided. The commonly used model for the shear contribution of transverse web reinforcement is the truss analogy. It has been shown that the contribution of light transverse reinforcement is at least 50% more effective than predicted by the modified truss analogy (ACI-ASCE Committee, 1974). The commonly used equation for calculation of the contribution of the reinforcement contribution is:

$$V_S = A_V f_y d/s \qquad (2.13)$$

where A_S is the cross-sectional area and f_y is the yield strength of the transverse reinforcement. This equation is derived from the well-known truss model developed by Morsch (MacGregor, 1992), which assumes the inclined crack has a horizontal projection equal to the effective depth of the member. The beam member is modelled as a truss by taking the stirrups as tension members, the concrete between the cracks as diagonal compression members and the longitudinal reinforcing bars as bottom chord tension members. The truss model recognizes that an increase in force in the web tension members (i.e., stirrups) will result in an increase in force in the bottom tension members (i.e., rebars) since this force will be in addition to the tensile force due to flexure. In order for the mechanism of the truss model to work, it is necessary that the stirrups are adequately anchored into the top and bottom chord so that they can transfer the force at the truss nodes. To ensure this, codes require that stirrups extend as high and as low as physically possible and as bar spacings and cover requirements permit. Equation (2.13) is based on the assumption that the full yield strength of the stirrups can be developed; the situation becomes more critical if the inclined crack intersects the stirrup very near the compression face. This would leave little length of stirrup above the crack with which it can anchor the stirrup to allow full f_y to develop.

In addition to the calculated contribution, V_s, of the transverse steel itself, the presence of stirrups aids the performance of the concrete, hence indirectly increasing V_c. The stirrups help keep the cracked surfaces of the concrete close together, increasing the benefit provided by aggregate interlock, or shear friction. By bearing against the longitudinal bars, stirrups also enhance dowel action. These two mechanisms (shear friction and dowel action) are important components of shear resistance, especially after cracking.

Another approach to deal with the problem of behaviour in shear is the Compression Field Theory, developed by Collins and Mitchell (1991). Although it resembles the truss model, it does not assume the angle of the cracks (or, orientation of principal compressive stress). Rather, this angle is calculated using compatibility as well as equilibrium conditions, and material stress-strain relationships. Further research led to the Modified Compression Field Theory (MCFT) which includes the contribution of tensile stress in the concrete between cracks, previously neglected. This allows MCFT to be used to predict the shear capacity of members without stirrups. The MCFT requires an iterative procedure to analyze sections under different combinations of moment and shear. The complexity of the procedure makes it rather tedious to apply. In order to more efficiently carry out the analysis for the purposes of this research, a software program called 'RESPONSE' was used (Collins and Mitchell, 1991) to obtain the co-incident shear and moment capacities at a section.

Appendix A describes the results of an earlier testing program which was carried out on four Type 'E' girders. The objective of this testing was to determine the actual shear and moment capacities of the Type 'E' girder and to compare the predictions made using the different methods described above. The shear results for one of the 9.14 m long girders are presented graphically in Figure 2.6, in which the predicted values are nominal strengths What is immediately apparent is that none of the methods predicted the capacity of the member accurately. The random spacing of the stirrups made it difficult to analyze the section. Although they are not spaced out consistently close enough to make the truss analogy valid, it is over-conservative to ignore their contribution. The load path established during the test was suited to the unique arrangement of stirrups. The random spacing of stirrups in this girder was typical of all girders tested (in tests described in Appendix A, as well as in the main testing program). It is not realistic to inspect every girder in every bridge individually to determine accurately the reinforcement provided.

Although using the design stirrup spacings will at times result in over-conservative evaluations, this may not always be the case.

An evaluation of the bridge was carried out in accordance with Clause 12 of S6-88 and shear and moment ratings were obtained. The results of the shear evaluation are summarized in Table 2.1. The capacities were determined in accordance with the criteria set forth in S6-88, using the nominal (specified) material strengths. The moment ratings are all well above unity, indicating adequate capacity in flexure. The shear ratings indicate that the girders are shear deficiencient between 2200 and 3600 mm from the ends of the members. In this region, the shear force due to the applied loads is still relatively high, yet the shear strength has already dropped off due to the widely spaced stirrups.

The other issue to consider is inspection. The inventory of 50 bridges constructed with Type 'E' girders has been inspected, particularly for shear cracking, locating stirrups etc.. This was carried out in such detail precisely because analyses indicated the possibility of shear problems. Although other problems, such as spalling, were often observed, shear cracking in particular was noted on 31 of the 50 bridges. At times these cracks were found almost at midspan (2.7 m to 3.7 m from supports), mostly at inclinations of 30 to 45 degrees. Thus, visual inspections as well as analyses, indicate that a shear problem may exist in these bridges.

2.4 Strengthening for Shear Deficiencies

The problem discussed in the previous sections exists not only for the Type 'E' girder bridges but for many other concrete bridges and girders in Alberta and elsewhere. Over the last 30 years various solutions have been implemented to upgrade existing structures for both shear and flexure. Ideally, a good repair technique will possess the following: ease of implementation; minimal disruption to use and service of the bridge during construction; minimal addition of dead weight and/or loss of clearance; efficient labour techniques; rapid installation; minimal disruption to the existing members; adequate behaviour and durability under service conditions (e.g. fatigue, corrosion, fluctuating temperatures, creep).

One basic method is to remove concrete (damaged or otherwise) sufficiently to allow placement of additional reinforcement. Concrete is then cast to reform the section,

perhaps increasing the sectional dimensions if required for strength or cover purposes. This method has been reported for both shear and flexural upgrading (Pakvor, 1991; Tankut and Ersoy, 1991). One concern here is to ensure that the bond between the old and new concrete is adequate. In other research, fibre reinforced concrete was used to replace the concrete removed (Andrews and Sharma, 1990). These methods have shown satisfactory results in restoring or increasing the capacity of the members. Although this method would probably be necessary if the concrete itself was damaged or deteriorated, it may not be the optimal solution in other situations. It is an arduous, labour intensive process, difficult to implement on existing structures. It is often of paramount importance to maintain traffic over the bridge while repairs are underway. This would be difficult if not impossible to accomplish while removing portions of the beams and some means of shoring would be required for work and concrete casting. Time is required for the concrete to gain adequate, even short-term, strength before it can be subjected to full loading. If additional concrete must be added over and above what was there originally, this will add dead load to the structure and probably will also affect clearances beneath the structure, both of which are undesirable side-effects.

Another group of solutions involves drilling through the deck and/or top flange of the bridge girders to install additional vertical or inclined stirrups. One such solution is described by Klein and Popovic (1985). An existing simple span T-girder highway bridge was found to be deficient in shear. The repair was made by drilling holes through the deck down into the web of the T-girder. The holes, oriented at 45 degrees, were filled with epoxy after which a reinforcing bar was inserted to the level of the bottom longitudinal reinforcing bars. Thus, the new 'stirrups' were well anchored into the top and bottom flanges. Figure 2.7 shows this repair technique.

A slightly different approach has the new stirrups installed externally, adjacent to the web. This concept has been applied successfully on various cross-sections of reinforced and prestressed concrete bridges. The strengthening of a T-girder bridge in this manner has been reported in the literature by Ramsay (1990) and a typical repaired cross-section in shown in Figure 2.8. Holes were drilled through the deck adjacent to the web of the T. Steel tie rods were inserted through these holes and connected to a pair of back-to-back steel channels which passed transversely across the bottom of the girder, flush to the bottom flange. This solution also provides good anchorage to the top and bottom chords. It is preferable to the previous technique described in that drilling is minimize, thus

reducing not only labour costs but also minimizing the chances of interfering with other internal reinforcement or otherwise damaging or disrupting the existing member. Also, the rods can be post-tensioned after installation, and can be checked and possibly tensioned again at a later date. One disadvantage that has been introduced is that now the steel is exposed to the environment and protective measures must be taken to prevent corrosion, which is an additional expense. With adequate corrosion protection this solution is effective, but it can still be expensive and labour intensive. A large number of these stirrup arrangements are required to strengthen an entire bridge. For example, about 800 stirrups were required to repair an 85 m prestressed bridge; 400 were required to repair a 63 m bridge. As many as 1100 tie rods were required to strengthen a 73 m long bridge. The photograph in Figure 2.9 is a view of a bridge strengthened in this manner; the solution would not generally be considered aesthetically pleasing.

The next group of strengthening solutions uses steel plates epoxied and/or mechanically fastened to the concrete surface. There have been numerous applications of gluing steel plates to concrete, especially for flexural strengthening and research has been undertaken in this area since the 1960's (Eberline *et al* (1986), Dussek (1980), Klaiber *et al* (1987), McKenna (1994) and Swamy *et al* (1987, 1989)). Epoxy-bonded steel plates have been used to strengthen bridges and buildings around the world and applications have been reported extensively in the literature. In order to use epoxy resin adhesives confidently in structural applications, certain factors must be considered when selecting and applying them. If the epoxies are appropriately selected for the application, strength is generally not a problem, but other important considerations include ease of application (e.g., workability of the glue, curing conditions, relatively rapid cure) and, most importantly, long term durability. The latter is particularly important for bridge use because of the service conditions which include exposure to fatigue-inducing loads (i.e., traffic), humidity, certain chemicals and fluctuating temperatures. Assurance is needed that the bond between the steel plate and the concrete will not degrade in time and that the creep deformations will be negligible. A general presentation of the use of epoxies in civil engineering, their development, properties and application can be found in (Mays and Hutchinson, 1992).

Reports pertaining to flexural strengthening using steel plates will not be covered here as the subject is well documented elsewhere. References will be made here if they apply in a general way or if they are related to non-strength issues (such as durability).

Experimental research has been reported by Iyer (1989) who bonded steel plates to prestressed, precracked beams with structural adhesives as well as mechanical fasteners. Tested under both static and cyclic loads, they showed improved strength, deflection and crack control with very little response to the cyclic loading. Johnson (1981) also bonded steel plates to the tension face of beams. There was no failure in the adhesive/bond layer but premature failure occurred due to the build-up of high shear stresses in the concrete at the ends of the plates which caused the concrete to shear horizontally above the longitudinal steel. This is a very common failure mode and many have tried to alleviate this specific problem. Mechanical fasteners near the ends of the plate, in addition to the glue, help prevent this. Ladner (1983) tested similarly strengthened concrete beams but was primarily interested in determining the stress distribution between the concrete and the steel plates near the ends of the plates and in modelling the load transfer mechanism between the two. He showed how these high shear stresses that develop can actually decrease the vertical shear capacity of the section, thus perhaps requiring shear strengthening as well. This last issue was also raised by Johnson (1981) who attempted to quantitatively estimate this loss of shear capacity. The shear peeling phenomenon, which is a rapid and catastrophic failure, has also been considered by Oehlers (1990) who showed that this failure mechanism depends on the shear strength of the concrete, not on the shear strength of the adhesive. This is clear as this kind of failure always occurs horizontally through the concrete, parallel to, but above, the glue line.

Further to experimental work, there have been many reported case studies of field applications, most of them in Great Britain, Europe and Japan. Although almost no research has been reported on shear strengthening, there are a few reports of applications. One very early application was in South Africa in 1967 (Fleming, 1967). Mild steel plates were glued to the web faces of laboratory specimens. Although the testing was limited in scope, an improvement in shear capacity was achieved. No particular problems were reported as to debonding or other behavioural problems and the technique was then applied to the strengthening of concrete members in an existing structure. Another early application was in France in the late 1960's when a reinforced concrete bridge was strengthened for both flexure and shear (Bresson, 1972). For shear strengthening, three millimetre thick steel plates were bonded to the web of I-girders along the full length of the bridge. Shear and flexural strengthening were also applied in Zurich to strengthen floor beams to carry additional load (Hugenschmidt, 1976). This practical application was preceded by tests on comparable members where shear angle plates were used in the high

shear zones in addition to flexural plates on the bottom flange. The specimens exhibited good bonding and stiffness characteristics. Although the finished steel surface had to be protected against both corrosion and fire, this method was chosen because it minimized the decrease in headroom and maximized the speed and efficiency of reconstruction. In 1978, steel plating for shear as well as flexure was used to upgrade floor beams in a London office building (Parkinson, 1978). Design and clearance restraints required that the plates be glued to the inclined beam sides rather than to the bottom of the flange. In this manner, they could contribute to both shear and flexure simultaneously. Anchorage bolts used at the plate ends against high shearing stresses also added assurance of safety in the event of a fire, as epoxies typically do not exhibit good behaviour at elevated temperatures.

In the early 1990's a simply supported prestressed concrete inverted T-beam bridge in Scotland was strengthened with steel plates bonded to the bottom tension flanges (Taylor, 1992). The main attractions to using this method were that there would be minimal disturbance to service as all work could be carried out from the underside. Although there was some concern as to the long-term durability/integrity of the bond between steel and concrete, it was decided that some debonding could be tolerated since it would not cause catastrophic failure and the plate(s) could be replaced/rebonded if necessary. As an added precaution, mechanical fasteners (i.e., resin anchored bolts) were used at each end of the plates. It was believed that long-term creep in the adhesive would not be a problem as the design was intended predominantly to assist with the live load (i.e., short term) capacity.

Several cases in Britain have involved the flexural strengthening of highway bridges with bonded steel plates; in fact, it has been reported that there have been an average of one or two applications of plate bonding repair solutions a year (Mays and Hutchinson, 1992). Bridge loading tests have demonstrated increases in flexural stiffness and decreases in crack openings under load. One of these bridges, at Quinton on the M5, was inspected regularly after repairs were made in 1975. After 12 years, there were only isolated occurrences of minor debonding and these affected areas had been exposed directly to leakage of water and chlorides (Calder 1988; Calder 1989).

There are several concerns when steel plates are epoxy bonded to concrete members and these will be summarized in the next few paragraphs. One of the main advantages of

the steel plating method is that all work can be carried out from beneath the superstructure and it is not necessary to disturb the deck or do any drilling. However, the weight of the plates makes the gluing work more difficult. Generally, they must be held in place under pressure until cure is complete, to ensure a good bond. More seriously, there have been concerns over the years as to the durability of the resin glue under adverse environmental conditions, under sustained or repeated loads, and the effect of creep.

One of the prime concerns is the possibility of corrosion at the steel/concrete interface due to ingress of moisture at this sensitive location. Long term exposure tests (2 to 10 years) have been reported by Calder (1988, 1989). Steel plates were bonded to one face of small concrete laboratory specimens using an epoxy adhesive. The specimens were exposed to various harsh environments, including high rainfall, marine, industrial environments, under both loaded and unloaded conditions. Although some corrosion between the steel and epoxy was found on plates removed from all specimens, this did not seem to significantly affect load carrying capacity. However, it was also found that satisfactory results depended critically upon the type of epoxy resin used, and such good results could not be obtained when certain epoxies were used. Corrosion remains a concern when steel is used, whether this is in the form of bonded plates, rods, or other. Preventive measures must be taken, such as galvanizing the exposed components, or using special coatings.

Research on epoxies that has considered their behaviour at high temperatures shows that their strength deteriorates rapidly with increasing temperature. Figure 2.10 shows the effect of temperature on typical epoxies. There is virtually no degradation in shear strength of cold-cure epoxies between -50 and +35 degrees Celsius. In fact, shear strength is higher at temperatures lower than typical application and service temperatures (say, 10-20° C). Most of the reported tests on long-term exposure to realistic outdoor environments have been conducted in Britain, where the typical temperature range that concrete bridges are exposed to is -20 to +38 degrees Celsius (Mays and Hutchinson, 1992). There has not been much research on the behaviour of these adhesives at extremely low temperatures, more characteristic of harsh Canadian climatic conditions.

There is also the question of behaviour under cyclic loading which has not been as extensively researched, although Hugenschmidt (1976) reported that beams tested under cyclic loads performed no differently from those tested under static loads. Fatigue

problems may be avoided or minimized in some situations, by designing the repair work appropriately.

Some of the disadvantages of the steel plating method may be alleviated by using, instead of steel plates, advanced composite materials (ACM) or fibre-reinforced plastics (FRP's). These are relative new-comers to civil engineering but have some beneficial properties which may make them preferable to conventional materials in some applications.

2.5 Advanced Composite Materials or Fibre Reinforced Plastics

Advanced composite materials (ACM) were originally introduced and used in the aeronautics, mechanical, chemical and automotive industries. They were considered attractive for use in these fields because they have an extremely high strength to weight ratio, they are non-corrosive, non-electromagnetic, have generally good fatigue behaviour and can be easily and precisely formed to suit the application. Although still quite expensive, their unique properties can make them competitive with more traditional materials, such as steel, in certain applications.

The term advanced composite material can refer to any material made up of two or more constituents which generally are taken to be advanced industrial man-made substances. Fibre reinforced plastics (FRP) are one of the largest subcategories of ACM's and one of the most commonly encountered. Although the two terms are used interchangeably, the materials used in civil engineering are actually FRP's. As the name suggests, these composites consist of high strength fibres (of various types) held in a relatively weak plastic resin matrix. The fibres provide the major contribution of strength and stiffness of the composite and most of its other desirable properties. The matrix serves primarily to hold the fibres in place in proper alignment and to distribute the load to them from point of application. In general, its properties are far less desirable than those of the fibres. The properties of the composite material depend largely on the properties of the fibres and matrix used, and the relative proportion in which each component is present.

FRP's have been and can be produced in a myriad of forms, tailored to the application. Although this is one of their attractive features, it does make it difficult to describe the material in general terms. Unlike other structural materials, there are no

standards, and cannot be, in the traditional sense since so many manufacturers produce their own proprietary products. They are a family of materials with widely varying properties rather than a single material with well-defined properties. Not only are a variety of different fibres and plastics used, modifiers or fillers are often added to enhance or diminish certain properties. FRP's can be supplied as a finished end product by the manufacturer in a variety of structural shapes or in the form of bars, tendons, wire meshes, cables, plates/sheets or as micro fibres to be used as an additive to concrete (Mufti *et al*, 1991). Alternatively, the FRP may be supplied to the end user in an unfinished (semi-cured) state. The composite is finished when the remainder of the resin is added by the user and must then undergo specific curing conditions to produce the final product. While products supplied fully cured were probably cured under high temperatures and pressures, these partially cured products are designed to cure at 'normal' service temperatures

The fibres may be made of glass, carbon, or aramid. Glass fibres are still most commonly used because there is more experience, historically, with them and because they are much less expensive. However, carbon fibres seem to be gaining interest for use in structural applications despite their higher cost because some of their properties are superior to those of glass in some areas such as durability in marine environments. Aramid fibres are also used.

Fibres may be oriented randomly within the matrix, in certain prescribed alignments, or unidirectionally. As all the attractive properties of the composite depend on the fibres, the greatest benefit is gained when it is loaded in the direction in which the fibres are oriented. When the load is applied at a different orientation (away from that of the fibres), the properties of the matrix begin to dominate. This phenomenon is especially dramatic when composites are highly directional. For instance, if a unidirectional composite is loaded in its principal direction, the properties are almost entirely those of the fibres. As the load is applied at an angle to this principal direction, the effect of the fibres decreases until, when the load is applied perpendicular to the fibres, the properties of the composite are merely those of the matrix. This effect can be seen in Figure 2.11; although shown in particular for a glass fibre-reinforced plastic (GFRP) material, this is typical of FRP's in general. Many FRP's used in structural applications are unidirectional, such as bars, tendons, and unidirectional plates or sheets.

Some typical properties for various fibres, matrices and composites are shown in Table 2.2. Normal and high-strength steel and concrete are included for comparison. Even though the matrix diminishes the strength and stiffness characteristics of the fibres, the composite still has impressive ultimate strength.

FRP's are generally linearly elastic to failure; that is, they do not have a yield point, as seen in Figure 2.12. Although they show no ductility, in the conventional sense, they do not behave like brittle materials, which typically have lower strengths and exhibit problems under impact loading. Most composites are typically not quite as stiff as steel, though considerably stiffer than concrete. Special high modulus composites do exist, but they are far more expensive. Although the ultimate tensile strengths are impressive, what is of far greater interest is to make this comparison by considering the strength/weight ratios, which are much higher than for traditional materials such as steel or concrete.

Although the strength properties of FRP's are well-established, there are other concerns to be addressed related more to serviceability. Long term loading can be a serious consideration because the matrix is highly susceptible to creep, due to the manner in which the material responds at a molecular level. Therefore, the composite creeps as well but the degree to which this is a problem depends on the fibres. Since most fibres are not sensitive to creep, the problem is minimized in FRP's with continuous, unidirectional fibres, since then if the composite is loaded mostly in the fibre direction, the influence of the matrix is minimized. It may be possible to alleviate the creep problem by learning how to design for it, just as this problem can be dealt with in the design of prestressed concrete or wood members. Carbon fibres are virtually creep free and thus creep of the CFRP is due essentially to creep of the matrix. This may not have a detrimental effect on the composite because, as the matrix softens, the carbon fibres may become more well-aligned in the direction of the load, thus avoiding loss of strength under sustained loads. On the other hand, aramid fibres are sensitive to creep (Holloway, 1993) and thus AFRP strains more due to creep than do other composites. The performance of GFRP's is almost as good as CFRP's.

Fatigue resistance is also highly directional and, in general, unidirectional, continuous fibres show the best fatigue behaviour. The fatigue resistance varies according to the type of fibre present in the composite; carbon fibres are superior, followed by aramid, then glass (Holloway, 1993). Figure 2.13 shows this comparison graphically for

CFRP's, GFRP's (glass FRP's) and KFRP's (Kevlar (aramid) FRP's). It is this quality of CFRP's that make them more attractive, especially in situations where cyclic loading exists, as in bridge structures. Further information on fatigue characteristics of fibre/resin composites can be found in the literature (Hilado, 1979).

Temperature effects can affect both the matrix and fibres. Resins used for matrices are susceptible to deterioration at elevated temperatures, much as are the adhesives discussed in Section 2.4. The response of the material to fluctuating temperatures depends on the thermal coefficient of expansion, α. This coefficient differs for matrix and fibres, and is quite different from that of concrete or steel to which the composite may be bonded (Table 2.2). In the case of a sheet or plate glued to concrete, although α of the adhesive or matrix may be dramatically different from that of concrete, if the glue layers applied are thin enough compared to the overall member scale, negative effects may be minimized. One report describes tests showing that the behaviour of GFRP tendons at high temperatures is the same as for pre-stressing steel at high temperatures. (Miesseler and Wolff, 1991) Some tests have shown that unidirectional glass fibre or graphite reinforced plastic composites tended to lose strength and/or stiffness at low temperatures or at cyclic temperatures (+24°C to -180°C) when loaded in the fibre direction (Dutta, 1989). However, the results varied depending on the fibres used and even varied amongst different graphite fibre products. Also, such low temperatures are more extreme than need to be designed for in civil engineering applications. Like many of the FRP properties, testing should ideally be carried out on the specific product to be used.

Environmental effects: One of the attractions of FRP's is that they are non-corrosive, but it is still important to consider how they may react in other, potentially hostile, environments to which they may be exposed. If a composite absorbs water, significant reduction in properties by as much as 25 to 30% can occur. This detrimental effect can be guarded against by using water-resistant resins, or by choosing products which have exhibited water-resistant properties. Freeze-thaw will probably have an even more severe effect and the material should be tested for this exposure. The polymer matrix is sensitive to photodegradation and break down of the matrix in this manner will eventually also affect the fibres. Photodegradation, i.e. exposure to ultra-violet light, can be minimized by additives or by protective covering of the finished product, such as painting. Concrete is an alkaline environment and if FRP's are used internally they can be adversely affected. Glass fibres, in particular, are adversely affected by an alkaline

environment and this is one reason why carbon fibres may be preferable for use in concrete structures. Resistance to other chemicals has been reported (Ichimasu *et al*, 1993a, 1993b) but, again, this behaviour depends also on the specific composition of the components in question.

Economics: In general, the FRP materials are more costly, on a per weight basis, than steel. However, the cost discrepancy decreases if the cost per force provided is compared, due to the significantly higher strength-to-weight ratio of FRP's. The other important consideration is the labour cost involved. The low weight of this material makes them easy to handle and install, and the application process requires no special skills. Perhaps especially on retrofit work of bridges, the cost savings due to labour savings can be substantial if the time required for retrofit and traffic disruption could be minimized. Finally, some of the benefits provided by the FRP's (e.g., non-corrosiveness) may help offset their higher costs. Although the potential for these materials to become economically competitive with more traditional materials and methods exists and has already been explored, their application has not yet been fully exploited (Ballinger, 1992; Bickley *et al*, 1992; Head, 1992).

Summary: The above paragraphs have pointed out some of the characteristics of FRP's. It is important to note that any particular FRP material is likely to possess some but not all of both advantages and disadvantages. The designer must decide which properties are most important for a particular application and then choose the appropriate material. In addition, as FRP research and development continues, different beneficial properties are introduced to different materials; the state of the art is continually changing. One disadvantage of many FRP's which was not mentioned above is their sensitivity to transverse pressure and therefore to damage, intentional or otherwise. This factor must also be considered in design.

2.6 Applications of ACM in Structural Engineering

As mentioned above, ACM's can be and are manufactured in a variety of forms such as pultruded structural shapes, bars, tendons and cables (for regular use and pre-stressing/post-tensioning), unidirectional plates and sheets, and as micro-fibres for use as an additive to concrete to form fibre-reinforced concrete. All of these forms have already found some use both in the design of new structures and in the rehabilitation of existing

ones. They are often used in conjunction with concrete, but have also been used with timber (Meier and Kaiser, 1991; Triantafillou and Deskovic, 1991) and may also be applied to steel or masonry.

In the last 10 years or so, a number of new structures, especially bridges, have incorporated glass, carbon or aramid FRP products. The earliest noted use of FRP's in road bridges dates from 1982, in Bulgaria and China (Head, 1992). The earliest known pedestrian bridge using FRP members was constructed in London in the early 1970's, and many other pedestrian and road bridges have been constructed since then, especially in the last five years. The first bridge using pre-stressed glass tendons was the Ulenbergstrasse bridge in Dusseldorf, Germany in 1986 (Khalifa *et al*, 1993). These examples are not only important so that more ACM bridges can be designed, but they will give invaluable information on long term, fatigue and exposure effects of many different types of ACM products under different uses, loads, and climates. This information can also be used in choosing appropriate products for retrofitting and increases confidence in their safe use.

At the moment, FRP's have perhaps their greatest potential for use in the rehabilitation of structures. Although they are still expensive, they become economically competitive when used in a more limited way, in a manner especially suited to take advantage of their unique beneficial properties. Also, engineers may be more comfortable implementing these materials, which have only ten years practical application in civil engineering, if the overall safety of the structure does not depend entirely on their performance. That is, if strengthening is added to a bridge to help carry additional live load, there is not as much chance of catastrophic collapse; the structure can be monitored for signs of deterioration while knowing the basic familiar structure is still there carrying the majority of the loads. This cautious approach to using new and unfamiliar materials was applied in the recent construction of a new highway bridge in Calgary. CFRP cables were used in the prestressing of six of the thirteen bridge girders. A fibre optical system was installed in order to monitor the behaviour of the bridge in the long term and provisions were made for replacement of cables if problems arise at a later date (Mufti *et al*, 1991).

While tendons and rods have and can be used for strengthening structures, much of the research and application has been in increasing the strength of concrete members by bonding FRP plates to the surface in a manner similar to steel plating. Almost all case

studies encountered have been associated with flexural upgrading, and there are as yet only incidental references to shear strengthening. However, a great deal can be learned from research on flexural strengthening which may then be extended to shear strengthening applications.

In a bridge in Japan, carbon fibre-reinforced plastic plates were bonded to the underside of a concrete slab in two mutually perpendicular directions (Ichimasu *et al*, 1993a, 1993b). The goal was to reduce stresses in the existing rebars to acceptable levels by current standards. Because the materials have no yield point, the "allowable stress" was taken as 60% of the specified breaking strength. The use of various CFRP products was investigated and it was found that unidirectional pre-impregnated carbon fibre sheets were the most appropriate for the particular application. The rehabilitation was successful in that the composite sheet did decrease the measured stress in the internal steel reinforcing bars.

A similar product has been used to upgrade bridge columns, concrete chimneys and beams and floors (Ballinger *et al*, 1993). This research, prompted by the need for seismic upgrading, focussed on the use of CFRP unidirectional prepreg (similar to that described above) and carbon fibre strand (CRS). Columns and chimney stacks were found to have insufficient flexural steel and transverse spirals, i.e. not enough confinement, and therefore did not have enough shear strength or ductility. The solution was to use the CFRP unidirectional prepreg sheets longitudinally to provide flexural reinforcement and the CRS strand wound around the column to provide the shear strength. The amount of flexural reinforcement required was calculated quite simply by requiring the area ratio (carbon fibres/steel) to be equivalent to the stress ratio (yield strength of steel to CFRP design strength). The latter was defined by applying a 1.5 safety factor to the specified ultimate strength. The design for shear was based on the assumption that the shear force acting on the columns should be resisted only by the fibres. The area quantity of fibres required was calculated as it had been for the flexural reinforcement. The contribution of the CFRP to shear was calculated using the same code equation used for steel stirrup design. Test results on columns thus strengthened showed increases in flexural strength, shear strength and ductility. Note that the strands used for shear resistance were wrapped completely and continuously around the column thus providing confinement to the concrete, increasing its effective strength and ductility. This type of seismic upgrading of columns is

being increasingly considered and/or used in California, where glass and aramid fibres are being used to confine bridge columns.

The Ibach Bridge, a continuous multispan box beam bridge in Switzerland, was repaired in 1991 using CFRP plates externally bonded to the tension faces of the boxes (Meier *et al*, 1992). The light weight of the CFRP sheets allowed work to be more easily accomplished as a lighter mobile platform could be used rather than the heavier scaffolding that would have been necessary if steel had been used as the repair material. This minimized obstruction to traffic beneath the overpass. Load tests were performed after the repair was completed to confirm the success of the procedure. After 18 months of monitoring, no problems were found with the strengthening (ENR, 1993). The success of these projects has led to the planning of a retrofit program for another bridge in Switzerland. Extensive cracking on the post-tensioned slab of this bridge will be "bandaged" with CFRP strips bonded to the damaged surface.

Much of the research on the use of FRP plates concrete beam strengthening has been carried out over the last decade at EMPA in Switzerland under the guidance of Urs Meier who has been the strongest proponent of FRP's. In Japan, many private organizations as well as government agencies are involved with research into all aspects of composite materials and their application in civil engineering, including external bonding to concrete members (Mufti *et al*, 1992). In North America, Triantaphillou (MIT) and Saadatmanesh (University of Arizona) have published extensively on their research into various aspects of the FRP bonding concept. More recently, research has begun in Canada (Mufti *et al*, 1991; McKenna, 1993).

Research at EMPA into FRP flexurally strengthened beams began in 1984 and progress is regularly reported in the literature. The work has involved the flexural strengthening of laboratory reinforced concrete specimens and has investigated not only the strength characteristics of the technique but also behaviour under fatigue and temperature cycling. Primary failure modes were caused by high shearing strains in the concrete along the bond line near the ends of the plates (as was seen with steel bonded plates), by rupture of the sheet in the constant moment region, or by shear cracks which could cause failure by creating a discontinuity as the section translated in the event of a shear crack opening up, as shown in Figure 2.14. Typically, the strengthened beams failed at higher ultimate loads than did the unstrengthened beams but there were definite

decreases in ductility. Both these effects depended on the nature of the original beam: percentage of steel, over- or under-reinforced etc.. In addition, better crack control was observed; cracks were well distributed and narrower (Kaiser, 1989; Meier and Kaiser, 1991; Meier *et al*, 1992).

Kaiser also investigated thermal cycling and fatigue loading of beams with CFRP on tension flanges. After 100 cycles between -25 to +20 degrees Celsius no degradation was exhibited in loading capacity, even though the coefficients of thermal expansion are very different for FRP's and concrete. Fatigue tests, in some cases under high humidity conditions, were carried out on similarly strengthened beams. In all cases, failure of all the internal steel reinforcement bars (either by fretting fatigue or yielding) preceded failure of the bonded CFRP plate.

Saadatmanesh and Ehsani (1990), in addition to confirming early results of static tests, also looked at other specific issues such as proper choice of epoxies. They found that if the epoxy performs well, both the cracking behaviour and the ultimate capacity improved and they concluded that tough epoxies, having enough strength and stiffness to transfer the shear force between the FRP plate and the concrete, were most suitable for this application. Although all strengthened beams showed increases in flexural capacity, the beams with lower steel reinforcement ratios showed a greater increase in ultimate load. All beams showed better crack distribution and finer, smaller cracks. Ductility, in general, decreased, although the degree to which it did so varied depending on the ductility of the same beam before FRP strengthening.

It is also possible to prestress the sheets being applied to the member (Triantaphillou and Deskovic, 1991; Triantaphillou *et al*, 1992c). CFRP unidirectional sheets were used to prestress materials with a shear strength higher than that of the adhesive used (e.g. some woods, steel) and materials with a shear strength lower than the adhesive used (e.g. concrete). The prestressing was carried out by first pretensioning the sheet, gluing it to the concrete surface, curing, and then releasing the ends of the sheet. Alternatively, the beam may be cambered, the sheet applied; after camber is released, a prestressing force is introduced.

Ritchie *et al* (1991) investigated a range of variables in tests of 16 under-reinforced beams. This study not only used a variety of different composites (glass, carbon, aramid

fibres) but also steel plates for comparison. Other variables included fibre orientation (0°, 0°/90°, random), modulus of elasticity (11,700 to 72,400 MPa), ultimate strength (160 to 1490 MPa). A rubber toughened epoxy adhesive was used in all cases because it was found to have the best load transfer and brittle failure characteristics. An average increase in stiffness of 40% and in strength of 19 to 99% were observed. The increase in stiffness was probably so great because relatively small specimens were used (150 mm x 300 mm x 2740 mm). Most failures were shear failures in the concrete near the ends of the plates, parallel to the rebar. None of the plated beams exhibited the ductility the control beams did; however, the steel plated beams showed somewhat more ductility than the other materials, although still not as much as the control beams. In order to prevent premature failure due to horizontal shear in the concrete near the plate ends, fibreglass angles were used to anchor the sheets (Figure 2.15). Some improvement in anchorage was seen but, more interestingly, it was noted that a side effect of this solution was increased vertical shear capacity.

Deblois *et al* (1992) used both uni- and bi-directional GFRP sheets for flexural strengthening. Increases in strength between 30 and 70% were observed and stiffness, initially similar to the control beam, was maintained far longer. In order to avoid premature failure by horizontal shearing in the concrete near plate ends, mechanical anchorages were used to improve the connection to the concrete. This improved the strength by about 18%, and stiffness somewhat. After some of the small beams failed prematurely and unexpectedly due to vertical shear, bi-directional sheets were bonded to the vertical web faces. This strengthening increased the shear capacity by 17% to 31%.

The question of high shear stresses near the anchorage zone and subsequent premature failure has risen in every testing program leading to the implementation of solutions such as mechanical anchorages. Sharif *et al* (1994) looked at this problem specifically and suggested a relationship between plate thickness and this type of premature shear type failure. In addition to steel bolts anchoring the fibreglass into the member, fibreglass jackets were used. The same GFRP material used to strengthen the beams in flexure was also used to form jackets around the beam near the anchorage zones. The jackets, which extended over the full depth of the beam, not only alleviated the anchorage problem but also controlled diagonal shear cracking near the ends of the beams (Figure 2.16).

One recent study investigated the creep characteristics of different FRP's bonded to the tension flanges of reinforced concrete beams. Plevris and Triantaphillou (1994) developed an analytical procedure to model the behaviour of the system under sustained loads, taking into account creep properties of the concrete as well as an existing model for creep of composites. Parametric studies and tests lasting up to 300 days were performed to investigate the effect of the type and area fraction of CFRP and of the area fraction of the steel reinforcement on the long-term response of the strengthened beams. Simulations were used to compare the effect of various thicknesses of glass, carbon and aramid FRP's. The best performance was exhibited by the CFRP strengthened beams, which showed almost no discernible negative reaction due to creep. GFRP strengthened beams behaved almost as well, while AFRP strengthened beams did not fare as well. Unlike carbon or glass fibres, aramid fibres themselves exhibit poor creep characteristics, and this affected the behaviour of the members.

No research specifically dealing with shear strengthening of concrete members with FRP's was found in the literature. However, when side plates were used for other reasons, increases in shear capacity were reported. The flexural testing reported also aids in the consideration of non-strength problems, as these apply just as importantly to shear applications. Some problems associated with strengthening of concrete structures in general were introduced, such as anchorage, failure in the concrete due to that material's low tensile and shear strengths, the importance of bond, long-term loading effects and sensitivity to transverse pressure.

Table 2.1 Results of Clause 12 (S6-88) evaluation of 9.14 m Type 'E' girder (from Appendix A)

Distance from end of girder (mm)	Factored dead loads V_D (kN)	Factored live loads V_L, for truck loading type: CS1 (kN)	CS2 (kN)	CS3 (kN)	Factored Resistance Vr (kN)	Live load resistance factor LLRF CS1	CS2	CS3
600	43.6	203.3	214.4	193.3	419.3	1.8	1.8	1.9
775	41.7	198.8	208.7	188.1	284.9	1.2	1.2	1.3
1000	39.2	193.1	201.3	181.4	284.9	1.3	1.2	1.4
1470	34.1	181.1	185.8	167.5	238.2	1.1	1.1	1.2
1980	28.5	168.1	169.0	152.3	234.2	1.2	1.2	1.4
2235	26.3	169.1	169.0	152.2	170.0	0.8	0.9	0.9
2910	18.7	151.1	151.0	136.0	170.4	1.0	1.0	1.1
3660	10.3	131.1	130.9	117.9	170.4	1.2	1.2	1.4

Table 2.2 Properties of various materials (Holloway, 1990; Mufti *et al*, 1991)

Material	Density (kg/m^3)	Tensile Strength (MPa)	Modulus of Elasticity (GPa)	Coefficient of Thermal Expansion ($x10^{-6}$/deg.C)
Traditional:				
Steel[1]	7850-8130	300-2000	200	11.7
Concrete[2]	2150-2700	25 - 100	25 - 50	10
Matrices:				
Epoxy resin	1100-1350	40-100	3 - 5.5	45 - 65
Polyester	1200 - 1400	45 - 90	2.5 - 4.0	100 - 120
PVC (rigid)	1400	58	2.8	50
Fibres:				
E-glass	2560	1500 - 2500	70	5.0
Carbon (high-modulus)	1950	2000	380	-0.6 to -1.3
Carbon (high-strength)	1790	3800	235	--
Aramid	1450	2700 - 3500	120	-2.0
Fibre reinforced plastic composites:				
Uni-directional laminate glass fibre/polyester	1600 - 2000	400 - 1250	20 - 50	--
Carbon fibre/resin epoxy	1930	800 - 2350	120 - 141	--

[1] Lower limit-structural steels; upper limit-prestressing strand

[2] Modulus of elasticity based on $E = 5000\sqrt{f'_c}$

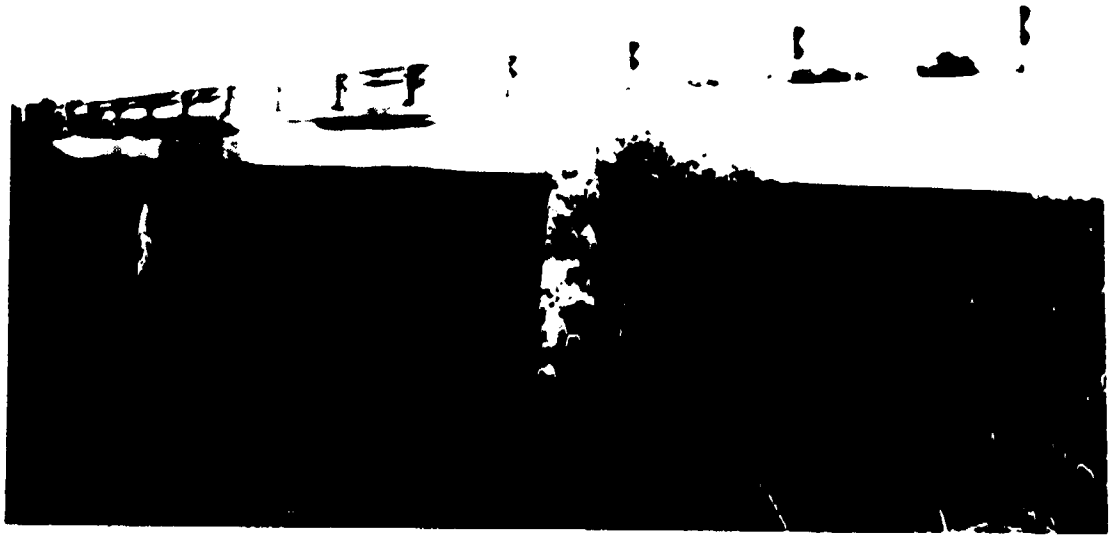

Figure 2.1 Photograph of Typical Type 'E' Girder Bridge - Dogpound Creek Bridge, on Highway 22, Southern Alberta

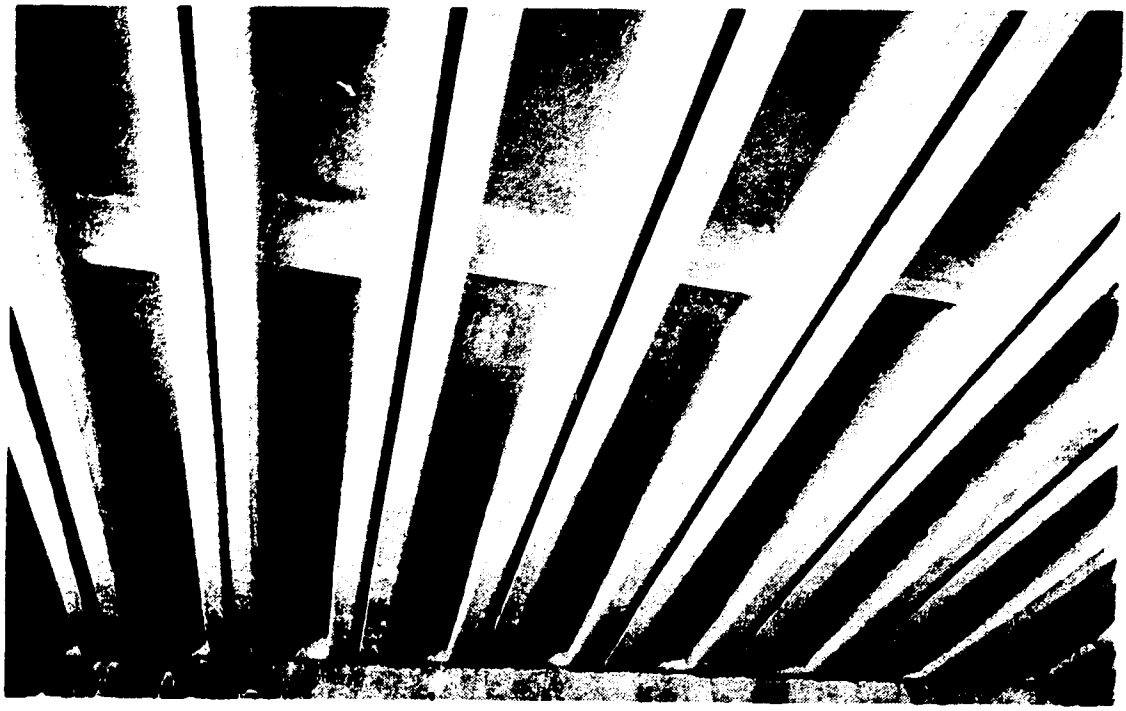

Figure 2.2 Underside of superstructure of typical Type 'E' girder bridge

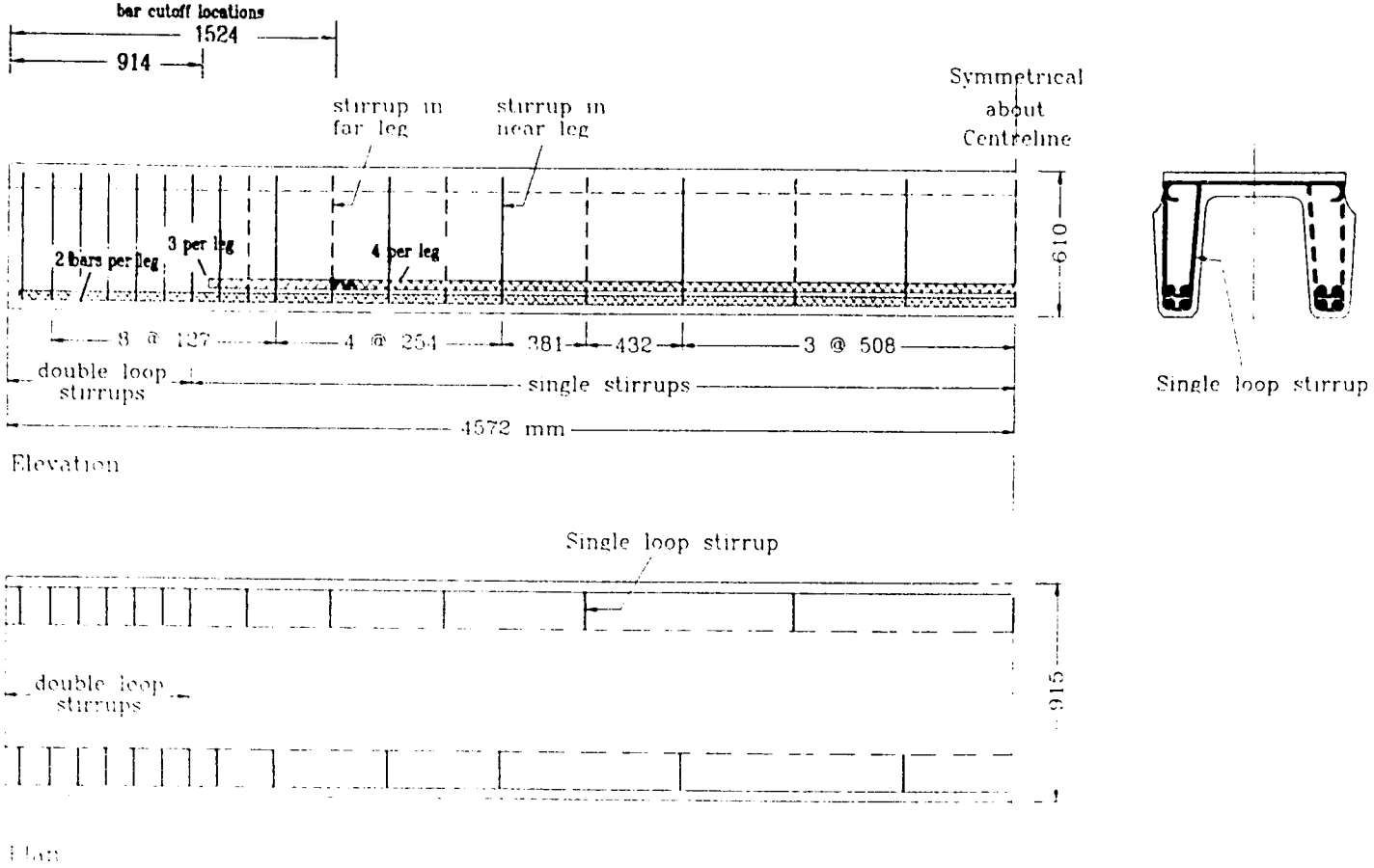

Figure 2.3 Elevation, plan and cross-section of Type 'E' girder

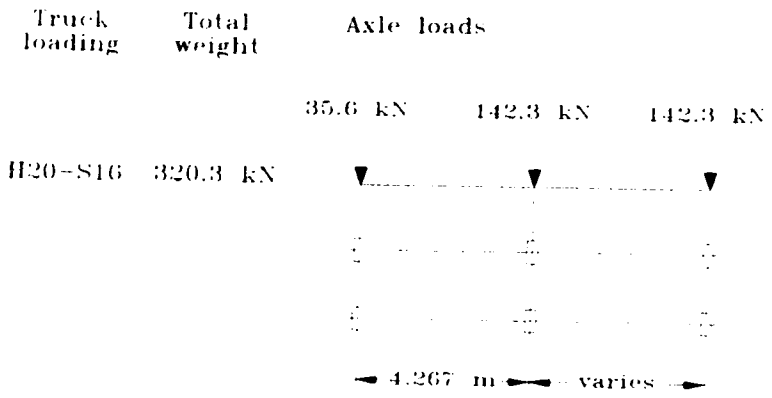

Figure 2.4 Original design truck loading - AASHO 1957, H20-S16 truck

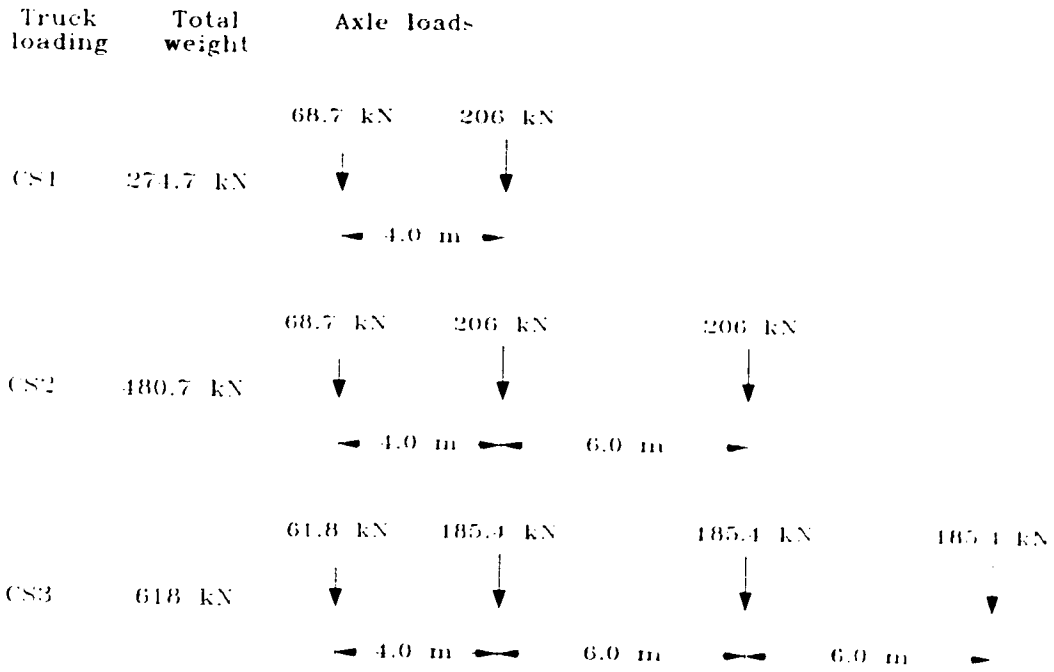

Figure 2.5 Current Alberta Transportation design trucks (Alberta Transportation and Utilities, 1993)

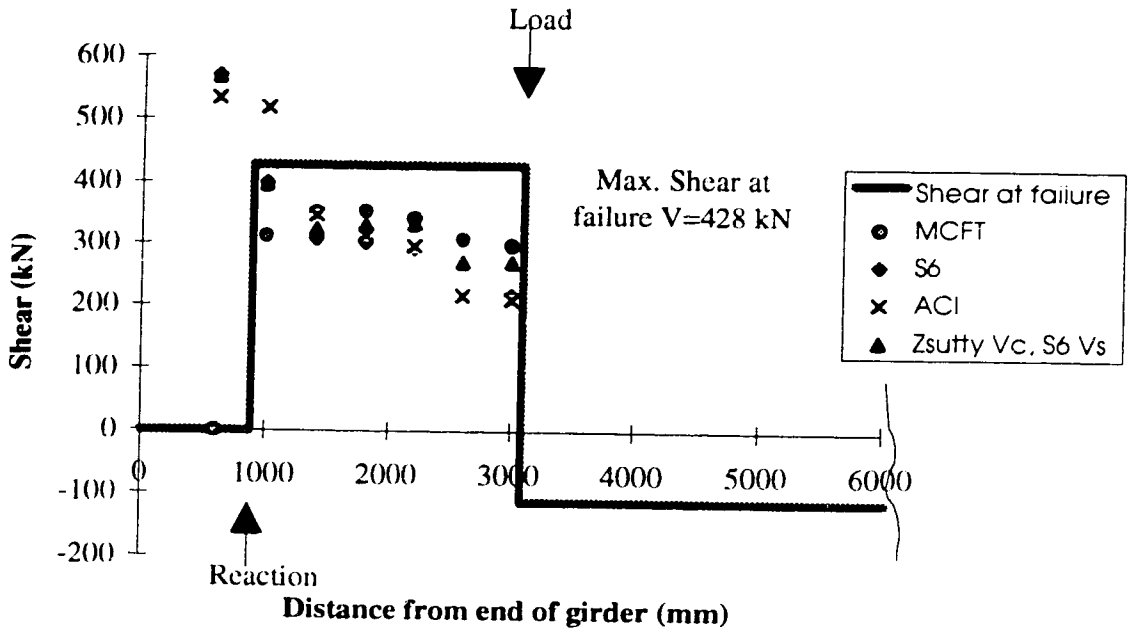

Figure 2.6 Type 'E' girder - In situ shear strength, actual and predicted

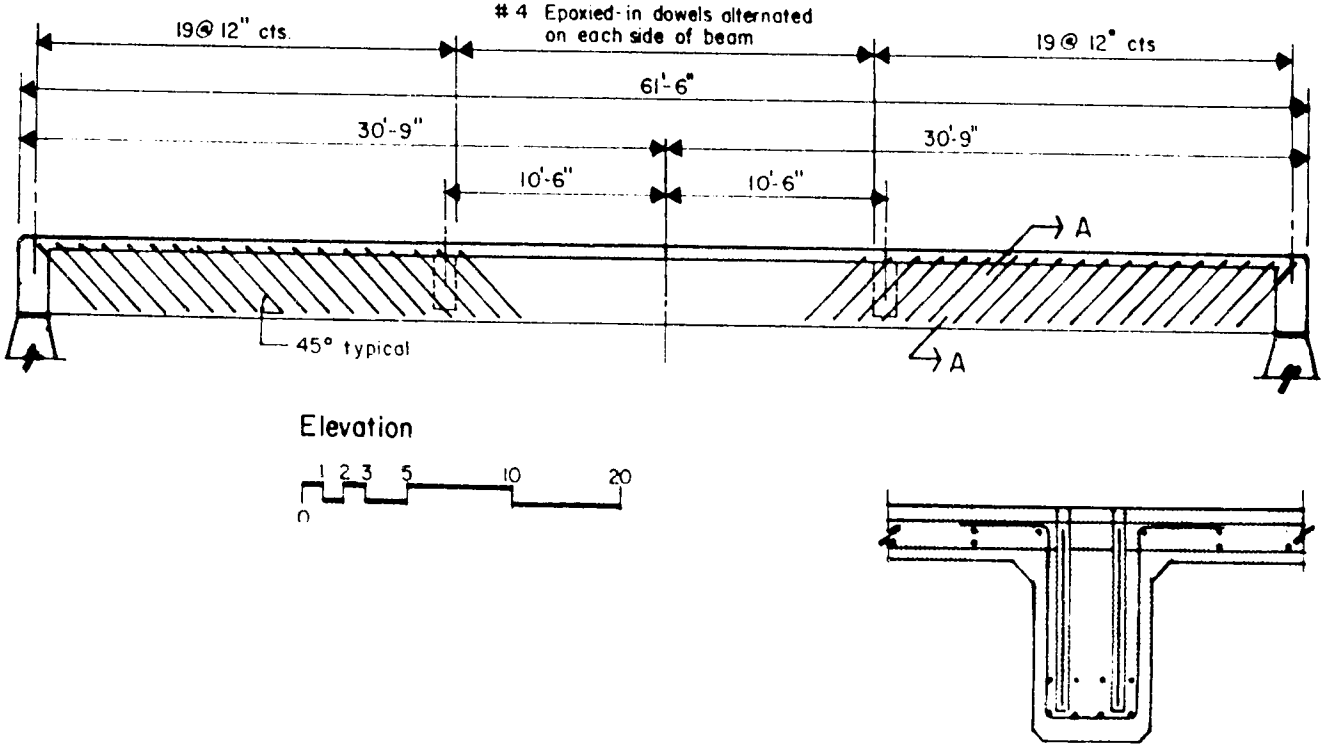

Figure 2.7 Repair of T-beam bridge by insertion of steel stirrups (Klein and Popovic, 1985)

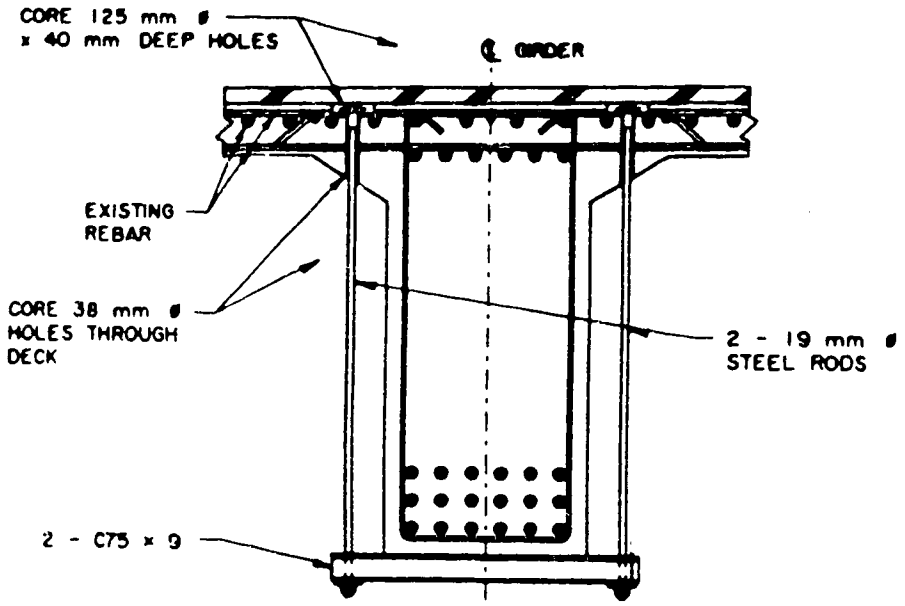

Figure 2.8 Shear strengthening of T-beam bridge using external steel stirrups (Ramsay, 1990)

Figure 2.9 Prestressed concrete T-beam bridge strengthened using external stirrups

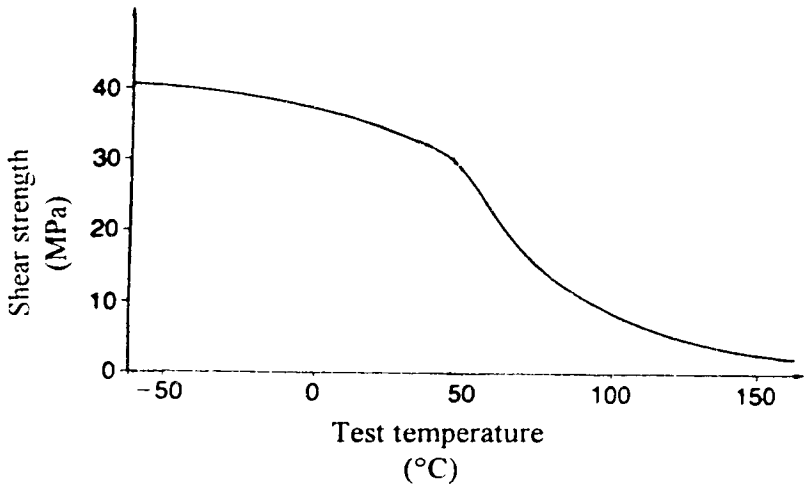

Figure 2.10 Shear strength of cold-cure epoxies as a function of temperature (Mays and Hutchinson, 1992)

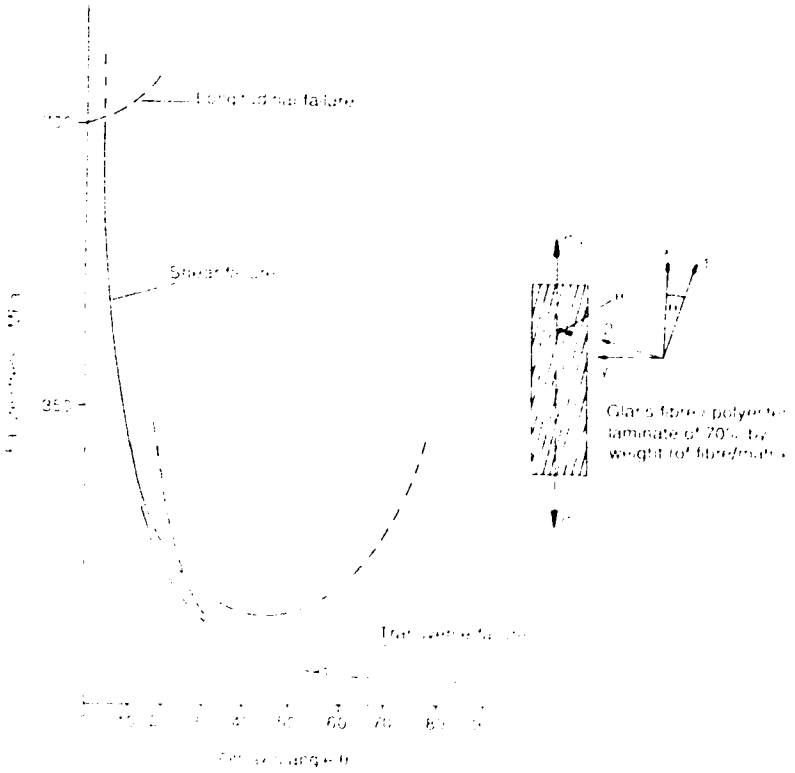

Figure 2.11 Typical failure stress of unidirectional GFRP with respect to axis orientation (Holloway, 1993)

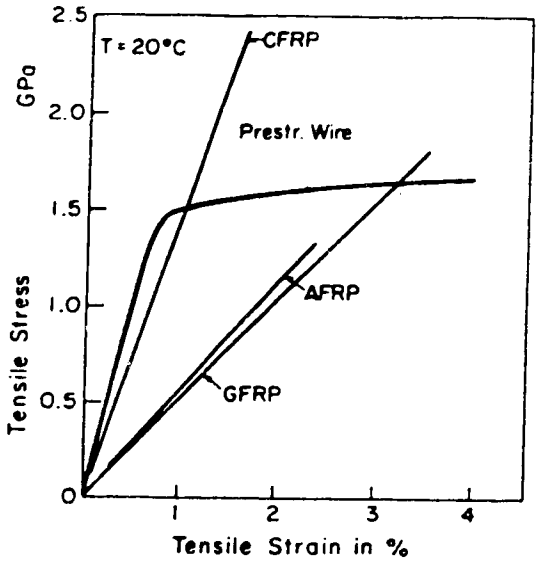

Figure 2.12 Tensile stress-strain curves for various materials (Erki and Rizkalla, 1993)

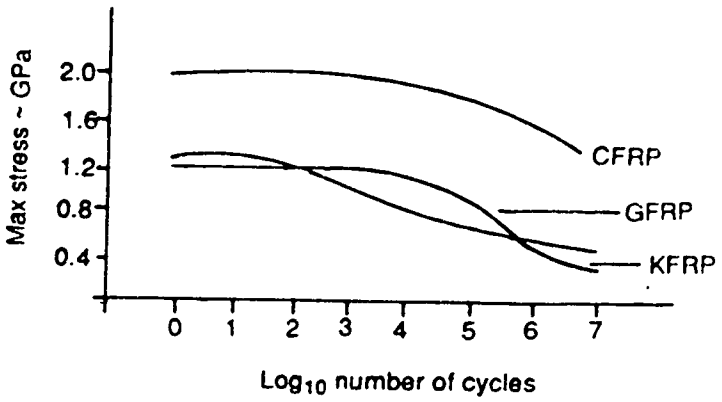

CFRP: carbon fibre reinforced plastics
GFRP: glass fibre reinforced plastics
KFRP: Kevlar (aramid) fibre reinforced plastics

Figure 2.13 Typical S-N curves for unidirectional composites (Holloway, 1993)

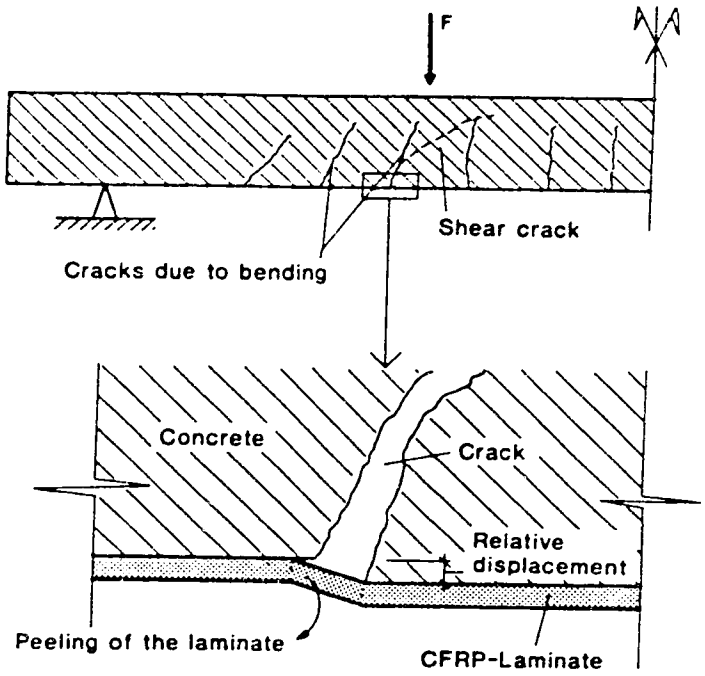

Figure 2.14 Failure of CFRP plated concrete beam by propagation of shear cracks (Meier and Kaiser, 1991)

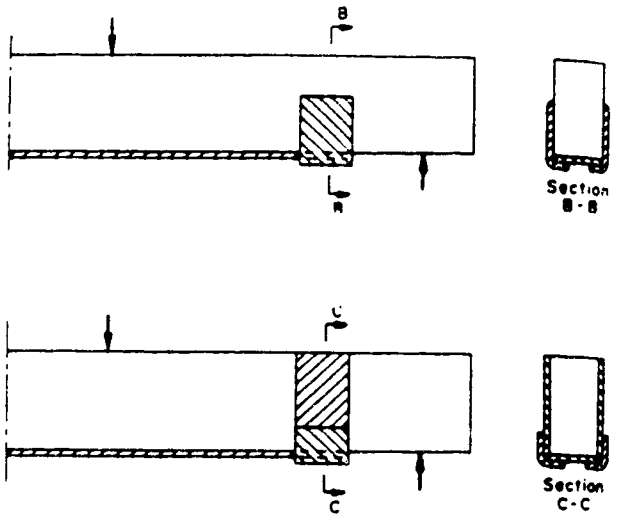

Figure 2. 15 Anchorage of longitudinal plates bonded to bottom flanges of concrete beams using fibreglass angles (Ritchie *et al*, 1993)

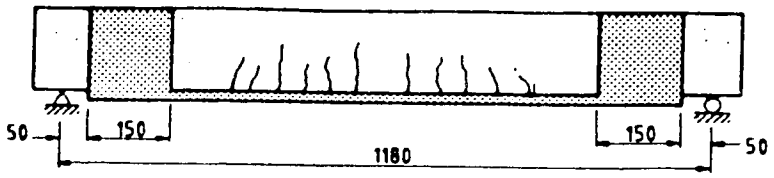

Side View

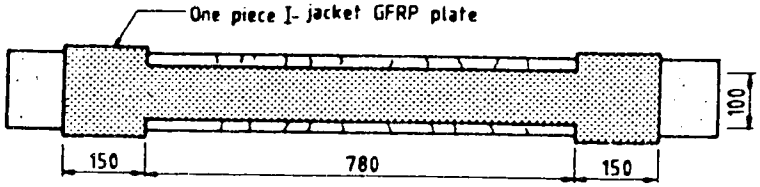

Bottom View

Figure 2.16 Fibreglass jackets used to improve anchorage of plates bonded to tensile flange of concrete beams (Sharif *et al*, 1994)

3.0 Experimental Program

3.1 Introduction

The experimental program consisted of tests of three pre-cast reinforced concrete Type 'E' girders salvaged from a demolished highway bridge in Alberta. They were strengthened for shear externally using CFRP sheets bonded to the webs and loaded to failure. The results were compared to the unstrengthened condition. The objectives were to determine the contribution of the CFRP sheets to the shear strength, if any, and to determine the way in which they altered and/or improved the behaviour of the system as a whole. All girders were tested under symmetrical two-point loading, producing a constant moment region in the centre and two equal shear spans. Each shear span of each girder was strengthened in a different manner; after failing one side, the failure was reinforced and the girder was retested to fail the second shear span. This allowed a total of five shear tests to be carried out.

The girders are referred to simply as Girder 1, Girder 2, Girder 3. The girders were oriented east-west during testing; thus, there are North or South legs, and East or West shear spans. Girder 1 was tested twice: G1-T1 and G1-T2. Girders 2 and 3 were both tested three times and have the additional suffix -T3. This terminology will be used in this and the following sections.

3.2 Description of Test Specimens

All tested girders were removed from the same bridge in September 1993. The plan of the bridge from which the girders were removed is shown in Figure 3.1, with the test girders shown hatched. Girders near the exterior of the bridge were avoided as some of these showed distress, such as corrosion spalls, due to greater exposure. A total of eight girders were salvaged from the bridge and three of those in the best condition were chosen for testing.

All three girders were 9.14 m (30') long Type 'E' girders. The member is 610 mm deep, 914 mm wide, and is hat-shaped in cross-section. Typical cross-section details and elevation are shown in Figures 3.2 and 3.3, respectively. Designed as simply-supported members, the girders have flexural reinforcement consisting of eight #8 (25 mm)

longitudinal bars and transverse reinforcement consisting of #3 (9.5 mm) bars. The design and geometry details, initially obtained from the original drawings provided by the Bridge Branch of Alberta Transportation, were confirmed by measurement of the actual members tested. This included the use of a rebar detector for locating stirrups and longitudinal bars. The cross-sectional dimensions and overall lengths were as described on the drawings, within a reasonable margin of error. There were minor losses of section at the ends of the girders or along the shear key due to the salvaging process or at other odd locations on the bottom flange due to spalling. These anomalies were not extensive and did not interfere with the testing.

A peculiarity of this bridge type is that, over most of the girder's length, the stirrups alternate from leg to leg (single loop stirrups). This means that, although the maximum spacing was specified according to Equation 2.7 (AASHO-57), it is actually twice this distance if considering only one leg. The specified distances between stirrups from original drawings are shown in Figure 3.3. In the elevation, a solid vertical line indicates a single loop stirrup in the near leg while a dashed line indicates a stirrup in the far leg. Double loop stirrups, i.e. a loop in each leg at the same cross-section, occur only near the ends of the girder, outside the tested region.

For testing and analysis purposes, the actual stirrup positions were used, as determined prior to tests with a pachometer. In general, for all three girders, the actual locations differed significantly from the specified locations. Not only was the spacing very irregular, but the gaps were often greater than the maximum specified. The actual stirrup locations are shown in Figures 3.4, 3.5 and 3.6 for Girders 1, 2 and 3, respectively. The stirrup spacings, per leg, varied from 440 mm to 1100 mm. In these figures, each stirrup shown represents a stirrup loop in one leg only.

Although no pre-existing shear cracks were noted on any of the girders, some flexural cracks did exist and these were noted if they occurred within the test region. Due to improper lifting during handling and transporting, several large cracks formed near midspan from the top flange, down (normally a compression zone). Generally, the cracks were not considered significant as they would close during testing, under positive bending conditions. No obvious effect on the results was observed. Occasional bad patches of concrete, e.g. honey-combing, were observed, particularly at the West end of Girder 1.

Although this was noted, it did not appear to affect the test results, nor did the concrete cores removed from near this region appear anomalous.

3.3 Material Properties

After testing the girders, samples of concrete and steel were removed for material testing in order to determine the in situ condition of the members. All samples were removed from outside the tested region, to minimize the presence of cracks in cores, or highly stressed regions in steel reinforcement. Since the girders had already been in service for many years this precaution only helped minimize, not obviate, the probability of damaged samples, although care was taken to avoid problem areas.

Limited material testing was also performed on specially prepared samples of the CFRP sheets.

3.3.1 Concrete

Twelve 75 mm x 150 mm cores were removed from each of the specimens after testing. Three cores were removed from each leg, at each end of the girder, from outside the loaded region. The cores were taken from a level approximately 250 mm from the top of the girder, where the width of the tapered leg ensured a sufficient length of core. The cores were prepared and tested in accordance with ASTM C42-90 (Standard Test Method for Obtaining and Testing Drilled Cores and Sawed Beams of Concrete, 1990), ASTM C617-87 (Standard Practice for Capping Cylindrical Specimens, 1987), CSA-A23.2-9C (Compressive Strength of Cylindrical Concrete Specimens) and CSA-A23.2-13C (Splitting Tensile Strength of Cylindrical Concrete Specimens). Prior to testing, the specimens were soaked in a curing tank in lime saturated water at laboratory temperature (~20° C) for at least 40 hours and were tested immediately upon removal. As the concrete was too weak for grinding, the ends were capped with sulphur mortar. Correction factors for the moist-cured conditions, the length-to-diameter ratio, and for the non-standard diameter were used (Bartlett and MacGregor, 1994). The mean compressive and tensile strengths, along with the corresponding standard deviations, of the concrete cores removed from the three girders are presented in Table 3.1.

3.3.2 Steel Reinforcement

Samples of both longitudinal tensile reinforcing bars and stirrups were removed from the girders and tested in uniaxial tension in accordance with ASTM Standards A615 and A370. The static yield and ultimate stresses were obtained for each specimen, if possible. An extensometer mounted at midheight of the specimen was used for strain measurements in order to obtain a stress-strain curve for calculation of the modulus of elasticity. Each of the eight #8 (25 mm) bars were tested for Girders 1 and 2. As the results were very close, only four bars were tested for Girder 3. Six #3 (9.5 mm) stirrup samples were tested for Girders 1 and 2; four samples for Girder 3. Table 3.2 lists yield and ultimate tensile strengths, and moduli of elasticity for both longitudinal reinforcement and stirrups. Representative stress-strain curves for each are pictured in Figure 3.7. The ductility the curves show was equally clear from observation of the failure surfaces. The only exceptions were for specimens on which stress raisers could clearly be seen; for example, weld notches where rebars and stirrups were connected. It is noted that this type of detail may lead to fatigue problems in the structure.

3.3.3 CFRP Sheets

3.3.3.1 CFRP Material Description

The composite used in this testing program was a carbon fibre-reinforced plastic (CFRP) sheet product, referred to as 'UD (unidirectional) tape', manufactured and supplied by Mitsubishi-Kasei Corporation of Japan. It consists of a single layer of unidirectionally arranged carbon fibres in a pliable sheet form, pre-impregnated with an epoxy resin and partially cured. The sheet is bonded to the concrete substrate using an epoxy resin which also forms the remainder of the matrix. Research has already been carried out using this material in concrete strengthening applications, and has been successful in many aspects (Ballinger *et al*, 1992; Ichimazu *et al*, 1993a, 1993b). The manufacturer's specified material properties are summarized in Table 3.3.

3.3.3.2 CFRP Material Testing

Material testing standards do exist for the uniaxial tension testing of fibre reinforced plastics, such as ASTM D3039-76 (Standard Test Method for Tensile Properties of Fiber-

Resin Composites, 1976). Although the testing procedure is straightforward in theory, the nature of the material used in this program makes it inherently difficult to achieve good results as it is particularly thin and flexible. Generally, there is no problem in obtaining the modulus of elasticity, but the ultimate capacity is extremely difficult to reach and typically failure occurs prematurely at or near the grips long before the ultimate strength can be achieved by breaking of the fibres. One possibility is to bond together more than one layer, allowing for better gripping conditions and perhaps better stability. However, interlaminar shear strength is very low for such composites and premature failure tends to occur interlaminarly.

Although it is important to be able to determine the actual ultimate tensile strength of the sheets, it is likely that the extreme stress levels will not be reached in the applications such as those described in this thesis. As the composite is bonded to a much weaker material, i.e. concrete, failure is expected to occur in the weaker substrate before fibres break in tension. It may be sufficient for design purposes to evaluate the modulus of elasticity and a 'lower bound' to the breaking strength. In addition, the precise laboratory conditions, including special lay-up procedures and autoclave curing, which are used in order to perform a successful tensile test are not very realistic when compared to the actual field application. In the field, lay-up is not as controlled, irregularities may be present (e.g. tiny voids) in the matrix or adhesive, and the material is bonded to a substrate. Perhaps more realistic results would be obtained from samples laid-up in a manner similar to the practical application.

A testing program was designed with two objectives in mind. First, as discussed above, some method to obtain a tensile strength and a modulus of elasticity was required. Even if this fell short of the specified values, the test values could perhaps be considered design minimum values. The second objective was to investigate development length and anchorage requirements. The bond to the concrete was, in general, excellent. However, in order to develop the strength of the sheets, some minimum development length is required. This development, or anchorage, length was used as a variable in this material testing.

Each of the three tests conducted involved two 150 mm x 150 mm x 500 mm concrete blocks with a compressive strength of 31 MPa. Single CFRP sheets were bonded to the two vertical sides of each of the two blocks, thus connecting them, as can

be seen in Figures 3.8 and 3.9. The 235 mm gap between the blocks was necessary for testing purposes. The blocks were pushed apart, placing the sheets into tension, until failure occurred, either by debonding, concrete failure or fibre breakage. The average thickness of one sheet, when cured, was 0.26 mm; each strip was 100 mm wide. A 400 mm length of the sheet was always bonded on one of the two blocks. On the second block, the bonded length was 100 mm, 200 mm, and 300 mm, for Tests 1, 2 and 3, respectively. The concrete surface was prepared and the CFRP sheets were laid-up in the same manner as they were for the girder tests. For the central portion of the sheet, which was not bonded to the substrate, care was taken to properly prepare both sides.

The gap between the blocks allowed placement of a load cell and a 200 kN capacity hydraulic jack which was used to push the blocks apart. One block was fixed to the supporting surface while the other rested on ball-bearing rollers so that it could move freely longitudinally. Relative displacement of the blocks was measured with 12.5 mm LVDT's mounted on the blocks, on both sides of the specimen. In order to obtain a stress-strain curve, 5 mm electrical resistance strain gauges were mounted on the surface of the CFRP sheets. Five gauges were used, two placed on each exterior face of the sheets, near the edges, the fifth placed mid-height on the inside face of one of the sheets (Figure 3.8).

Each specimen was loaded slowly and incrementally to failure in approximately 25 load steps. At each load step, the load was held for one or two minutes. All three tests proceeded similarly, to similar load levels. The stress-strain curves are shown in Figure 3.10. Failure was typically sudden, with no visual warning beforehand. Only in Test 1 were tiny 'puckers' observed in the sheet near the short bonded end, with the edge of the sheet pulling away from the concrete very slightly. These signs appeared early in the test (at about 65% of the failure load) but showed no further change until just before the final load step, when some more 'puckers' appeared (Figure 3.11). There were no visual forewarning signs whatsoever in Test 2 or 3. The only warnings were the crackling noises heard in all tests. The loads at which these noises were first heard are marked on the stress-strain curves in Figure 3.10.

In each case, failure occurred by failure of the sheet. Typically, the fibres appeared to break near the free edge of the block, which acted as a stress raiser as this surface between concrete edge and CFRP sheet was not perfectly smooth. Figures 3.11, 3.12, 3.13 and 3.14 show the condition of the blocks and sheets after failure. In Figure 3.12

(Test 1), the shorter development length may have precipitated failure; the ultimate load was almost 25% lower than in Test 2 or 3. In the second and third tests, the development length did not appear to have influenced the results. As can be seen in the photos, the fibres show clear signs of breakage.

The results of the tests are summarized in Table 3.4, and compared to the specified values. The sheets in these tests failed at barely 25% of the ultimate specified tensile strength. However, the specimens did not fail by tension in the CFRP sheets and thus the failure stress cannot be compared to the breaking strength which is a CFRP material property. Rather, the results reflect the behaviour of the composite CFRP/concrete block system. Even under far from ideal conditions, they still exhibited a strength exceeding many ordinary structural steels. However, as is typical for composites, they showed essentially no ductility.

The average modulus of elasticity was calculated as E= 114.3 GPa, 81% of the specified E=141 GPa. This low value was obtained because the actual thickness of the fully cured sheet, including the additional resin added for bonding, was used in calculating the experimental value. Conversely, material testing by the manufacturer is performed on an uncured coupon so the cross-sectional area used is approximately 25% smaller than the fully cured area. Thus, the composite has only about 60% the stiffness of steel or, over four times the stiffness of ordinary strength concrete. The maximum strains measured in the CFRP at failure were about 5000 με. During the girder tests, strains as high as 5000 με were frequently reached and exceeded, at times as high as 10,000 με, indicating that higher levels of stress can indeed be sustained than was indicated in these small block tests. In the block tests, premature failure at relatively low load levels was instigated by stress raisers at the block edges. If these are not present, and the sheets are well bonded to an even surface, there is no reason why higher stress levels cannot be reached.

3.4 CFRP Strengthening Schemes

3.4.1 "Patterns" Used

There were several restrictions on the arrangement of CFRP sheets which could be used on the girder specimens. When the girders are installed in a bridge, the outer faces of their webs are almost flush against each other, with only a small gap between adjacent legs, as seen in Figure 3.15. In order that the strengthening technique be a practical

solution for use on this type of bridge, the limited access had to be taken into consideration. Therefore, with one exception, the sheets were bonded only to the inside faces and/or to the bottom flanges of the girders.

Although the composite sheet is quite flexible, a minimum 50 mm radius is recommended when bending it around corners. As can be seen in Figure 3.15, the member has corners rather than curves where it is chamfered and this resulted in less than ideal conditions for application of the sheet. Care was taken during application but it was not possible to entirely avoid over-bending the sheets around some corners.

The product manufacturer recommends a maximum of three layers of this particular material to be used, as delamination can be a problem when more plies are used. It was decided to use either one or two layers. When one layer only was used, it was oriented vertically. If a second layer was used, it was oriented horizontally. Although the sheets could be applied in different orientations, only these two mutually perpendicular directions were used. Another possibility would have been to apply layers at ±45°; however, as indicated from earlier tests on similar girders (Appendix A), the angle of the compression strut was expected to be only at about 25 to 30 degrees, due to the low quantity of transverse reinforcement. The horizontal sheets would probably do just as well in carrying a component of the principal stress, and one layer would help carry stress in either direction. The vertical fibres were expected to function primarily analogous to vertical steel stirrups, while the horizontal sheets were expected to contribute more through crack control.

The shape of the girder restricted the height to which the sheets could be extended. If possible, they should be carried up the entire height of the beam, in order to anchor into the compression zone, as is required for internal stirrups. Ideally, the best behaviour would be achieved if they could wrap over the top flange, or even back onto themselves. Under the circumstances, access was available only to 500 mm of the 610 mm depth (Figure 3.15). Although there was therefore little room for adjustment, the bonded length was varied from specimen to specimen.

The sheets were applied continuously throughout the shear span, and are shown as the shaded regions in Figure 3.16; the variations for each girder are summarized in Figure 3.17. Each shear span of each girder was strengthened in a different manner. Both legs

of any particular shear span were strengthened identically. Either one or two layers of CFRP were bonded to the webs. One layer was always oriented vertically. The second, if used, was oriented horizontally. The East shear span of Girder 1 was left unstrengthened in order to serve as a control. In the West span, two layers of CFRP sheets were used, the bottom layer oriented vertically and the top one horizontally. The vertical sheets extended between the top and bottom chamfers, 430 mm in length. The horizontal sheet was centred vertically on the inside face of the web leg, and was the width of the sheet (300 mm). This strengthening arrangement was repeated on the East shear span of Girder 2 as the first girder failed prematurely in flexure before failing the West span in shear. The West shear span of Girder 2 was strengthened with one vertical layer only. In this case, the sheet was extended slightly higher, along the chamfer to meet the underside of the top flange.

In the East span of Girder 3, the two layer scheme of the West span of Girder 2 was again used, with the difference that the vertical sheet was extended, at the bottom, to wrap right around the bottom of the girder and, at the top, 30 mm onto the underside of the top flange. The West span was strengthened with one vertical layer which not only wrapped around the bottom of the girder, but continued up the outer face of the web leg, as high as possible given that the concrete was sometimes chipped away where the grout key had been (about 340 mm height on the outer face). This last method is not practicable as a field application but gave an indication of the improvement possible if the member could be strengthened on both sides of both legs and so could be compared to the less desirable but necessary situation. In addition, the results of this test could be extended to the rehabilitation of more common girder cross-sections, such as I- or T- sections where access is available to both faces of the web. Note, however, that the bonded length was even shorter on the outer face and this may affect results more than the advantage gained.

After the girder failed prematurely in flexure in Test 2 of Girder 1, two measures were taken to avoid this situation in subsequent tests. First, the moment/shear (M/V) ratio was reduced by simply moving the load points towards the supports. Second, three longitudinal layers of CFRP sheets were applied to the bottom flange of Girders 2 and 3. Although it was not part of the objective of this experimental program to investigate flexural strengthening, it is well established that such reinforcing will increase flexural capacity (see Section 2.6). The main concerns in previous investigations have been anchorage lengths and debonding. Typically, high shear stresses in the concrete adjacent

to the FRP initiate failure at the ends of the plates. To avoid this problem, the sheets were extended well beyond the supports (Figure 3.16).

3.4.2 Application of CFRP Sheets

Before the CFRP sheets could be applied, the surface of the concrete had to be prepared. First, any sizeable cracks or voids were filled using an epoxy grout. As a clean, even surface of exposed aggregate is required, the surface was then finished with a disc sand grinder to remove uneven spots and laitance. After cleaning and air drying the surface, a recommended concrete primer was applied in the manner prescribed by the supplier. This consolidated the substrate in preparation for the application of the epoxy resin and the composite sheets. The surface preparation described is not unlike that required to bond steel plates to a concrete member, although it is simplified in that sand blasting is not required nor, in fact, is it even recommended as it produces a surface that is too rough.

A thin layer of the specified epoxy resin was applied to the prepared concrete surface. The pre-impregnated, semi-cured CFRP sheet was placed, then coated with another thin layer of the epoxy resin. The resin was worked through and between the fibres, thus forming both the composite's matrix and the adhesive with which it is bonded to the concrete substrate. The specified curing period is a minimum of seven days at 23°C. No girder was tested prior to this specified time period, taking into account temperature variations.

For convenience, the sheets were applied while the girder was upside down. Figure 3.18 shows Girder 3 in this position to illustrate the layout of CFRP sheets used. However, there is no foreseeable problem with carrying out the procedure described while the girders are in situ in a bridge. For this particular CFRP product, no pressure need be applied during curing beyond the hand pressure used at the time of application. This is unlike the case when steel plates are used, which not only require some means of holding the heavy plates in place, but also require considerable pressure during cure.

No protective finishing of the cured surface is required, although it may be painted for aesthetic purposes. If the surface is exposed where it may be subject to physical damage (e.g. abrasion), it may be protected by covering it with a layer of mortar.

3.5 Testing

3.5.1 Test Set-up

The general test set-up is shown in Figures 3.19, 3.20 and 3.21. All girders were tested in symmetric two-point bending over a 4.8 m simple span with two equal shear spans. The objective was to achieve as high a V/M ratio as possible in order to fail in shear in both shear spans before failing in flexure. The shear span-to-depth ratio (a/d) was thus minimized as much as possible while remaining within the beam behaviour range and avoiding arching action. Preliminary analysis (Appendix A) indicated that a/d=3.6 would be appropriate. This ratio was further decreased for Girders 2 and 3 after Test 2 of Girder 1 ended with a flexural failure. Shear spans were 1900 mm, 1600 mm, and 1600 mm for Girders 1, 2 and 3, respectively.

For two main reasons, the supports were located as far from the ends of the girder as possible while allowing a reasonable test length and without cracking the top concrete. First, they were located beyond all bar cut-off locations in order to avoid the complication of bar termination and anchorage problems, and to have the same moment capacity throughout the tested region. Second, this permitted testing of the length of girder with fewest stirrups, allowing potential for most improvement with the strengthening method. It is acknowledged that this was obviously not realistic given that these girders were designed to be simply supported at the ends, but the primary objective was to test for an increase in shear capacity under the worst case situation.

The girder was supported under each leg independently; that is, there was a total of four supports, each of which was monitored by a Strainsert flat-type load cell. All reactions had rollers and knife edges to allow translation and rotation in the longitudinal direction. In order to have good access to the underside and interior of the girders during testing, the specimens were elevated by resting the supports on stout stub columns which transferred the compressive loads directly to the laboratory strong floor.

The total load was applied by the MTS 6000 testing machine. A 5.2 m distributing beam transferred the load from the MTS compression head to two smaller distributing beams located at the two load points longitudinally along the girder. Rollers between the large and small distributing beams allowed the load points to move longitudinally during

the test. The load was transferred to the small distributing beams via two half spheres so as to create a point load midspan, and allowing free rotation about this point. The small distributing beams rested transversely on the test specimen and transferred the load at each load point (i.e., half the MTS load) to 200 mm square steel plate loading pads centred over each of the two legs. Figures 3.21, 3.22 and 3.23 show cross-sections of the test set-up.

The loading and support arrangements described allowed each leg of the girder to be loaded and supported concentrically and so the girder could be considered two separate beams side by side. Although theoretically identical, each shear span of each leg could have a different number of stirrups, at different spacings, and may also have different stiffnesses depending on variations in material properties. This set-up resulted in two statically determinate systems and, because the four load cells directly measured the force carried by each leg in each shear span, four shear spans could be analyzed. Although this was an artificial arrangement compared to the field condition, it simplified the analysis.

3.5.2 Instrumentation

As these were pre-existing specimens, most of the typical instrumentation for concrete test specimens, such as strain gauging of reinforcement, was not possible. The asymmetrical strengthening arrangement with CFRP sheets on only one face of each web leg meant that the behaviour was not necessarily symmetrical on both sides of the legs. As well, the behaviour of the CFRP sheets loaded in this manner was unknown. For these reasons, extensive instrumentation was used on the surface of the specimens.

Figure 3.24 shows the typical layout of the strain measurements on the web surface. Strains on the concrete surface on the outer faces of the girder were measured using a 200 mm Demec gauge. The Demec targets at each location were arranged to form a three-arm 45° strain rosette. In order to obtain similar readings on the inside face of the web, two of these rosettes were echoed on the inside using 2.5 mm LVDT's mounted on a specially constructed frame as seen in Figures 3.24 and 3.25. These measurements could be compared to the strains obtained from Demec readings on the outer surfaces. Electrical resistance strain gauges with a 5 mm gauge length were used to form 45° strain rosettes on the CFRP sheets. These rosettes were used extensively in order to obtain a distribution of strains over the strengthened shear span.

Figure 3.24 also shows the instrumentation used along one shear span; the same was used on the other leg of the girder. Vertical deflections were measured with 25 mm linear variable differential transformers (LVDT's) located under both legs, at each of the load points and at midspan. Longitudinal strains were measured using 200 mm Demec gauges at five locations vertically at midspan, on both outer faces, in order to obtain the longitudinal strain distribution through the depth of the beam. When CFRP sheets were used on the tension flange (Girders 2 and 3), strain gauges were mounted longitudinally on the sheet, in the centre of each leg, at both load points and at midspan. In both shear spans, 2.5 mm LVDT's mounted between the top and bottom flanges at stirrup locations measured overall depth change of the girder as an indirect measure of strain in the stirrups. These measurements, along with the visual aid of crack patterns, helped indicate if or when the stirrups were yielding. Lastly, four cable transducers spanning from loads and supports to fixed reference points beyond the ends of the girder, were used to measure any shear span changes. This movement was not expected to be significant because the girder was very stiff, especially with the supports much closer together than designed for.

3.5.3 Test Procedure

The girder was initially supported at its extremities on beam brackets connected to columns. During the test, these columns also acted as bracing in the event that the girder should fail catastrophically and kick out longitudinally. The girder was lowered onto the test supports by jacking, and plastered in place. The small distributing beams were plastered in place on top of the girder at the load points after which the large distributing beam was lowered into place. Great care was taken to ensure the girder was centred longitudinally and transversely and that load and reaction points were accurately located.

Before commencing the test, the dead load of the specimen was determined using the four load cells and all subsequent measurements did not include the effect of the dead load. The tests were stroke controlled and approximately 30 load steps were taken to failure, each test lasting about six and a half hours. Each increment corresponded to approximately 100 kN (MTS load) until the advanced stages (as indicated by cracking and strains and by the MTS load vs. stroke plots), at which time the increments were reduced to about 20 kN until failure occurred. Each load step was held 10 to 15 minutes allowing re-distribution of stresses and relaxation. At the beginning and end of each load step, data other than the Demec gauge readings were recorded by the data acquisition system.

During the waiting period, Demec readings could be taken, cracking patterns marked, and the interior of the girder inspected for any sign of disturbance in the CFRP sheets.

Each girder was tested at least twice. Each test was terminated when it was clear that no additional load could be carried. After the first test ended with failure of the first shear span, the specimen was unloaded completely. Some means of repairing the failed span was required and this was achieved by using external stirrups consisting of four 25 mm diameter threaded tie rods at each of six locations along the shear span. Holes were drilled through the top flange between the web legs, and rods were installed on either side of each web leg; part of the process is shown in the photograph of Figure 3.26. The tie rods were braced with 75 mm x 100 mm HSS members above and below the girder. Rods were torqued until snug, and pretensioning was not required. This repair technique can be seen completed in Figure 3.27. The second test was then begun and continued until the second shear span failed, which was then repaired similarly. The third test attempted to determine the flexural capacity of the girder in the constant moment region. Note that Girder 1 was only tested twice as G1-T2 ended with a flexural failure.

Table 3.1 Concrete core results

Specimen	Number of Samples	f'_c (MPa)	σ (MPa)	f_t (MPa)	σ (MPa)
Girder 1	12	27.1	1.7	n/a	n/a
Girder 2	12	27.7	2.2	n/a	n/a
Girder 3	12	28.5	2.5	2.58	0.36

σ: standard deviation

Table 3.2 Steel coupon results

Specimen	Number of Samples	f_y (MPa)	σ (MPa)	f_u (MPa)	σ (MPa)	E (GPa)	σ (GPa)
Longitudinal reinforcement (#8 bar, 25mm)							
Girder 1	7	338.5	6.72	532.7	16.65	208.5	5.57
Girder 2	8	337.8	10.54	536.7	16.87	212.7	6.28
Girder 3	4	345.9	3.74	547.2	7.55	219.3	3.31
Stirrups (#3 bar, 9.5 mm)							
Girder 1	5	378.5	3.56	545.9	6.61	213.3	7.70
Girder 2	6	377.3	7.08	549.8	8.89	210.9	6.70
Girder 3	4	389.9	6.71	554.9	5.45	220.1	2.15

σ: standard deviation

Table 3.3 Manufacturer's specified material properties for CFRP pre-preg

Material	Tensile strength (MPa)	Tensile modulus (GPa)	Volume fraction* (%)	Thickness (mm)
CFRP prepreg	2350	141	60	0.17
Carbon fibre	3920	235	n/a	n/a

* carbon fibre percentage in prepreg, by volume

Table 3.4 Test results of CFRP bonded blocks

Specimen	F_u (MPa)	$\frac{F_u}{F_u(spec)}$	E (MPa)	$\frac{E}{E(spec)}$	$\frac{E}{E_s}$	$\frac{E}{E_c}$
1	500.0	0.21	110.1	0.78	0.55	4.00
2	645.3	0.27	120.4	0.85	0.60	4.40
3	603.9	0.26	113.0	0.80	0.57	4.10

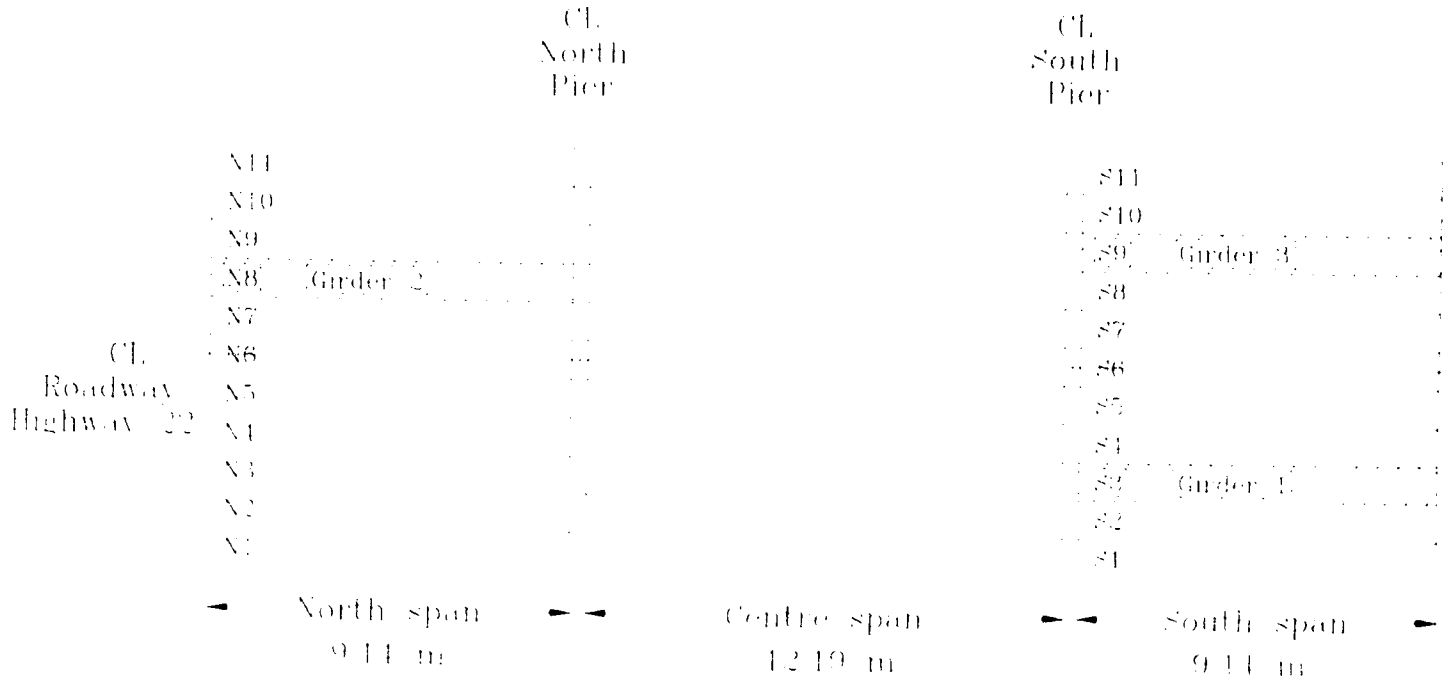

Figure 3.1 Schematic plan of Dogpound Creek Bridge indicating girders used in the testing program

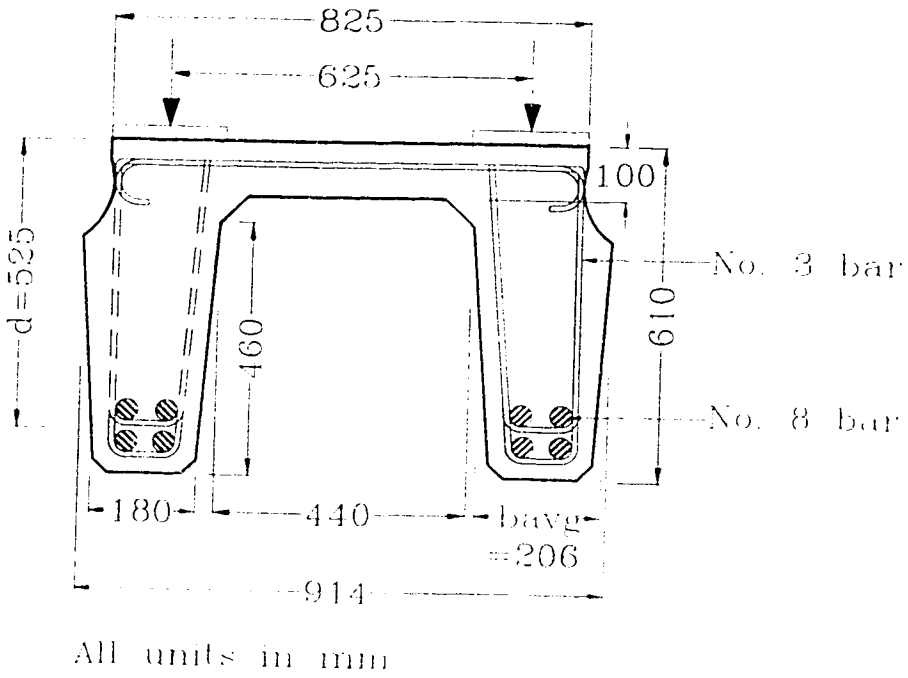

Figure 3.2 Cross-section details of Type 'E' girder

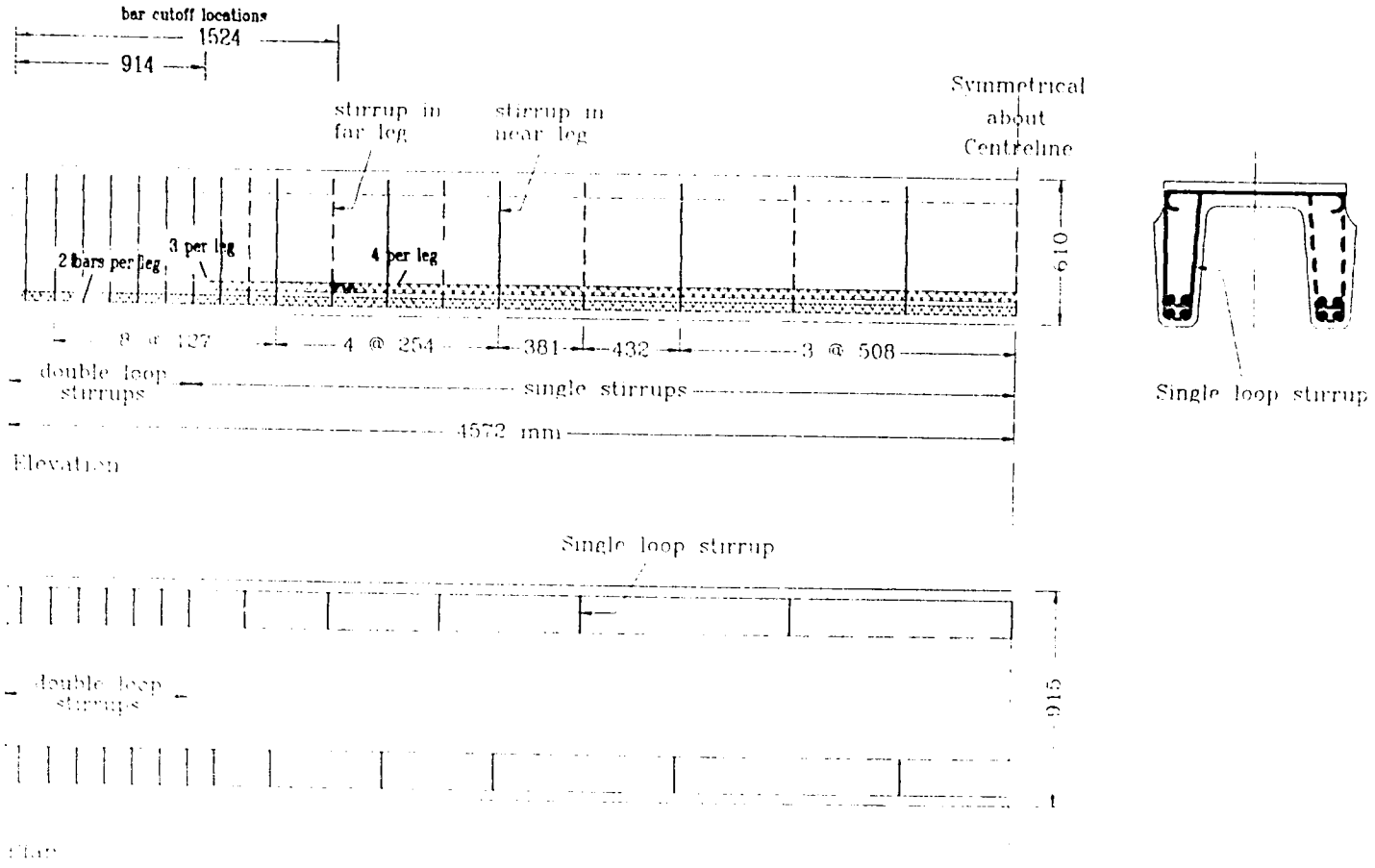

Figure 3.3 Longitudinal details of Type 'E' girder (Designed)

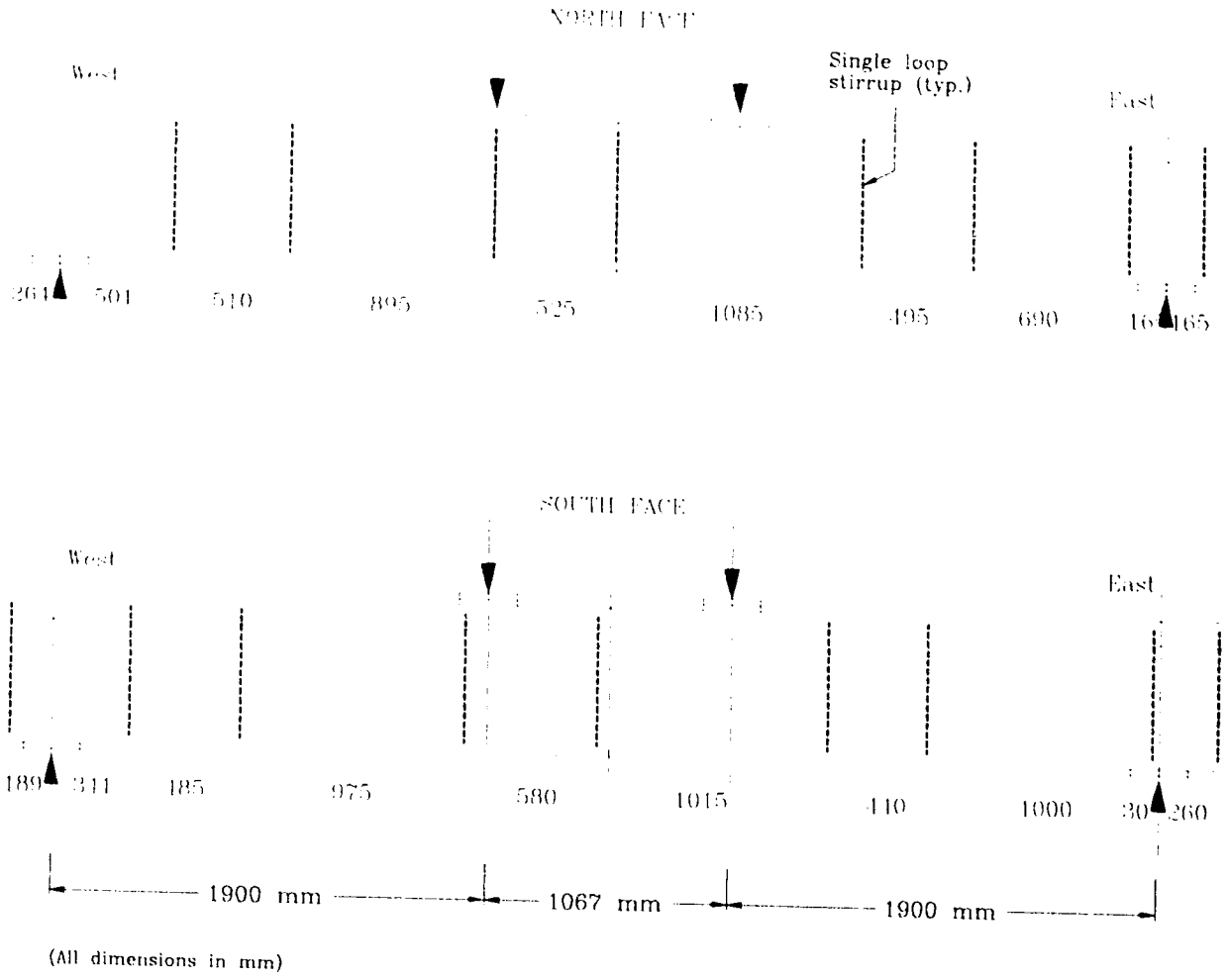

Figure 3.4 Girder 1 - Test set-up and stirrup locations

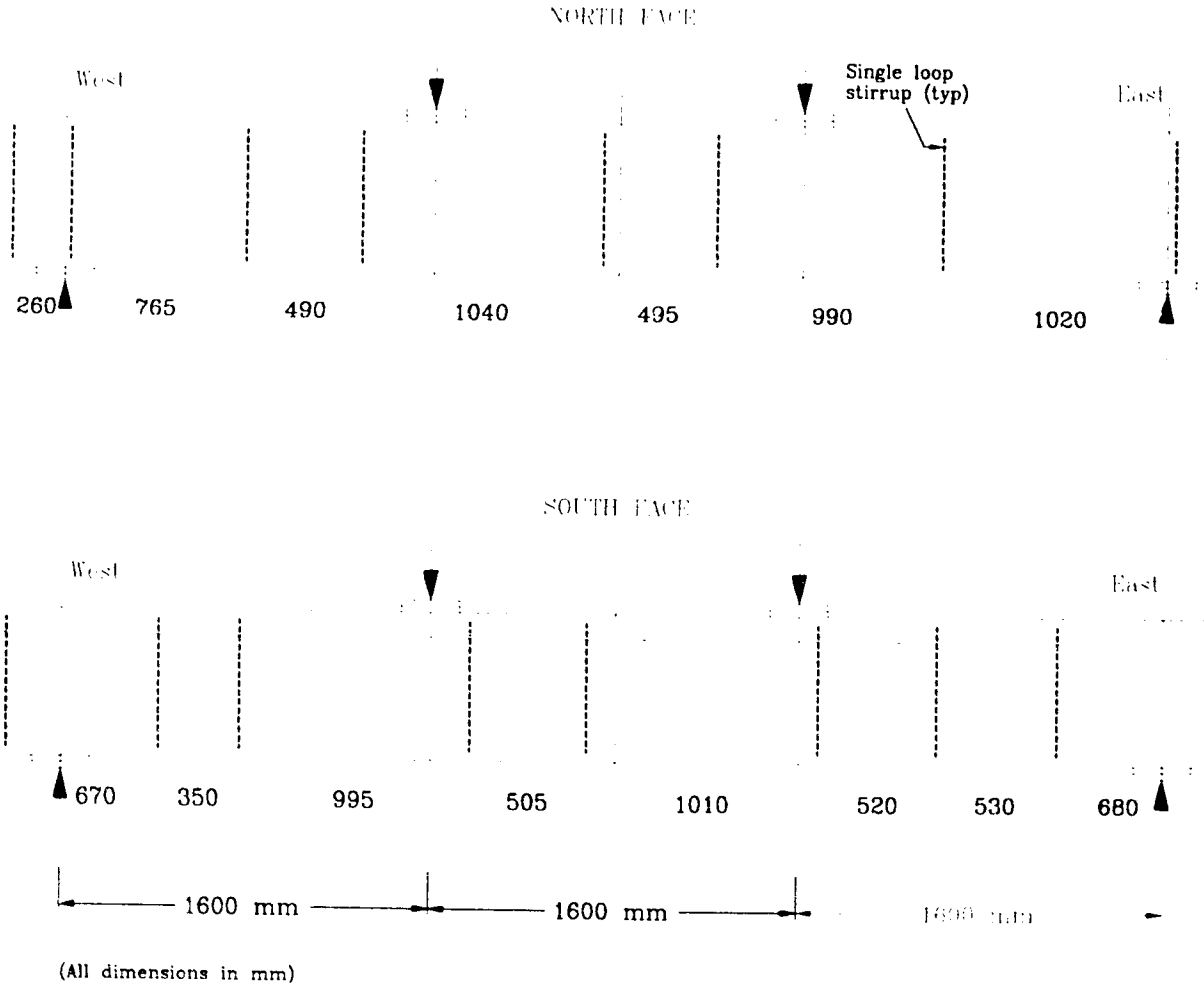

(All dimensions in mm)

Figure 3.5 Girder 2 - Test set-up and stirrup locations

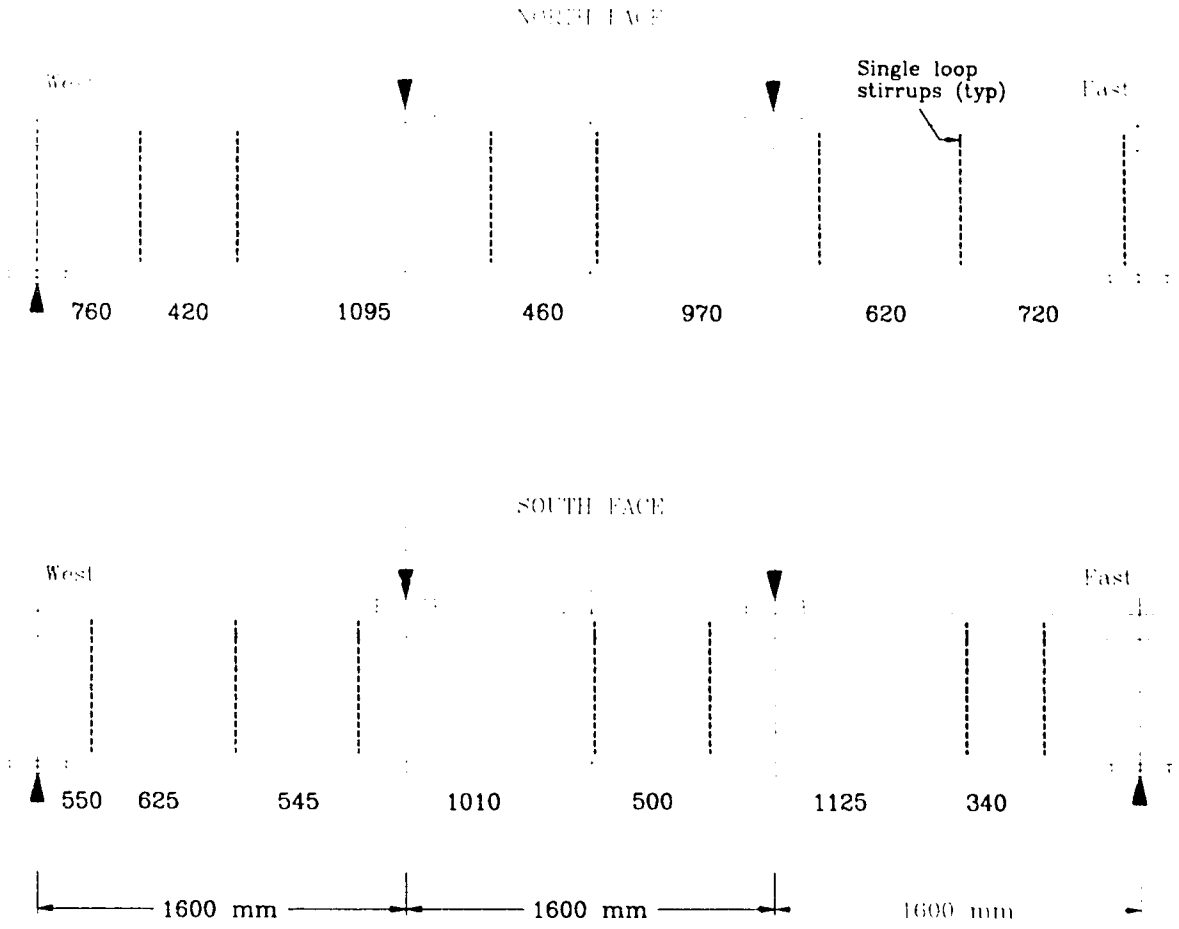

Figure 3.6 Girder 3 - Test set-up and stirrup locations

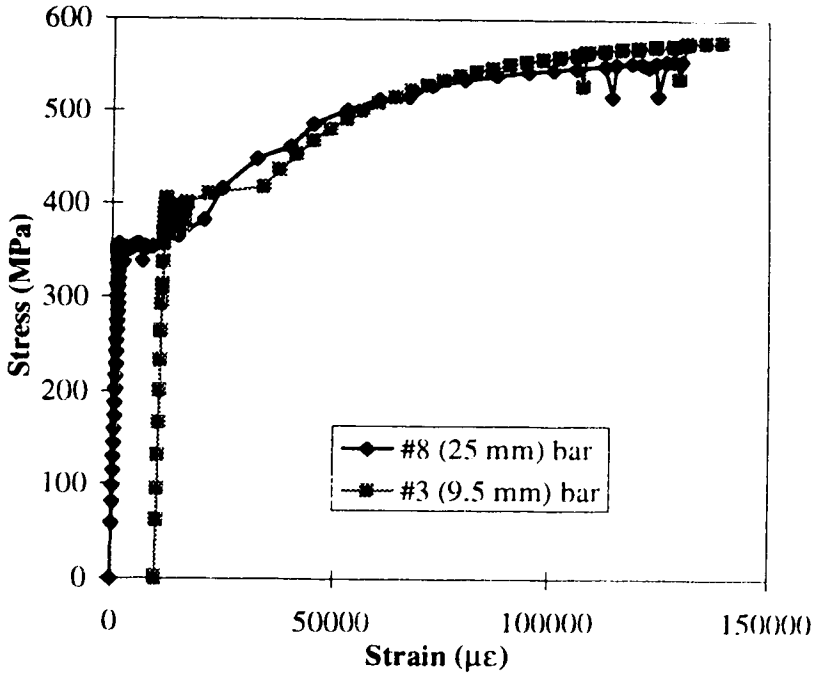

Figure 3.7 Representative steel reinforcement stress-strain curves

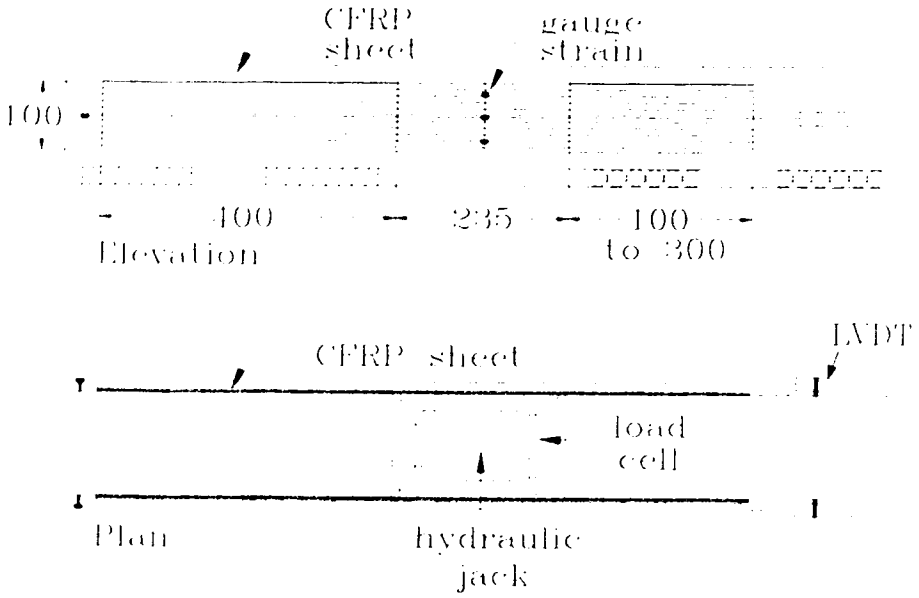

Figure 3.8 Schematic of test set-up for small concrete block tests

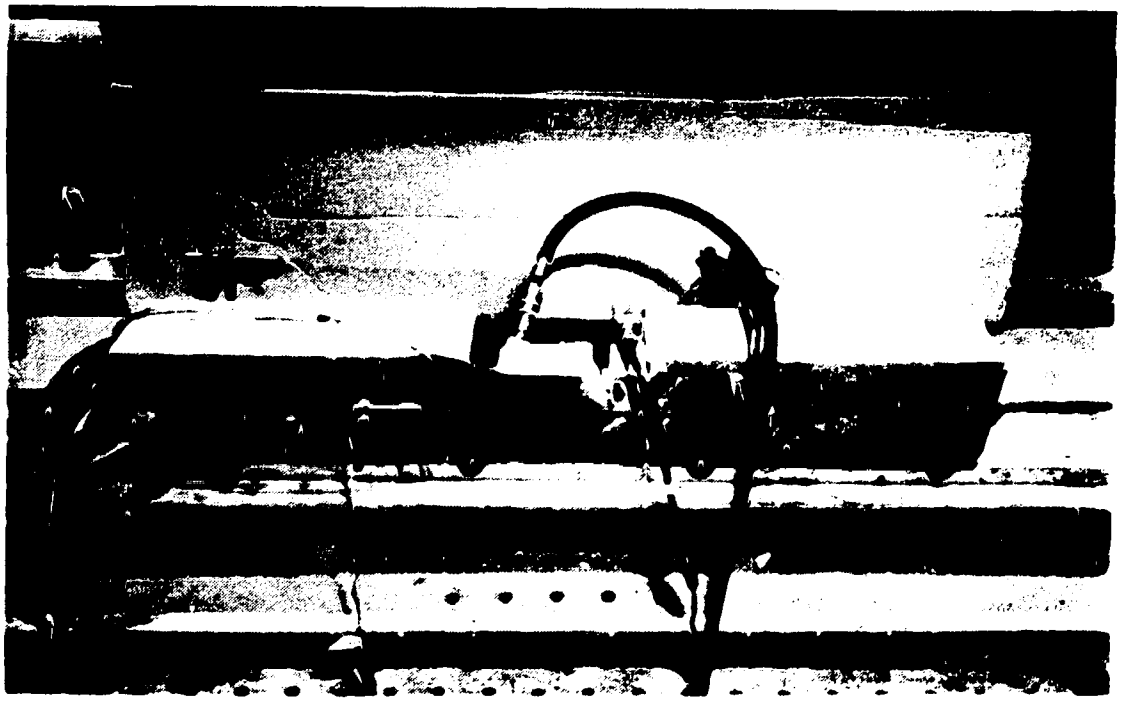

Figure 3.9 Test set-up for small concrete blocks bonded with CFRP sheets

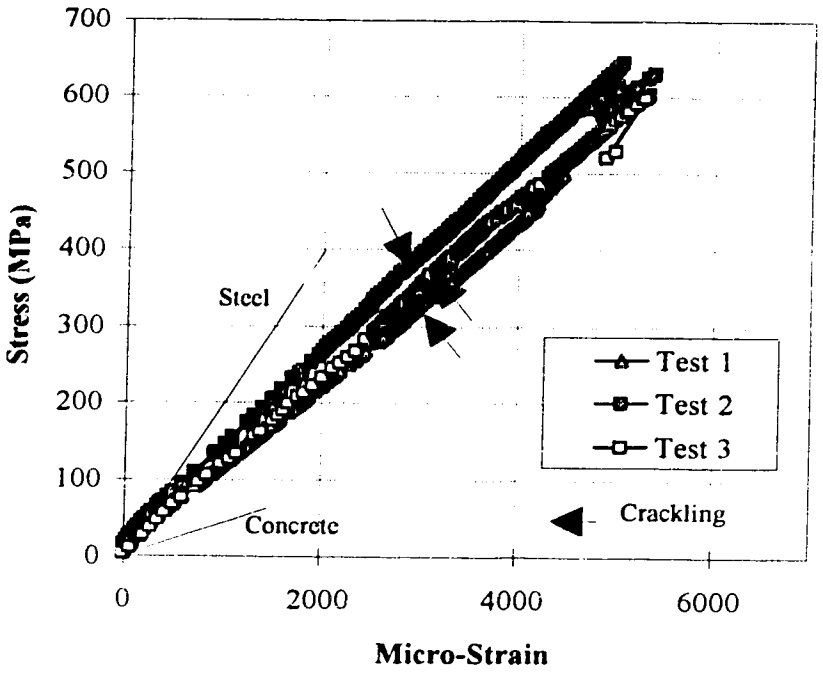

Figure 3.10 CFRP/Concrete block tests - Stress vs. strain curves

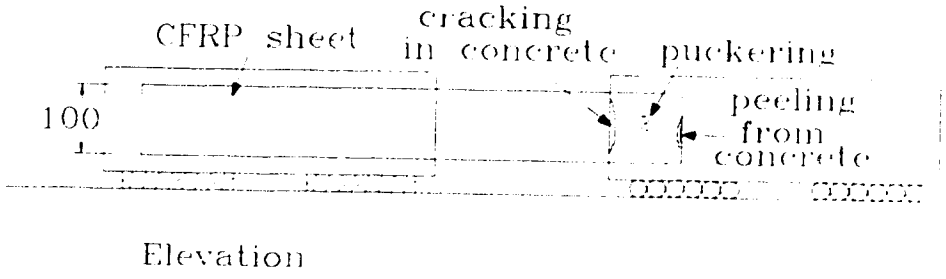

Figure 3.11 Signs of failure in small concrete block tests

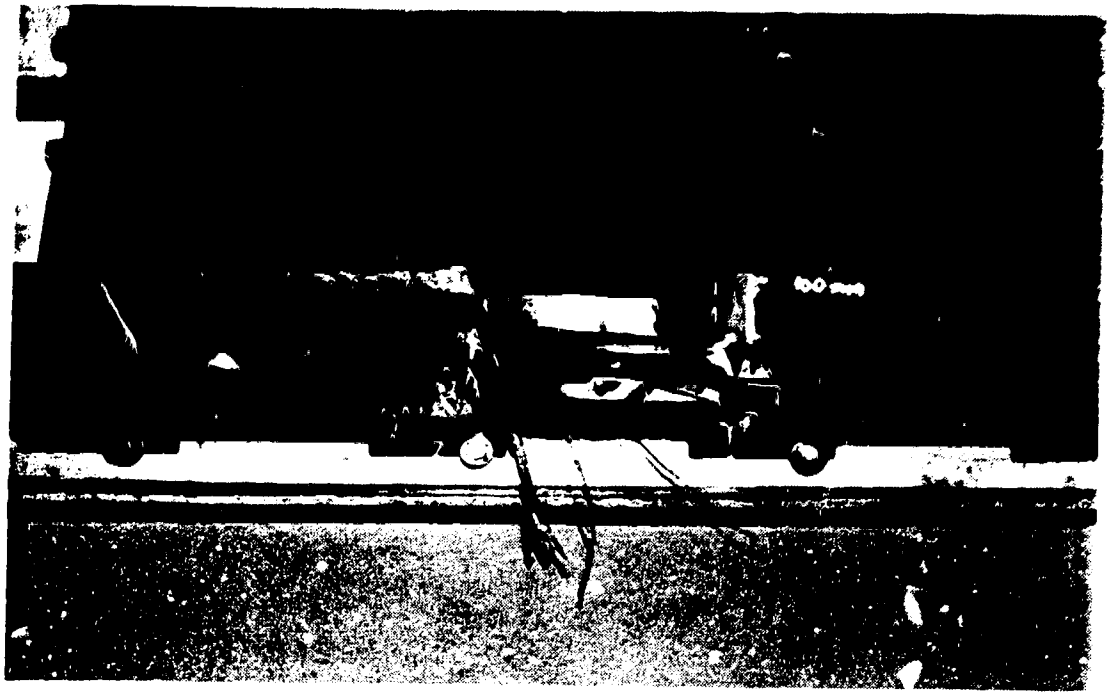

Figure 3.12 Block #1 after failure of CFRP sheets

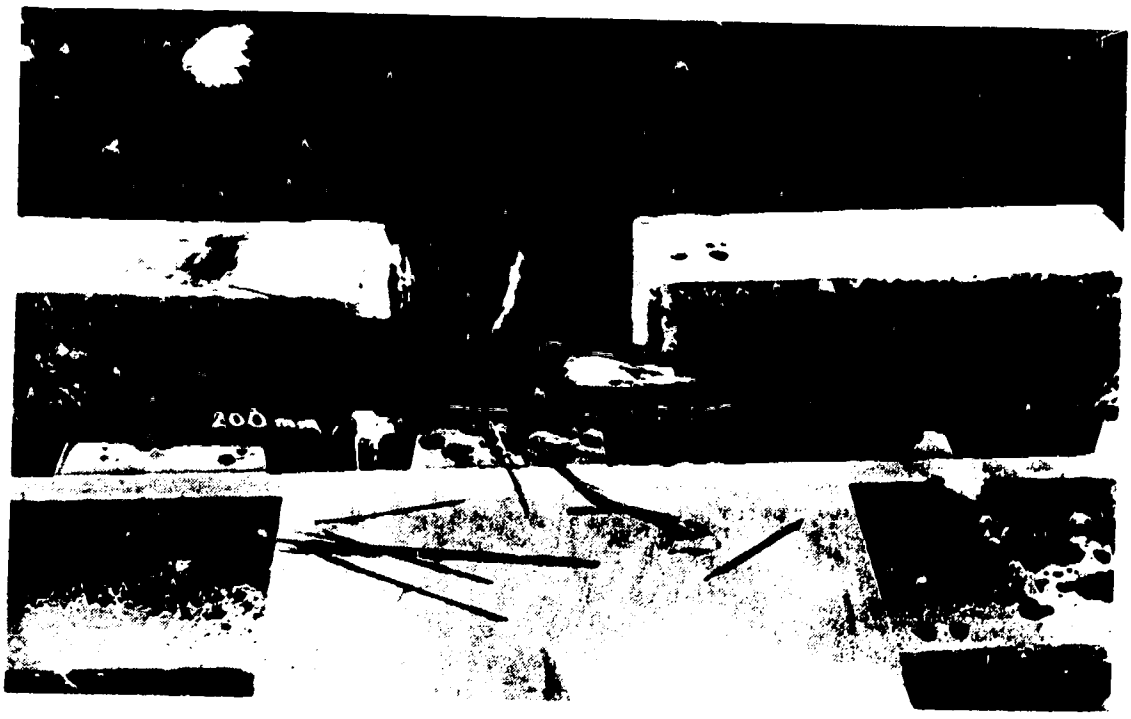

Figure 3.13 Block #2 after failure of CFRP sheets

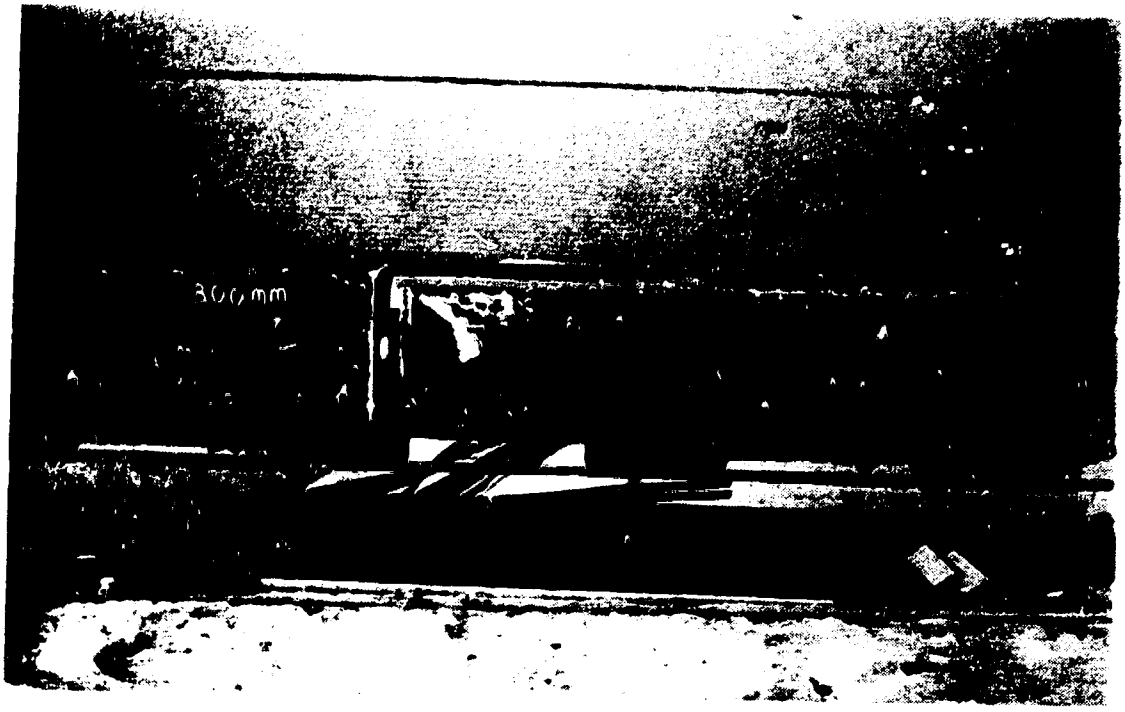

Figure 3.14 Block #3 after failure of CFRP sheets

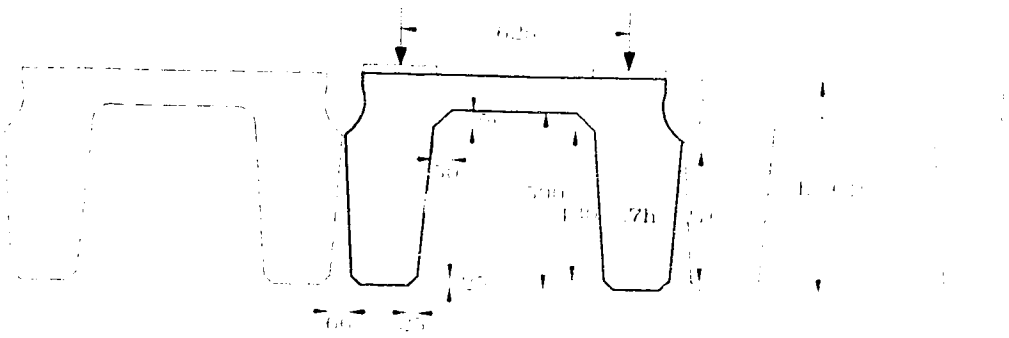

(All dimensions in mm)

Figure 3.15 Typical cross-section of Type 'E' girder indicating clearances

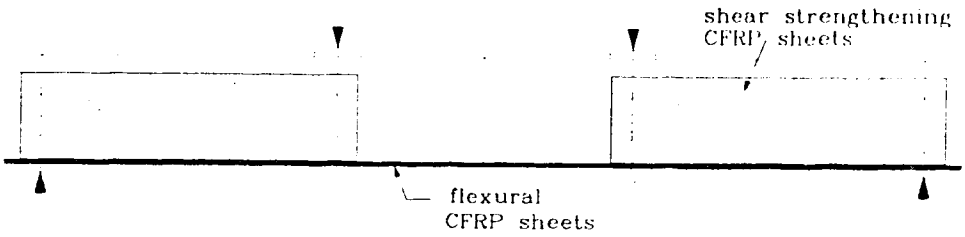

Figure 3.16 Typical extent of CFRP sheets through test span

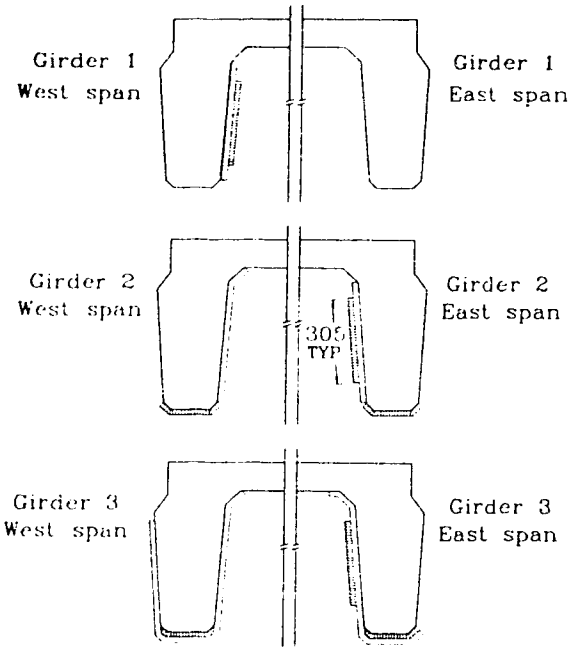

Longitudinal CFRP sheets
Vertical CFRP sheets

CFRP shear reinforcement - single sheets

CFRP flexural reinforcement - three sheets

Section	Length of vertical sheet (mm)
G1 - East span	0
G1 - West span	430
G2 - East span	430
G2 - West span	504
G3 - East span	700
G3 - West span	1070

Figure 3.17 Layouts of CFRP sheets on the three test girders

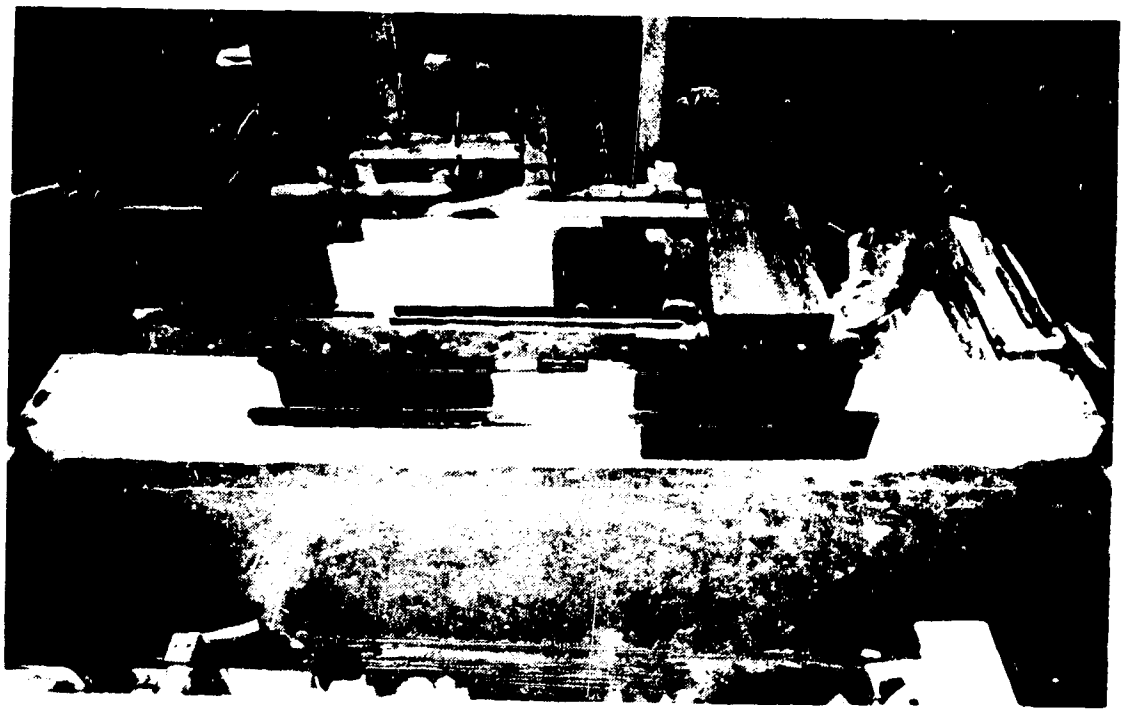

Figure 3.18 Inverted girder showing CFRP sheet layout immediately after application

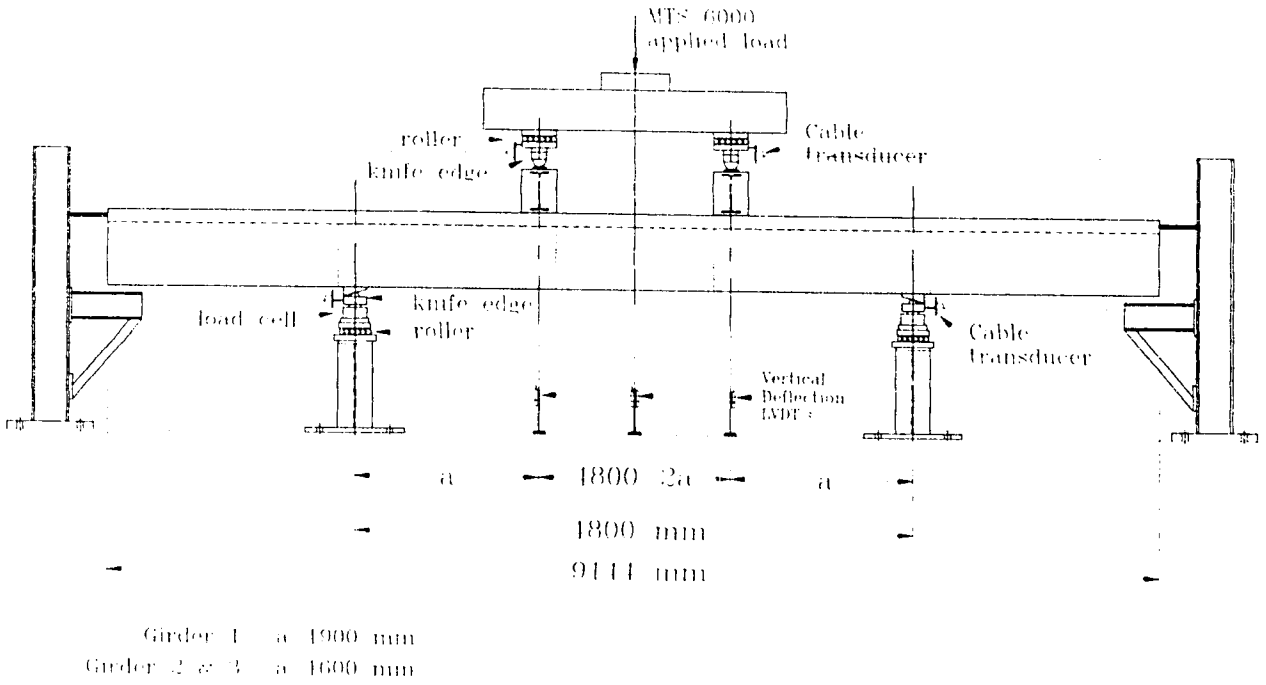

Figure 3.19 Schematic elevation of test set-up for girder tests

Figure 3.20 Overview of test set-up

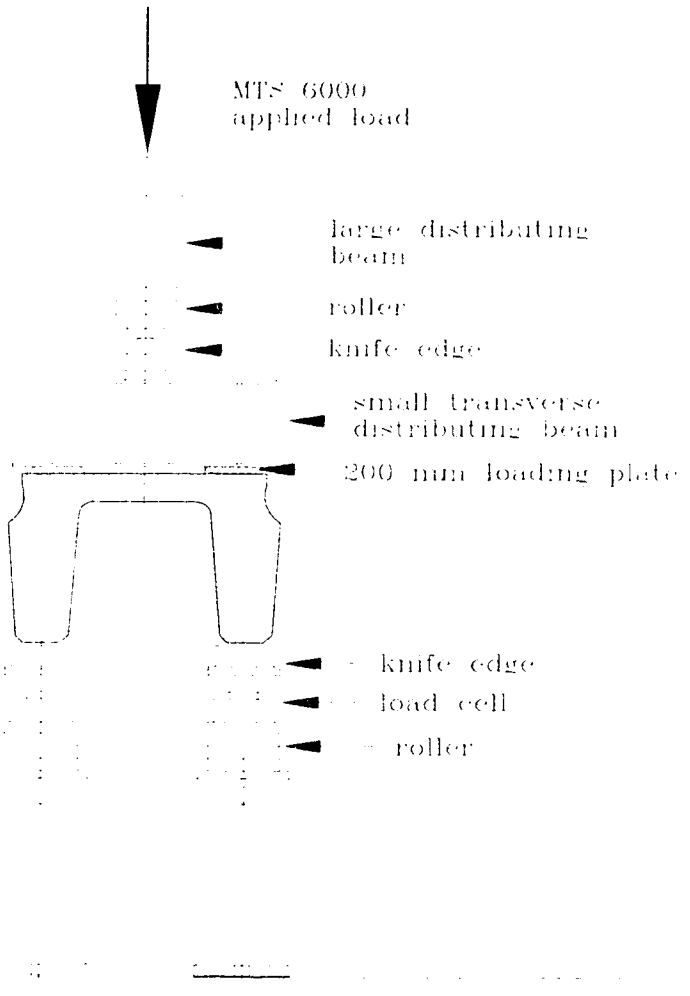

Figure 3.21 Schematic cross-section of test set-up

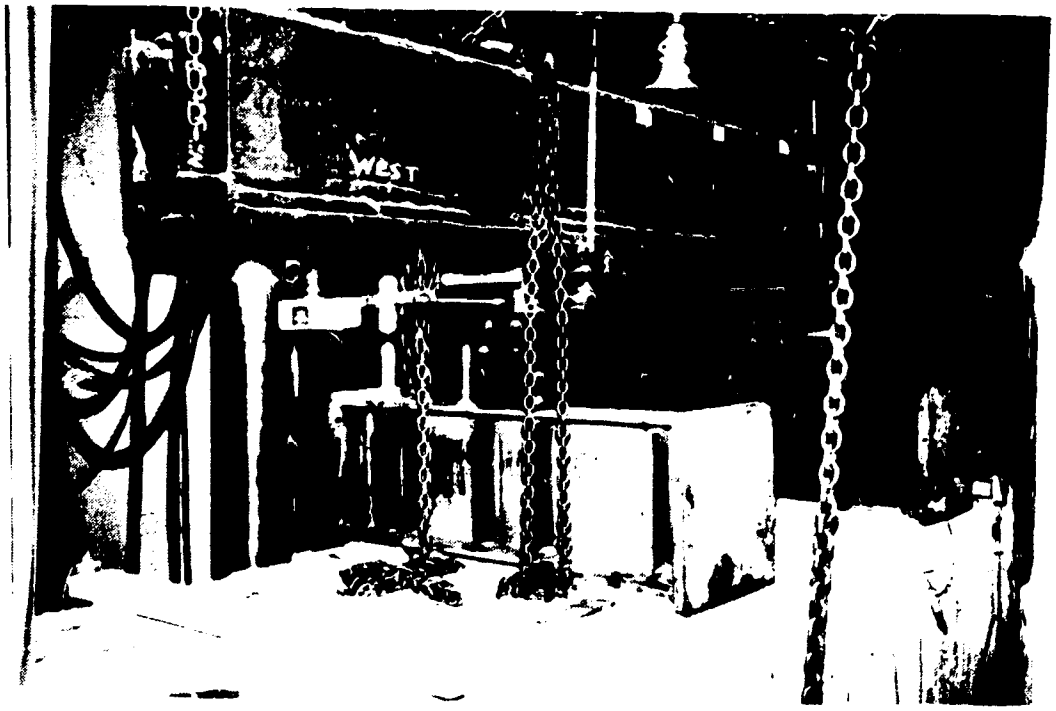

Figure 3.22 View of test set-up - Load applied and top of girder

Figure 3.23 View of test set-up - Supports and interior of girder

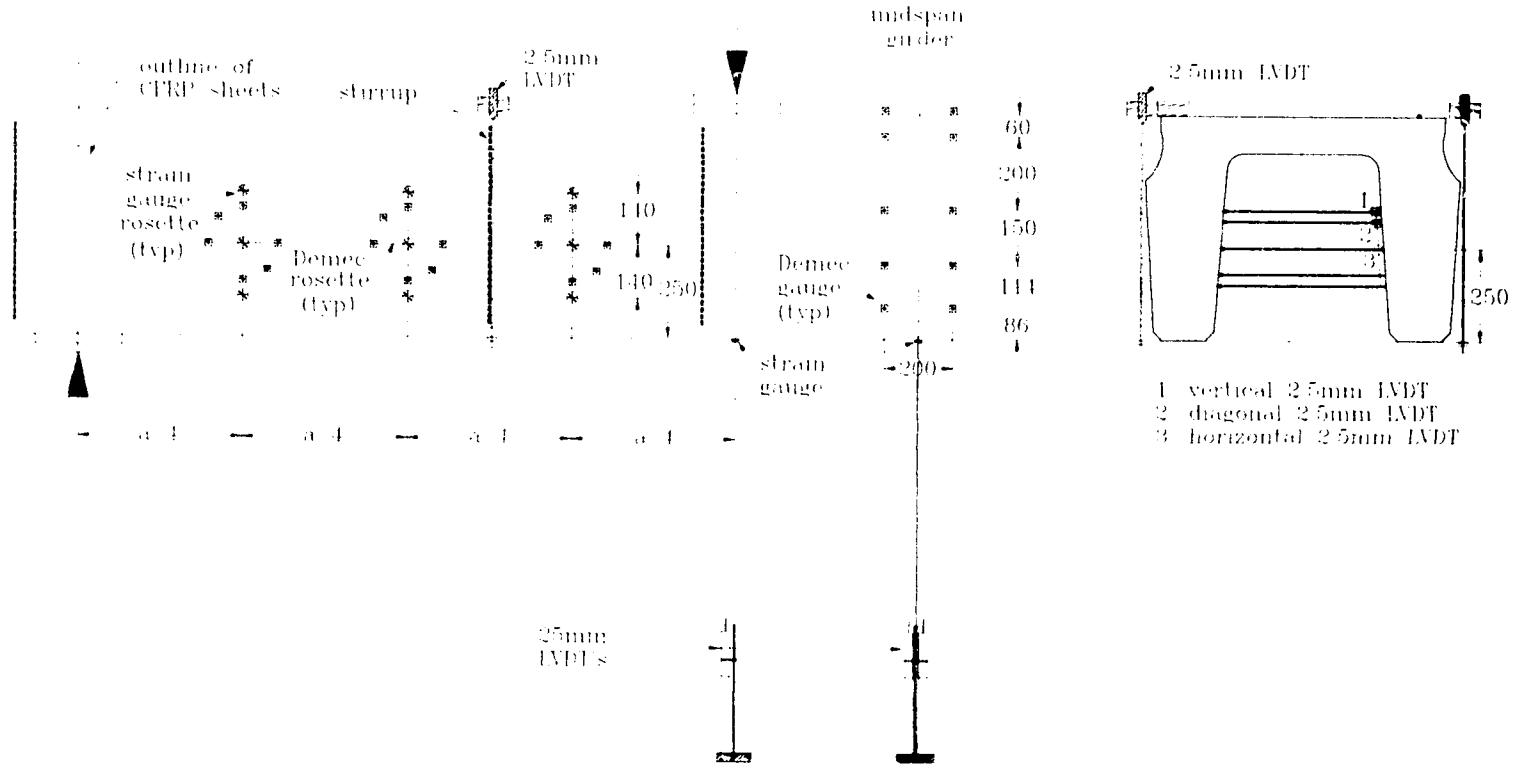

Figure 3.24 Layout of instrumentation

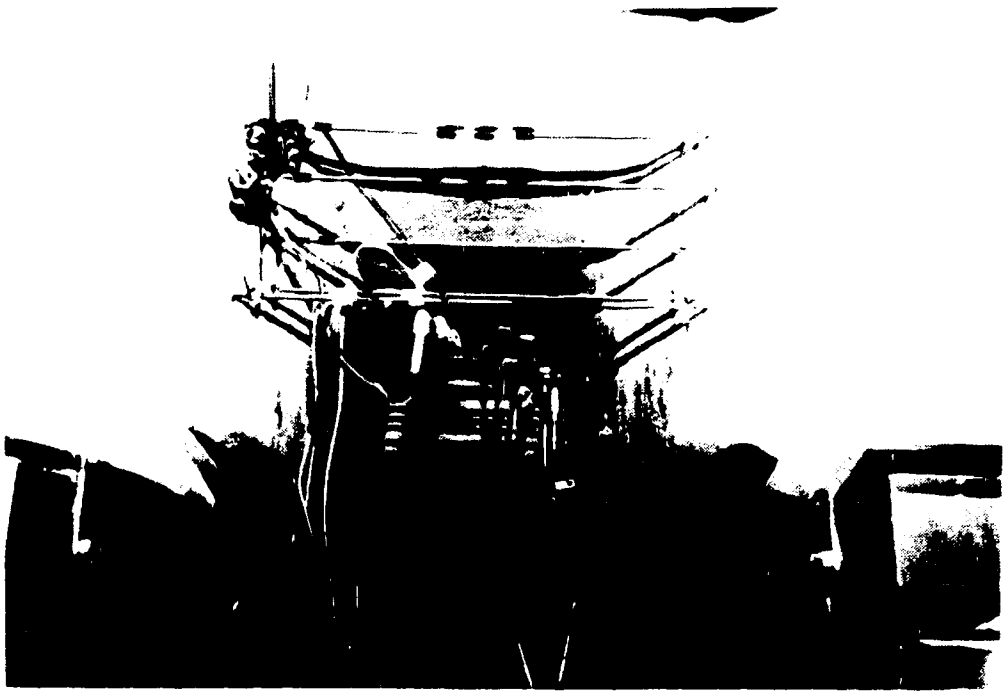

Figure 3.25 LVDT rosette arrangement on interior faces of web legs

Figure 3.26 Installation of external repair stirrups

Figure 3.27 Installed external repair stirrups

4.0 Test Results and Observations

4.1 Introduction and Overview

The experimental results of the testing program are presented in this chapter. Section 4.2 reports on the general behaviour of the three specimens with respect to the load-deformation relationships, including ultimate strength, stiffness and ductility. The progression of failure of the specimen during each test is presented for each girder in turn in Section 4.3. In the following discussions, loads referred to are the total MTS loads applied, unless otherwise noted.

4.2 Load Deformation Relationships

Load vs. deflection curves, shown in Figures 4.1, 4.2, 4.3 for Girders 1, 2 and 3 respectively, give a good idea of the general behaviour of the girders. During the shear tests, the load was increased until no additional load could be carried. They were generally not pushed further because it was not known how much damage could be easily and successfully repaired using the external tie rod stirrups. It was possible that the ultimate shear failure may be sudden and 'catastrophic', opening up the cracked section too much to be easily repaired. Therefore, the full load-deflection curve was not obtained for all the tests nor could the post-peak behaviour always be observed.

The curves are used as a reference to discuss three general aspects of the girders' behaviour and the effect of the CFRP sheets. First, the test results and general failure modes of the girders are briefly summarized. Then stiffness, which is one important characteristic of system behaviour, and ductility will be discussed.

4.2.1 Strength

All the girders failed in shear in both shear spans, by diagonal tension failure, except in Test 2 of Girder 1 (G1-T2) when shear failure in the second shear span was preceded by flexural failure in the constant moment region. A summary of the failure loads for each test of each girder is provided in Table 4.1 along with the corresponding shear and moment p[illegible]nt. After the shear failure of G1-T1, the test was stopped when the load began to drop off and so no post-peak behaviour was obtained. G1-T2 failed in a ductile

flexural mode. The test was terminated after a long plateau and not continued to complete failure. G2-T1 was also stopped once the load began to drop off with almost no post-peak behaviour being observed. Near the end there was a substantial drop of load and it is believed that the peak load would not have been recoverable. G2-T2 showed somewhat more ductile behaviour. G2-T3 failed in flexure suddenly and prematurely by failure of the CFRP sheets at a stress concentration. G3-T1 was stopped after several load steps of post-peak declining load. G3-T2 failed catastrophically in shear with almost no post-peak response. G3-T3 failed in the same manner as G2-T3, at almost the same load. In both shear failures of Girder 3, crushing of the concrete could be clearly observed both in the reduced compression zone in the top flange and in the diagonal compression strut.

Using Alberta Transportation CS rating trucks (Figure 2.5), the maximum shear and moment which a girder would experience at service loads were calculated. The calculation took into account the change in span lengths and followed S6-88 rules for load distribution and serviceability state. The maximum service load level corresponds to a total (MTS) load of 218 kN. This load level, $P_{service}$, is indicated on the load-deflection curves and is always well within the linear range for all tests.

Ideally, a properly detailed beam should fail in flexure before failing in shear to ensure ductile behaviour. One thing to note, if the shear span did fail in shear, was how close the girder was to flexural failure . The ultimate moment capacity of the unstrengthened girder is given by the results of G1-T2. Although stirrups and therefore shear strength varied from specimen to specimen, the results of G1T1 are still a good estimate of the in situ shear strength. Based on girders examined, the stirrup distribution of Girder 1 was fairly representative for regions of sparse stirrups (i.e., not within 1.5 m of the ends) which makes it a good estimate of the shear strength of the Type 'E' girder, especially since the stirrups vary so much that it is not reasonable to analyze every girder in every bridge based on actual spacings. More detailed analysis taking into account the specific stirrup details of each test shear span will be presented later in Sections 5.3 and 5.4, in order to determine the real contribution of the CFRP sheets to shear resistance.

Table 4.1 shows the ratios of V_{max} for each test to V_{max} for the unstrengthened (G1-T1) case. Although a close look is required to separate the shear contributions of concrete, steel and fibre sheets, the results shown here are a good indicator of the shear capacity increase demonstrated. Note that G3-T2 may actually have had a slightly higher

shear failure load but the test was stopped before a decline in load was observed in order to repair it for the third test (G3-T3). It is not expected that the ultimate peak load would have been significantly higher. Increases in shear capacities ranged between 18% and 64%.

In order to determine how close to flexural failure the girders were when they failed in shear, the ratios of the moment corresponding to the shear at failure to the moment capacity of the in situ girder (G1-T2) were compared. For example, in G1-T1, the girder failed in shear; the corresponding moment at failure was 574.5 kNm, 85% of the flexural capacity (676.4 kNm) of the member. This information is also included in Table 4.1. Except for G2-T1, the shear strengthening upgraded the girders enough that failure of the girder was limited by its flexural capacity. This is not immediately obvious because the flexural capacity of Girders 2 and 3 was increased by the addition of CFRP sheets on the bottom flange. In Figures 4.2 and 4.3, a horizontal line shows the peak load that would have been reached if Girders 2 and 3 had not been strengthened for flexure. Therefore, one goal of the research program was achieved -- shear failure prior to ductile flexural failure was prevented.

While G1-T2 and G2-T1 reached the same shear, V=356.0 kN, G1-T2 failed in flexure while G2-T1 failed in shear. By increasing the flexural capacity using longitudinal CFRP sheets, shear and flexural behaviours could be isolated. There is no real difference between G1-T2 and G2-T1 if the effect of the longitudinal CFRP sheets is excluded.

4.2.2 Stiffness

No increase in the stiffness of the member was observed for any of the strengthened girders. This applies whether the girder was strengthened for both flexure and shear, or only for shear. If stiffness of the system is defined as the slope of the linear portion of the load vs. deflection curve, G1-T1, G2-T1 and G3-T1 can be compared (Figures 4.1, 4.2 and 4.3). The slopes of the lines are almost identical which indicates that the bonded CFRP sheets had no discernible influence on the stiffness of the member.

Previous studies have reported substantial increases in stiffness for FRP strengthened beams (Ritchie *et al*, 1991). This was due primarily to the difference in specimen size and stiffness. The stiffness (EI) of the CFRP sheets, due to its small cross-

sectional dimensions, is much less than the stiffness of the Type 'E' girder. By using a transformed section (steel and CFRP transformed to concrete), it was determined that the fibre sheets contributed only about 0.5% to the overall member stiffness. Typically, in other research, the test specimens were much smaller, and the FRP materials used tended to be thicker; typical FRP contributions reported were on the order of 10% of the composite member section (i.e., concrete/steel/FRP). Consequently, it is not surprising that an increase in stiffness did not occur; the sheets had no effect on the stiffness of the member.

4.2.3 Ductility

Ductility is always an important concern for concrete structures. Design should ensure that shear failure is preceded by flexural failure precisely because the latter (at least, for well-designed, i.e. under-reinforced, members) is a ductile failure mode. Typically, shear failure is not ductile. Better shear behaviour can be obtained if closely spaced, thin stirrups are used rather than fewer, widely spaced, heftier ones. Not only do many small stirrups provide better crack control, they also help confine the concrete which improves its effective compression strength both in the compression flange and in the diagonal compression strut (Leonhardt and Walther 1964). It would be advantageous if the CFRP sheets could be found to provide the same benefit, by effectively acting like many tiny closely-spaced 'stirrups'. However, since they may only be applied to the Type 'E' girder in a limited manner, given the geometry, it may not be possible in this case.

Ductility normally is defined as:

$$\mu = \Delta u / \Delta y \qquad (4.1)$$

where Δu is the deflection at the end of the post-elastic range, and Δy is the deflection at yield (Park and Paulay, 1975). Table 4.2 summarizes the ductility factors for all the tests. In all the shear tests, the tests were terminated once the peak ultimate load had been reached and the load had begun to drop off; Δu was calculated at this last point. Except for G2-T1 (East span failure), the shear failures of CFRP strengthened sections show increases in ductility compared to the control, unstrengthened, section. Although the flexural failures of G2-T3 and G3-T3 do not appear to be as ductile as the flexural failure of G1-T2, these two tests failed prematurely, as described in Section 4.3. Therefore, these

ductility factors may be considered 'minimums'; the results are not conclusive. The results do indicate, however, that CFRP sheet shear strengthening may improve the ductility of a member in shear. Generally, ductility factors of 3 to 4 are recommended for concrete structures. The shear failures of G2-T2 and G3-T2 are in this range.

4.3 Progression of Failure

4.3.1 Introduction

This section will focus on the physical behaviour of the specimens during loading. Figures 4.4 to 4.8 show the tested spans of each girder (i.e. support to support), indicating main crack patterns and areas where sheets were damaged or peeled. Note that the west end of the girder is always on the left-hand side of the page. This means that while the exterior face of the south leg is shown, the interior face of the north face is shown. This presentation was chosen in order to show the cracking patterns in a consistent manner. Reference will be made in the discussion to locations along the girder labelled as, for example, N(orth)W(est)1(closest to support). The locations are defined in Figures 4.4 to 4.8. The term "peeling" will be used and it is important to note that this refers to a layer of concrete peeling away with the fibre sheet, such that failure is in the substrate rather than in the composite or in the bond line. If failure is in the bond line, "de-bonding" will be the term used.

For each shear span, Table 4.3 presents the shear cracking load, the (average) angle of the compression strut, the number of stirrups crossed, and the maximum measured vertical strains at stirrup locations. This information will be referred to in the following sections. The shear cracking load is defined as the load at which the first diagonal shear cracks form at the level of the neutral axis at an angle of 45 degrees or less. The maximum strains measured in each test are shown in Figures 4.9 to 4.17 for the first two tests of each girder. Each set of three strains shown at each target are, from top to bottom, for the vertical, horizontal and diagonal orientations, respectively. Note that strains referred to in the text are principal tensile strains measured on the CFRP sheets, unless otherwise noted. All strains are summarized in Appendix B which contains the complete set of measured strains for several stages throughout the tests.

4.3.2 Girder 1

Girder 1 had the same number of stirrups at similar spacings in each leg of each shear span Figures 3.4 and 4.4, 4.5. The unstrengthened (control) East shear span failed first, in diagonal tension shear failure, a classic failure mode for slender beams. The inclined failure planes were staggered for the two legs, depending on differences in stirrup spacings. Judging both by the crack patterns and the strains measured in the vertical LVDT's adjacent to stirrups, only one stirrup in each leg was effective in contributing to the shear resistance of the section (Table 4.3 and Figures 4.4, 4.5). The principal failure cracks were at an average angle of about 27 degrees, quite shallow due to the widely spaced stirrups. At the time when the East span failed, at Pmax = 605 kN, the crack distribution in the West span was much lighter and finer. After the test, the CFRP sheets in the West span were thoroughly inspected. No signs of distress were observed. The strains at various locations on the CFRP sheets and/or on the concrete surface at ultimate are shown in Figures 4.9 and 4.10. The maximum principal tensile strain reached only about 1700 $\mu\varepsilon$, as measured on the CFRP sheets.

After strengthening the failed East span with the external stirrups, the girder was reloaded. Nothing new was observed until after P = 550 kN, when shear cracks began to form in the West span, at different locations from the shear cracks which had developed in Test 1, due to higher strains building up in as yet uncracked concrete. After about P = 650 kN, flexural cracking began to dominate in the constant moment region. The girder began to fail in a ductile manner, having reached its maximum yield moment capacity at a load of Pmax = 712 kN before it could fail in shear in the strengthened shear span.

After the test, inspection of the CFRP sheets showed distress at only one location. This occurred where the worst shear cracking was observed on the outer face of the South West leg, near the top (SW3). The vertical sheet 'peeled away' from the member over a horizontal length of about 200 mm, from its top edge down to where it was restrained beneath the horizontal sheet (Figure 4.18). A vertical split occurred in the vertical sheet, from the top free edge, down to where it was apparently restrained by the overlying horizontal sheet. On the outer face, the diagonal shear crack passed by this location about 80 mm below the level of the top edge of the vertical sheet. At this location the sheet did not have enough bonded length above the crack to anchor it against the straining introduced by the opening crack. The sheet did not debond, but peeled off a layer of

concrete, with the failure occurring in the concrete rather than in the bond line. At a strain rosette on the surface of the horizontal sheet within 75 mm of this spot, a principal tensile strain as high as +7500 με was measured. High strains were also measured near NW1B (principal tensile strain to +4643 με). This straining is clearly echoed on the outside of the legs: these two locations had shear cracks passing through.

4.3.3 Girder 2

Soon after the shear cracking load in G2-T1 (at P=550 kN), cracking began to dominate in the middle of the North East leg, which had the greatest gap between stirrups (985 mm). No distress was noted in the CFRP sheets until after P = 650 kN, when slivers of the vertical sheet began to peel away, starting from the top free edge (near NE2) down to the level of the overlying horizontal sheet, similar to the effect seen in G1-T2, South-West leg (see Figure 4.18). Again, the overlying horizontal sheet may have retarded the peeling somewhat. By this point principal strains as high as +3811 με (at SW3M) and +2479 με (at NE2B) were measured. Soon after, distress in the sheet was noticed and crackling noises began to be heard as loading continued. These were not characteristic concrete cracking noises, but sounded more like wood cracking. This was caused by CFRP sheets peeling away the concrete substrate and, in so doing, not only cracking through the concrete but also failing through the resin matrix once the sheet had peeled away from the main body. Although there was no failure or breakage of the fibres, the matrix did fail once peeling commenced, as evidenced by the vertical 'slivers'. Once concrete peeled away from the main body, there was a release of strain; in the process, the weakened matrix failed.

Still in the NE leg, the vertical sheets appeared to 'bulge' away from the substrate near the top edge of the sheet. As load increased, this 'bulging' spread out down towards the level of the diagonal crack. The disturbance began at the top of NE2, and moved towards the North East support. At about P = 700 kN, beginning about halfway between NE2 and NE1, the vertical sheets began to also peel away upwards from the bottom edge of the leg up towards the level of the diagonal crack. Although peeling from the bottom edge began later, it eventually became more severe. As the load increased, the sheets continued to peel away the concrete substrate from both the top and bottom flanges towards the mid-height of the girder. Finally, diagonal tension shear failure occurred in

the North leg of the East shear span at Pmax = 712 kN. Figure 4.19 clearly shows the situation at failure, with the extent of the bulging zones outlined in white ink. The horizontal lines show where the horizontal sheet stretched over the bulging at the bottom edge, some fibres breaking in tension due to the restraint effort. However, the horizontal sheets did not seem to be effective in actually preventing the peeling away along the crack.

The distribution of strains in the CFRP at ultimate are shown in Figures 4.12 and 4.13. Initially, higher strains were measured in the West span. At ultimate, strains in the West span were only exceeded by those measured in the South East leg. It is likely that the greatest strains in the North East leg did not occur near strain gauges, and therefore could not be directly measured. High CFRP strains were measured first in the South West leg (SW2B); principal strains reached +3057 με / -2906 με by P = 400 kN. Although quite a lot of cracking could be seen on the outside of the leg here, there was no sign of disturbance in the sheets. By about P = 600 kN, strains as high as +3811 με / -988 με were measured at NW3M. At the same load level, the highest strains measured in the South East leg were +2174 με / -2046 με (SE3M) and not much more in the North East leg (NE2B: +2479 με / −1857 με). Near failure, the highest strains measured in the North East leg were +2252 με / −1594 με (NE2B) and +2590 με / −155 με (NE3T). At the same time, strains as high as +4100 με were measured In the West side and as high as +6241 με (SE3M) were measured in the South East leg.

Despite the higher strains measured in the South East leg, there were almost no signs of deterioration. The early stages of peeling away at the top edge, like those seen in G1-T2, were noted halfway between SE2 and SE3, and immediately west of SE3, seen in Figure 4.20. Well distributed shear cracks could be seen on the outside face of the girder but, because of the better stirrup distribution, these were still very narrow. Shear cracks were similarly well distributed on the outer faces of the West legs. No disturbance whatsoever was noticed on the West span CFRP sheets. The extra length of the sheets, extending up along the chamfer) in the West span seems to have prevented top edge peeling.

After strengthening the failed East span, Test 2 of Girder 2 began. Starting from about P = 760 kN (prior to any visible distress in the CFRP) crackling noises could be heard and continued until failure. The sheets showed no distress until about P = 825 kN, when the start of peeling off was observed near the top chamfer between NW2 and NW3.

In order to extend the sheets up the chamfer, they had to be bent around a relatively abrupt corner which made it difficult to get as good a bond to the concrete in the corner. Under increasing load, tension in the sheet straightened the bend and the sheet began to "pop off" along this corner although it remained well bonded above along the chamfer itself and below along the height of the web. This was typical of the first sign of distress seen in cases where the sheet was continued up around this corner of the girder. The portion above the corner, along the chamfer itself was still well bonded at P = 880 kN. At about P = 900 kN, the sheet began to peel away from the bottom edge, near NW2 and SW2, and the bulging started to progress down from the top chamfer corner. Eventually, a vertical 'split' developed in the sheets on both legs, as can be seen both in Figure 4.21 and 4.22. Most of the detaching occurred from the bottom up, while higher up, the sheet continued to bulge outward. Although this bulging continued up to the top flange, almost everywhere the CFRP remained attached to the concrete along the chamfer, and thus the tension in the sheets could continue to be mobilized over the full height of the sheets, unlike where the sheets pulled away completely from the bottom flange up.

By the time the peak load, Pmax = 923 kN, was reached, sheets had bulged or peeled away along the length of the crack line from both bottom and top, although the extra anchorage length along the chamfer still prevented complete detaching. Load was sustained for a few load steps past peak until the span failed suddenly and both North and South legs "popped" open; the load fell off to about half peak. The failure shear cracks were about 8 mm wide in the South leg but only about half as wide in the North leg, due to the distribution of the internal steel stirrups.

The strains measured at ultimate on the CFRP sheets of the West span are shown in Figure 4.14. Amongst the highest strains measured were near SW2M and SW2B, NW2M, SW3M and NW3M. Strains at many locations exceeded 3000 με. The highest principal tensile strain measured was +8951 με at SW2B, just before failure at which time the sheet peeled away to beyond this level.

With both shear spans now failed, Test 3 was simply an attempt to observe how much additional flexural capacity was added by the three layers of CFRP on the tension flange. Both shear spans were now braced with the external tie rod stirrups. Already, in G2-T2, the flexural capacity of the Type 'E' girder (as determined in G1-T2) had been exceeded by about 10%. In G2-T3, failure occurred prematurely and unexpectedly at P =

999.5 kN. The HSS sections which formed part of the external stirrup arrangement bore directly against the longitudinal sheets on the underside of the tension flange of the girder legs (see also Figure 3.27). As the load carried by the external tie rods increased, high stress concentrations were generated where the HSS bore against the sheets, eventually slicing through the sheet. The failure was sudden, explosive and unexpected with no warning signs beforehand. It is important to note that the fibres did not "break", that is, they did not fail tension. Rather, they were neatly cut as if by a knife edge. The sheet tore away from the concrete (pulling concrete with it) from the cut location at the HSS to as far as midspan, approximately 1200 mm. This failure occurred only in the North leg, while the sheets on the South leg remained intact. Figure 4.23 shows the situation after failure occurred. Once these longitudinal sheets peeled off, it could be seen that the bond to the concrete was not consistent. Where the bond was good, the failure occurred in the concrete and the sheet tore away chunks of concrete with it. Poor bond was wholly due to the irregular bottom flange surface of the concrete; it was quite rough with a slight longitudinal ridge created by the original formwork. The surface of the webs, in comparison, was very even and so these bond problems did not arise.

4.3.4 Girder 3

In the first test, G3-T1, the characteristic "crackling" noises commenced soon after the first diagonal shear cracking at P=500 kN. No disturbance was observed in the sheets until P = 850 kN (96% Pmax), when a slight bulging outward appeared at the top edge of the sheet on the outer face of the North West leg (immediately north of NW2) (Figure 4.24). Cracks in the concrete could be seen in the narrow gap between the 30 cm wide fibre sheets, even though the sheets remained undisturbed. By P = 800 kN, strains at NW2 had reached +3663 με / -897 με and at SW2 +3910 με / -30 με. By now, the strains in the East span had become much larger: +4498 με / -918 με (NE1), +7598 με / -1591 με (NE2), +7706 με / -1902 με (SE3) and +4014 με / +647 με(NE3). On the interior web faces of both the North and South legs of the West span, the sheets peeled slightly away from corner below the upper chamfer, the "typical" first sign of distress (as described already for G2-T2) (Figure 4.25). The disturbances in the West span remained stable in this condition throughout the remainder of G3-T1.

By P = 700 kN, the shear cracking in the East span was quite extensive, particularly in the North leg which had only one internal stirrup through the shear span. Although the

cracking in the South leg started slower and did not become as intense, the crack distribution was very similar in the two legs. By P = 850 kN (96% Pmax), the sheets on the East span were still intact but the strains were very high: +5661 με / -1141 με (NE1), +3917 με / +343 με (SE1), +9088 με / -2320 με(NE2), +8575 με / -1945 με (SE3), +4257/ +729 (NE2). No damage to sheets was observed until the peak load (Pmax = 883 kN) was reached. The sheets on the North leg "fell apart" in the following few load steps, as the load would slowly drop off, then was increased again, repeatedly. The load was raised again to a post-peak value of P = 880 kN. During those load steps, the sheets incrementally went from slight bulging along the top chamfer corner (similar to that shown in Figure 4.25) to the condition shown in Figure 4.26. As before, the sheets "bulged" away from the top chamfer corner down to the level of the inclined crack, remaining well bonded above along the chamfer itself and along the 30 mm on the underside of the top flange. At some locations, the sheets remained attached by a length of only about 30 mm along the top flange, having peeled from the chamfer as well, yet remained anchored by this very small length . The bulging region, outlined in white ink in Figure 4.26, extended about 250 mm below the chamfer and almost 1000 mm along the length of the span spanning, generally, between NE1 and NE2.

Some twisting of the fibres could be seen over the chamfer in Figure 4.26. By the time the shear crack opened to a width of 8 to 10 mm (as measured on the outer face of the leg), the relative vertical and horizontal displacement on either side of the crack were severe enough to strain the fibres in this manner. Figure 4.26 and Figure 4.27 show the inside and outside of the North East leg, respectively, at the same location. The fibres were able to span these deformations, and there was no fibre breakage despite the deformations. Usually, little disturbance was observed in the horizontal fibres, but this time the effect of the severe horizontal and vertical displacements can be clearly seen over the depth of the web adjacent to the North East support in Figure 4.26. The displacements were in fact shearing the sheets and bending the fibres. No horizontal fibres were broken in this location. Since the vertical fibres wrapped around the bottom of the girder leg, this relieved the stress on the horizontal fibres, as compared to the situation in G2-T1 when horizontal fibres broke as they stretched over the 'bulging' concrete.

For the first time in the testing, broken vertical fibres were seen. This occurred near the North East support, on the inside of the North leg, at the corner where they were bent around the chamfer. Although the stress concentration at this corner instigated the failure,

the load on these fibres was also very high. The vertical displacement adjacent to the support that the fibre sheets had to support can be seen in Figure 4.27. On the outside, where the fibres wrapped around and ended on the outside surface of the leg, they peeled away from the concrete.

By this time, the diagonal shear crack on the North East leg was about 8-10 mm wide, as measured on the outer surface of the leg. Although, in general, the girder seemed to be holding up well, it was decided not to push the load any further because this may have made repair of the specimen too difficult. The girder remained loaded for a further 40 minutes, dropping from Pmax = 883 kN to P = 705 kN (80% Pmax). The lines in Figure 4.26 show how the bulging progressed gradually during this time, from the lighter white lines to the heavier dashed line. Again, failure was by diagonal tension shear failure. This time, there was evidence of concrete crushing in the top flange compression zone which had been severely reduced by the encroaching diagonal shear crack.

The South East leg remained relatively undisturbed during all the activity on the North side. The failure pattern was similar on the South East leg, centred around SE3, but was much less severe. The failure zone was shifted towards the load points in the South leg because of the different stirrup arrangement. The highest strains recorded in the South leg were +3917 με / +343 με (SE2) and +8575 με / -1945 με (SE3).

In Test 2 of Girder 3, no further sign of distress in the West span was noted until about P = 650 kN (68% Pmax) when the bulging on the exterior face near NW2 expanded slightly. The situation remained stable until P = 850 kN (89% Pmax) at which time the crackling noises began. Throughout the ten minute period during which Demec readings were taken, the noises continued and the bulging near NW2 grew further; there was now a 30 mm gap between sheet and concrete. The highest strains measured by this point were +4075 με / -264 με (SW2) and +4589 με / -3349 με (NW2). Strains at ultimate are shown in Figure 4.18. The dotted lines along the chamfer corner (Figures 4.28 (NW) and 4.29 (SW)) show where failure began on the interior faces of both the South and North legs. Around P = 950 kN (99% Pmax) bulging began to progress from there towards the diagonal crack, although the sheets were still bonded above this point. On the North leg, the sheet split vertically about 10 cm west of NW2; the same thing occurred on the South leg, about 150 mm east of SW1. The white marks on the photographs show the progression of the failure. By now, on the exterior faces, a large section of sheet had

peeled away from the top free edge to the level of the shear crack. Figures 4.30 and 4.31 show the condition of the North West and South West exterior faces a few loads steps after reaching P=950 kN. The member continued to carry load over several load steps despite being in this condition, eventually reaching the peak load, Pmax = 956 kN. Then, upon trying to increase load further, the girder shot suddenly to the east as shear failure occurred suddenly and catastrophically.

Failure was virtually identical in both legs. Figure 4.32 shows the condition of the exterior face of the south leg at failure. Fibres broke at several different locations, both on the interior and exterior faces of the legs, but always near the bottom chamfer, along the corner. Again, this was due to the abrupt vertical displacement and the high stresses at this location. In other studies this kind of shear crack has caused failure by debonding of the longitudinal sheets or plates bonded to the tension face (Meier and Kaiser, 1991). This did not appear to be a problem here; the longitudinal sheets on the bottom flange were able to span this discontinuity, although the vertical sheets could not.

On the outside faces of the legs, the sheets could only be bonded over about a 430 mm height whereas on the inside, they extended up 510 mm, and even slightly onto the underside of the top flange. Although by the end there was peeling on the interior faces as well as on the exterior faces, in general the behaviour was much better on the inside faces with the longer bonded lengths. Figure 4.30 shows the progressive failure pattern on the outer face of the leg

In Test 3, the girder displayed much less stiffness due to damage sustained in G3-T2. The load did still increase and was approaching 1000 kN when premature failure occurred in the South leg in much the same manner as it had occurred in the North leg in G2-T3 (Figure 4.23). This time, however, failure did not occur at the location of the stirrup HSS. After G2-T3, some precaution had been taken to avoid stress concentrations by placing thick steel plates between the HSS sections and the underside of the girder, to spread out the load. This did not prevent the failure, but only shifted its location to where the longitudinal sheets were first crossed by the vertical sheet which wrapped over them underneath the leg. The stress concentration was caused by this point of discontinuity where the vertical sheets, which bore against the longitudinal sheets, sliced quite cleanly through them. Figure 4.33 shows a close-up of the failure surface.

Table 4.1 Summary of test results of girder tests

Test	M/V	MTS Load (kN)	Shear (kN)	Moment (kNm)	Type of Failure	$\frac{V}{V_{GITI}}$	$\frac{M}{M_{GITI}}$
G1 - T1	1.9	604.7	302.4	574.5	V	1.00	0.85
G1 - T2 *	1.9	712.0	356.0	676.4	M	1.18	1.00
G2 - T1	1.6	712.0	356.0	569.6	V	1.18	0.84
G2 - T2	1.6	933.0	461.7	738.7	V	1.53	1.09
G2 - T3	1.6	999.5	499.7	799.6	M	1.65	1.18
G3 - T1	1.6	882.8	441.4	706.2	V	1.46	1.04
G3 - T2 *	1.6	956.3	478.2	765.1	V	1.58	1.13
G3 - T3	1.6	993.3	496.7	794.6	M	1.64	1.17

* Test not continued to ultimate flexural failure
Note: Effect of own weight not included

Table 4.2 Ductility factors

Test	Δy (mm)	Δu (mm)	μ =Δu/Δy
G1 - T1	6.0	13.5	2.2
G1 - T2	6.0	32.5	5.4
G2 - T1	8.0	16.75	2.1
G2 - T2	8.0	27.75	3.5
G2 - T3	8.0	32.5	4.1*
G3 - T1	8.75	22.0	2.5
G3 - T2	8.75	29.0	3.3
G3 - T3	8.75	35.0	4.0*

Table 4.3 Shear cracking loads, crack angles, maximum stirrup strains

Shear Span	Test Failed	Vcrack (kN)	Average Θ (deg)	Number of Stirrups Crossed	Maximum Vertical Strains (με)
Girder 1					
S - E	G1 -T1	500	25	1	3000
N - E		520	30	1	3455
S - W *	G1 -T2	500	27	0.5	3293
N - W *		540	28	1	3275
Girder 2					
S - E	G2 -T1	550	26	0.5	1330
N - E		550	32	0.5	3542
S - W	G2 -T2	450	29	1	3871
N - W		550	25	1.5	11826
Girder 3					
S - E	G3 -T1	500	30	1	5184
N - E		600	28	1	10344
S - W	G3 -T2	n/a	26	1	8249
N - W		n/a	30	1	15333

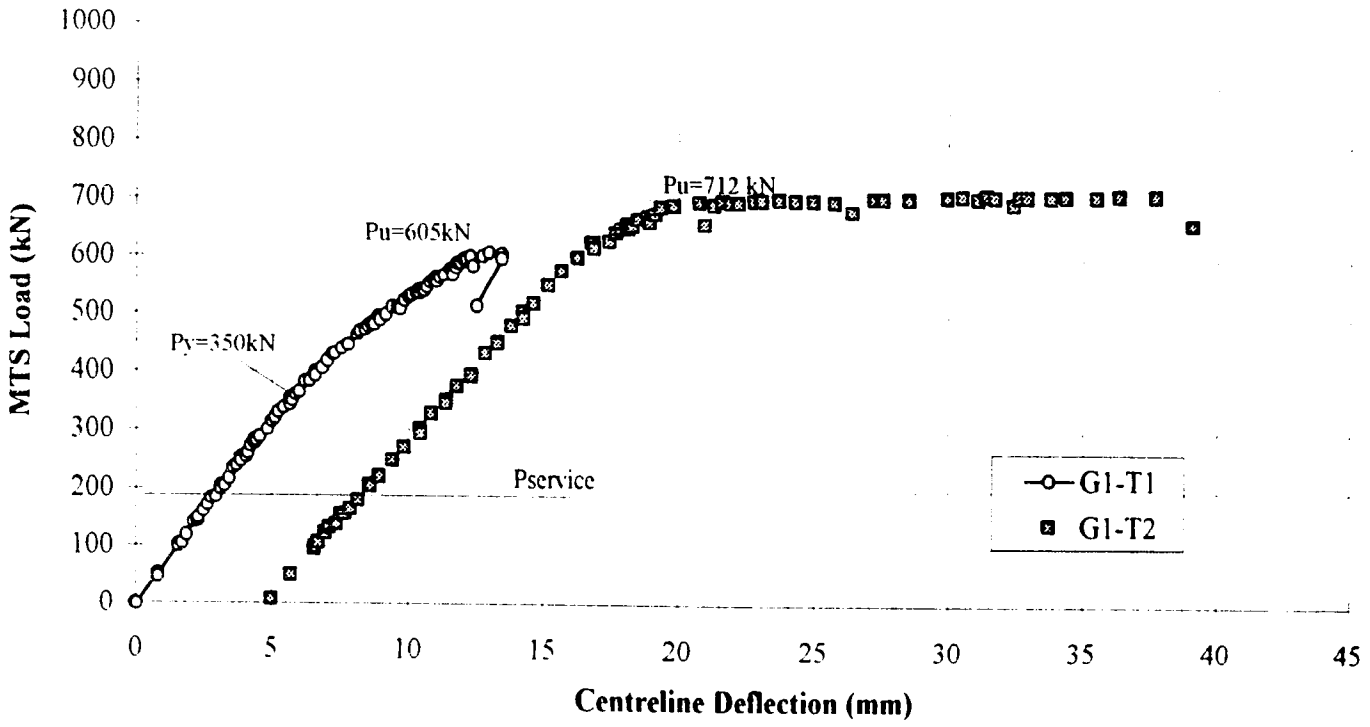

Figure 4.1 Girder 1 - Load vs. deflection curves

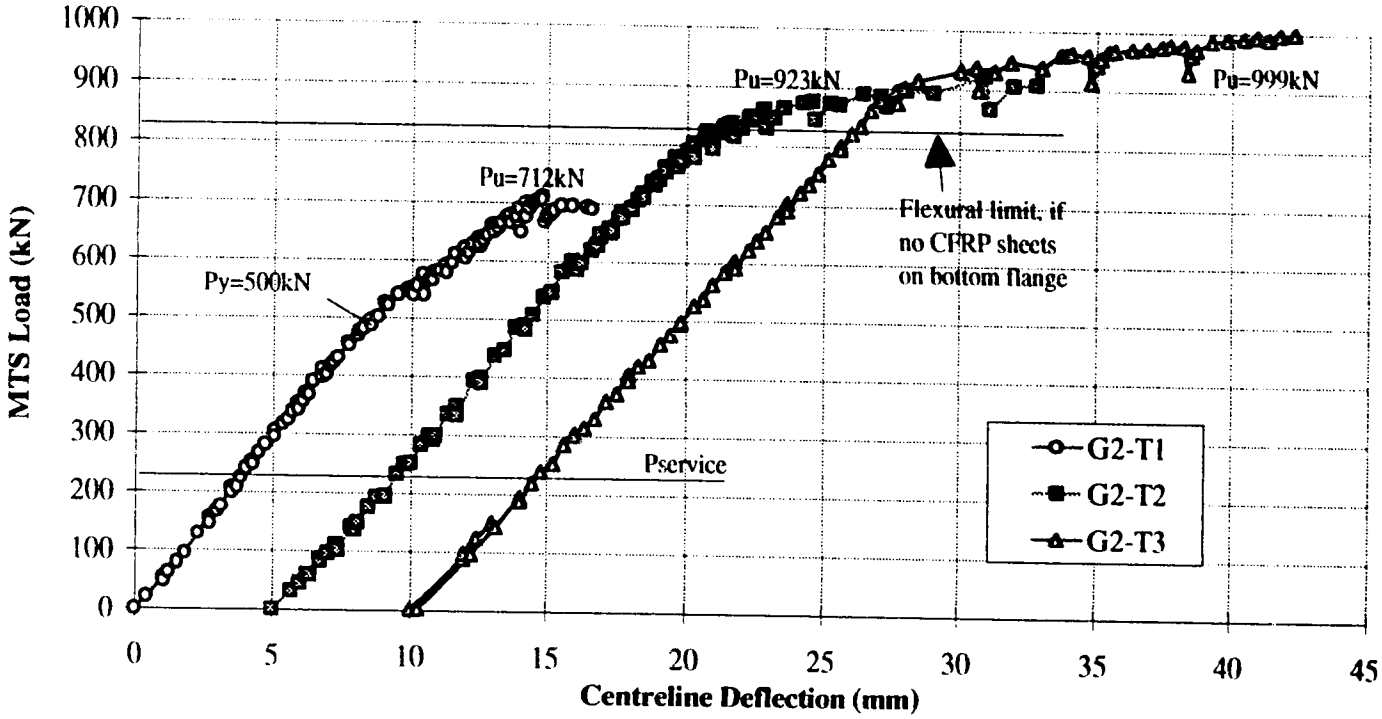

Figure 4.2 Girder 2 - Load vs. deflection curves

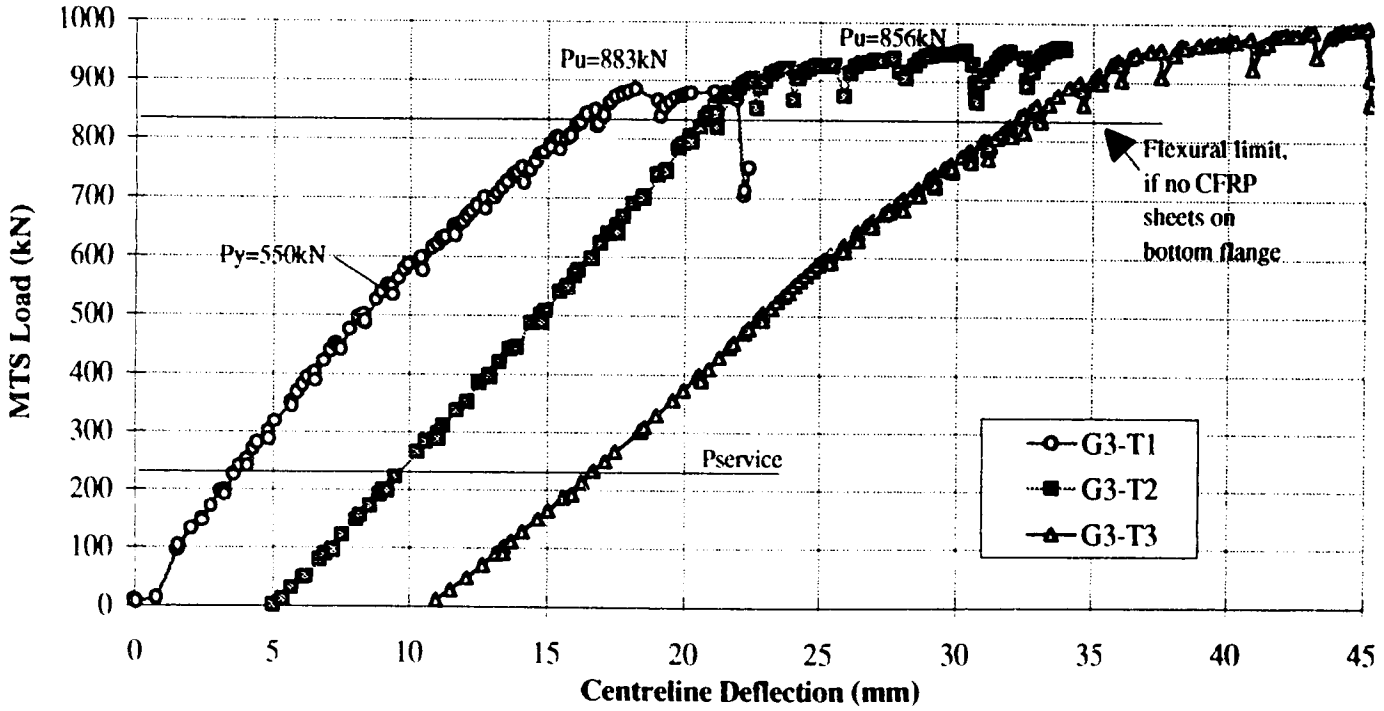

Figure 4.3 Girder 3 - Load vs. deflection curves

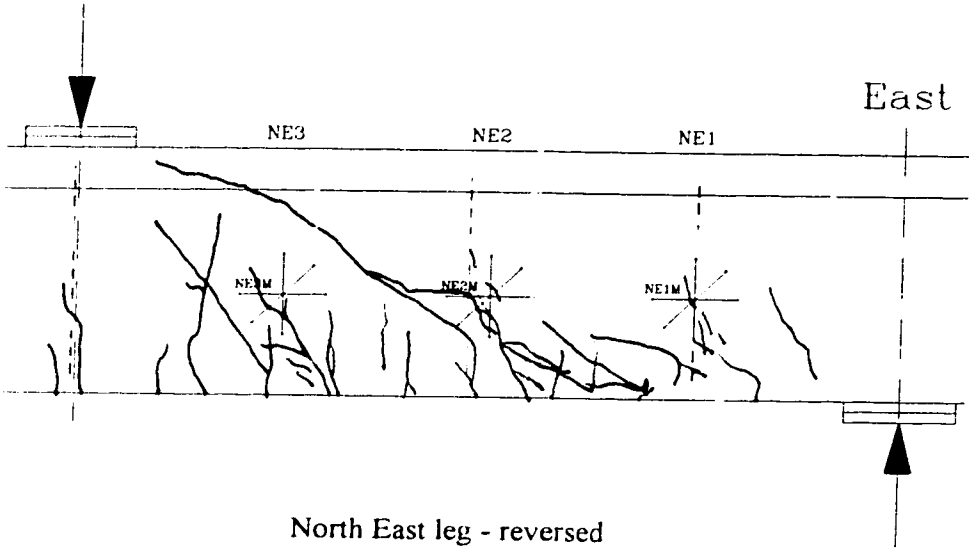

North East leg - reversed

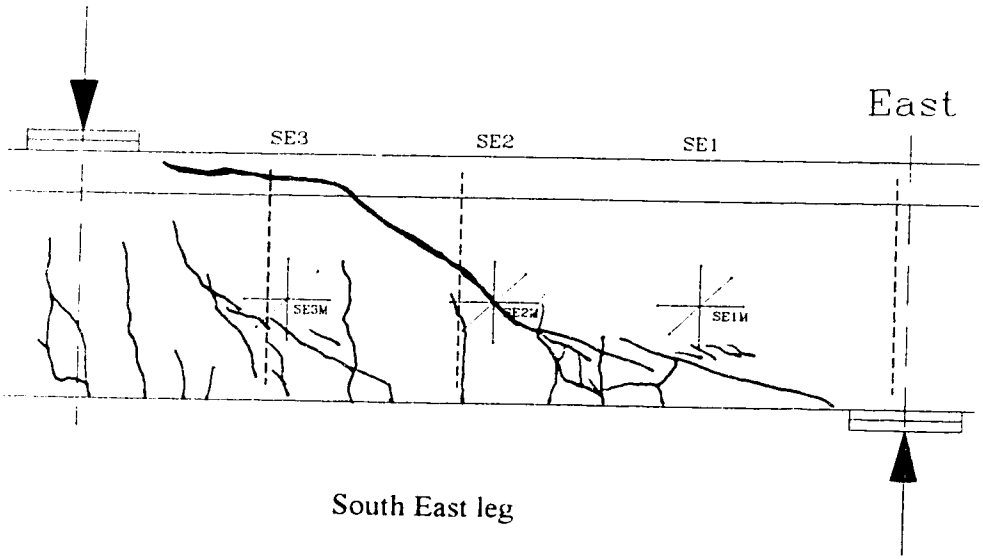

South East leg

Figure 4.4 Girder 1, East span - Crack patterns

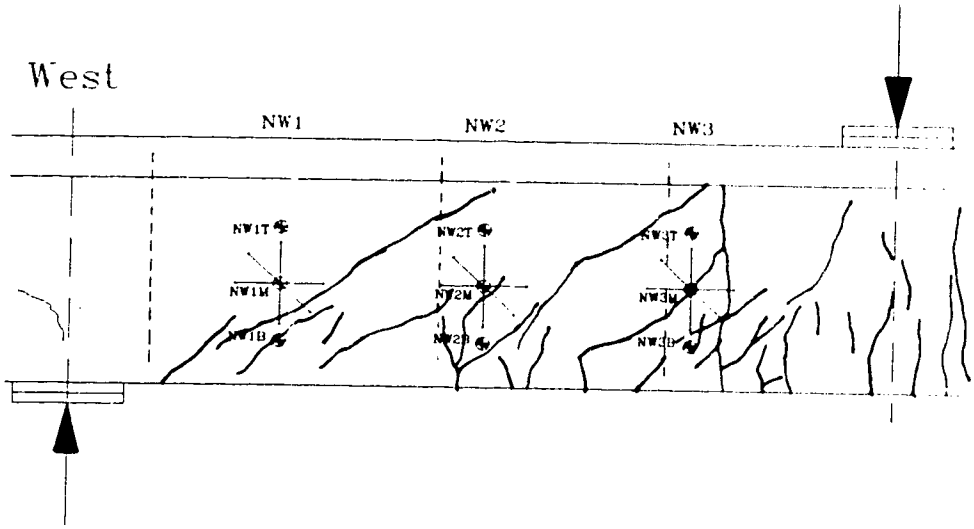

North West leg - reversed

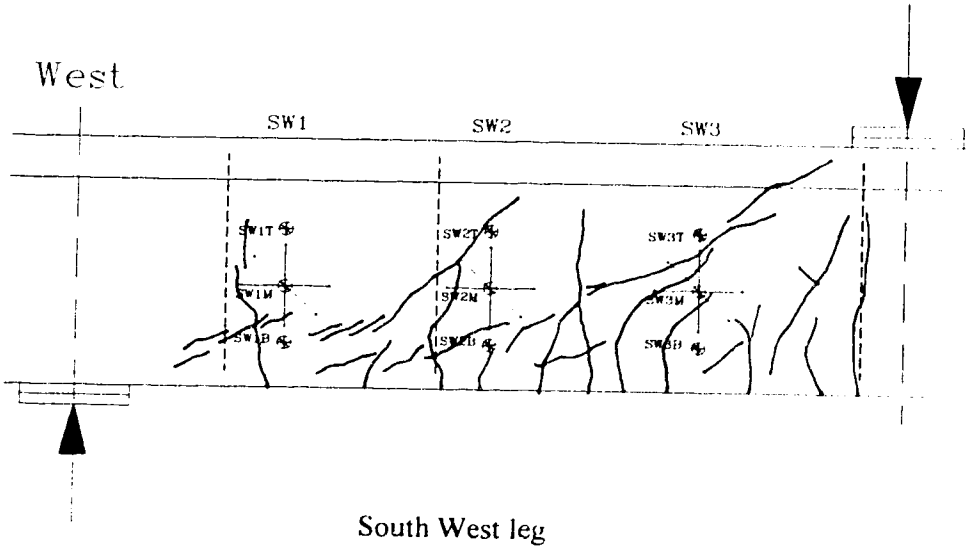

South West leg

Figure 4.5 Girder 1, West span - Crack patterns

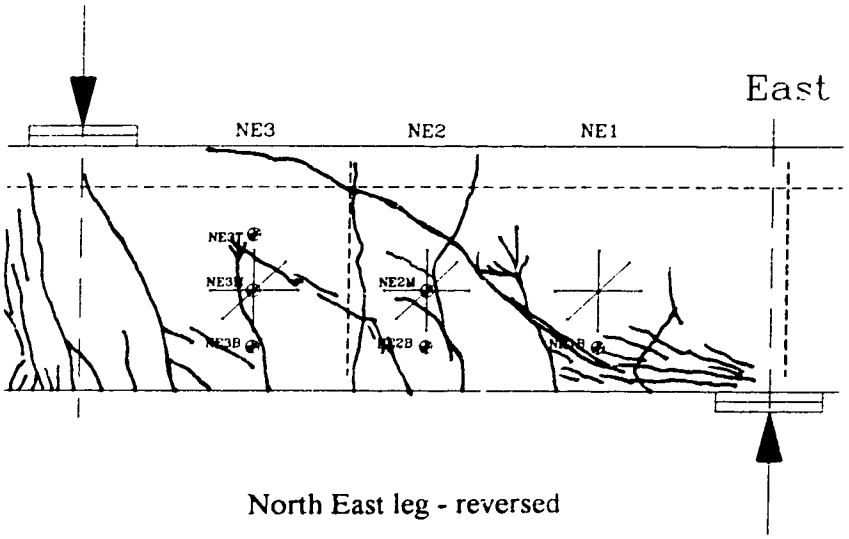

North East leg - reversed

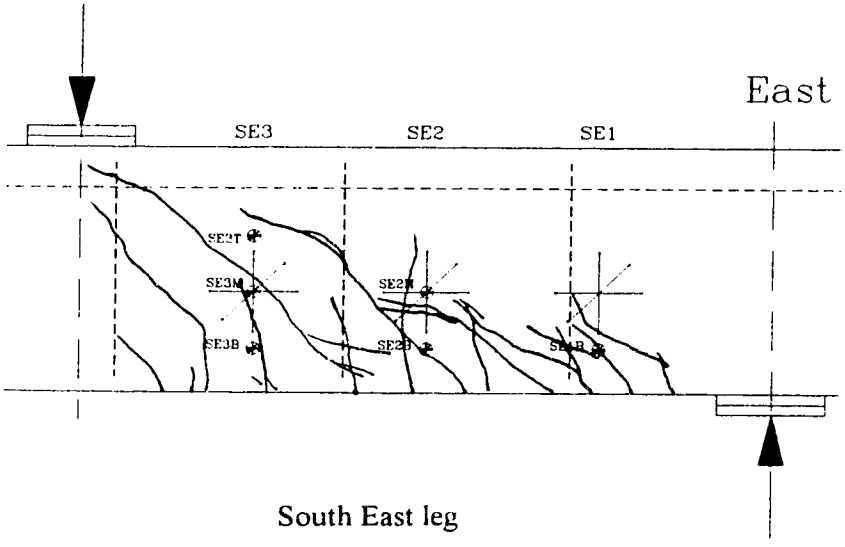

South East leg

Figure 4.6 Girder 2, East span - Crack patterns

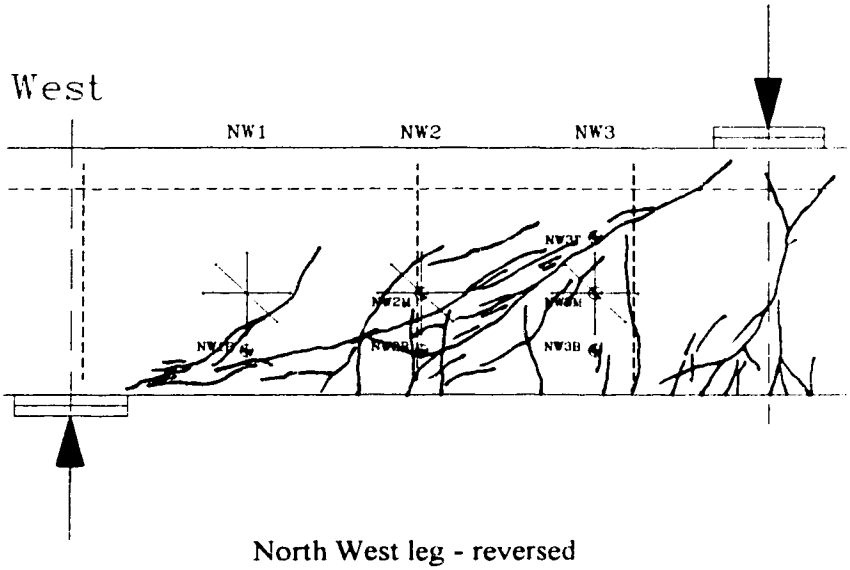

North West leg - reversed

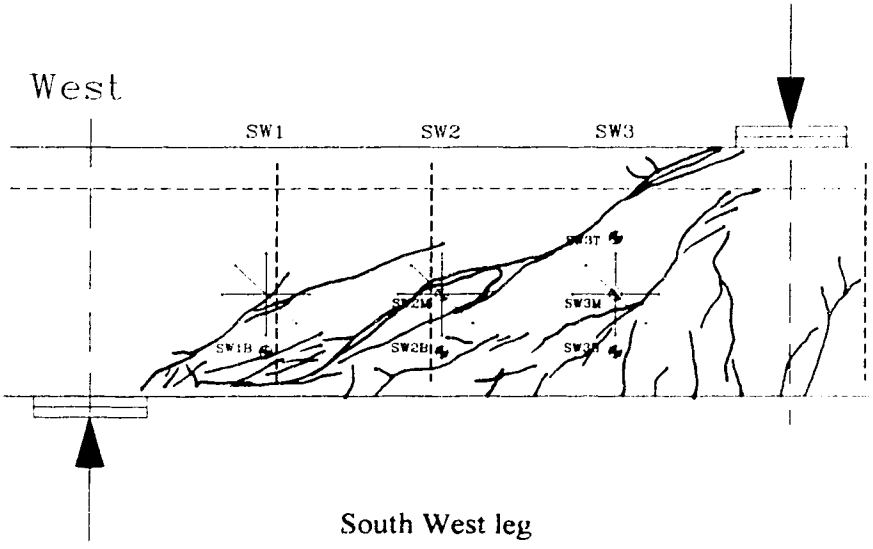

South West leg

Figure 4.7 Girder 2, West span - Crack patterns

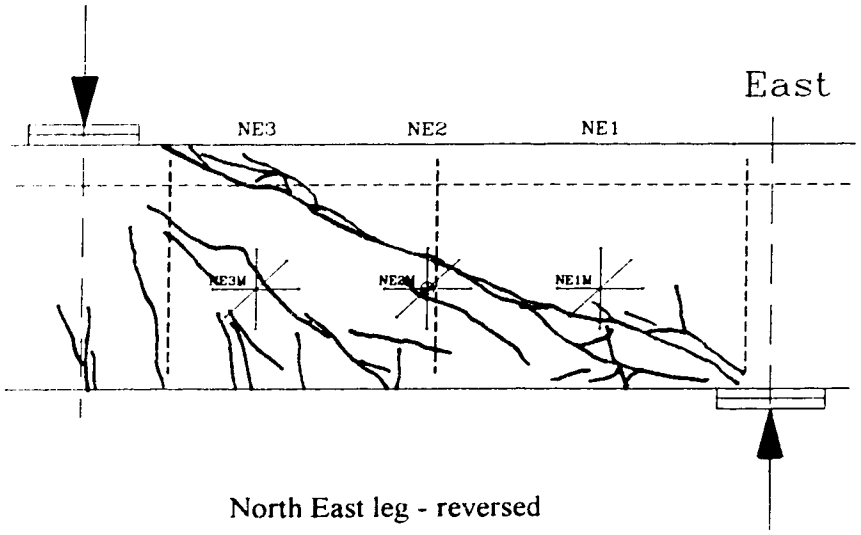

North East leg - reversed

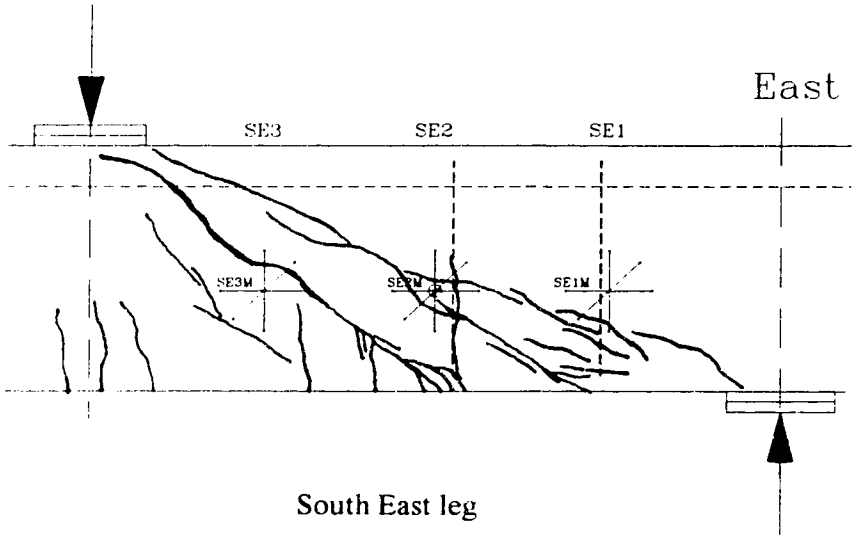

South East leg

Figure 4.8 Girder 3, East span - Crack patterns

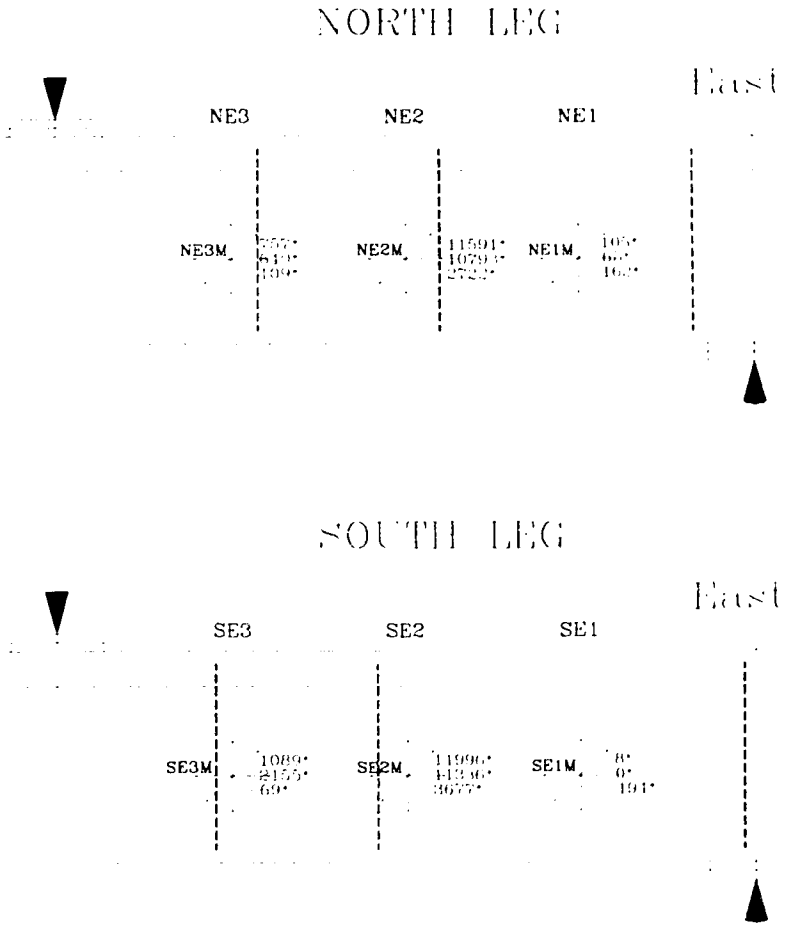

Figure 4.9 Girder 1, Test 1, East span - Maximum vertical, horizontal and diagonal strains (με)

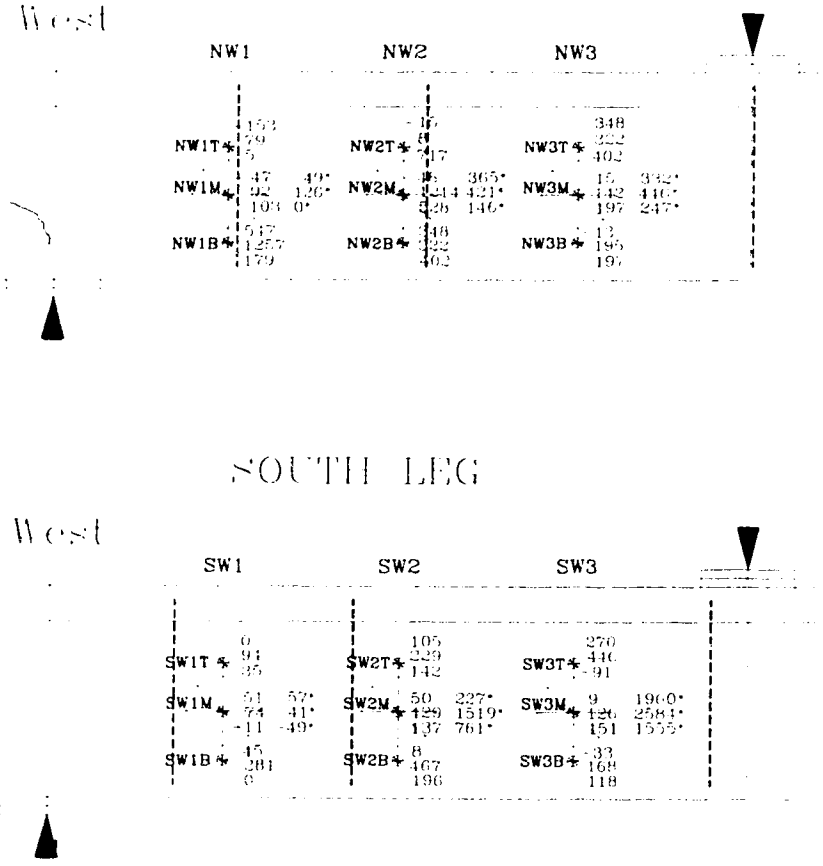

Vertical, horizontal, and diagonal strains are shown

* Starred strains are concrete strains over gauge length shown (200mm)

All other values are strain gauges measurements on CFRP (5mm gauge length)

Figure 4.10 Girder 1, Test 1, West span - Maximum vertical, horizontal and diagonal strains (με)

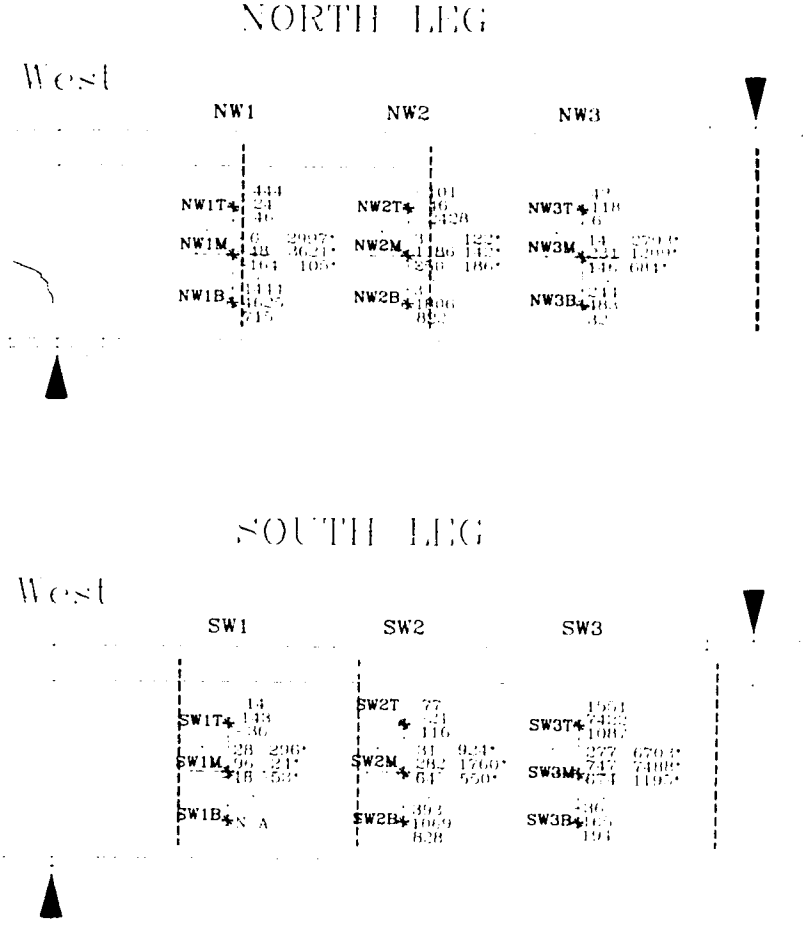

Figure 4.11 Girder 1, Test 2, West span - Maximum vertical, horizontal and diagonal strains (με)

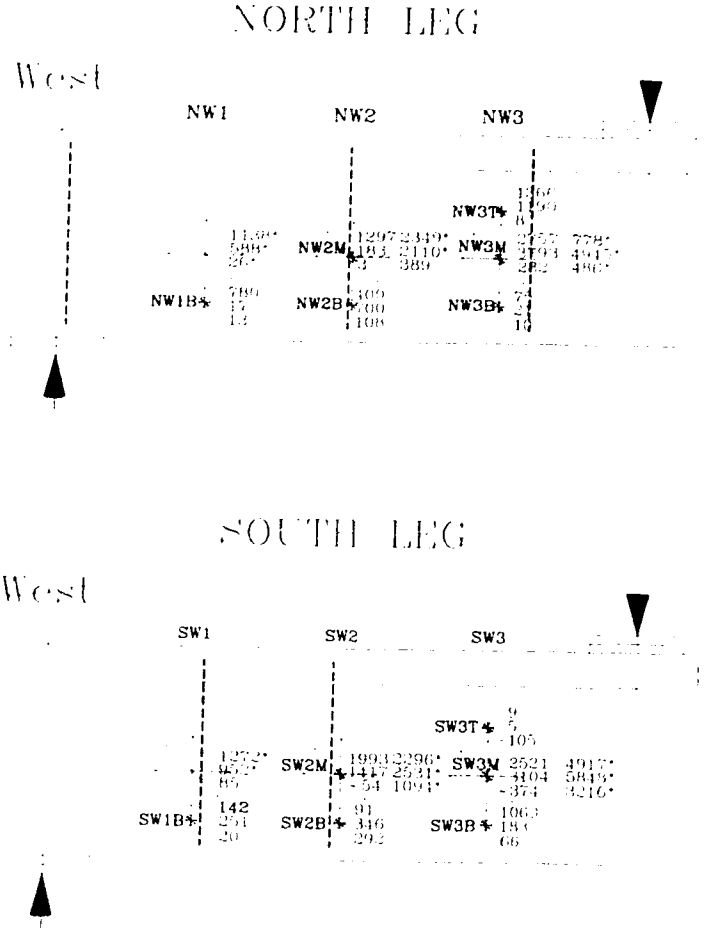

Figure 4.12 Girder 2, Test 1, West span - Maximum vertical, horizontal and diagonal strains (με)

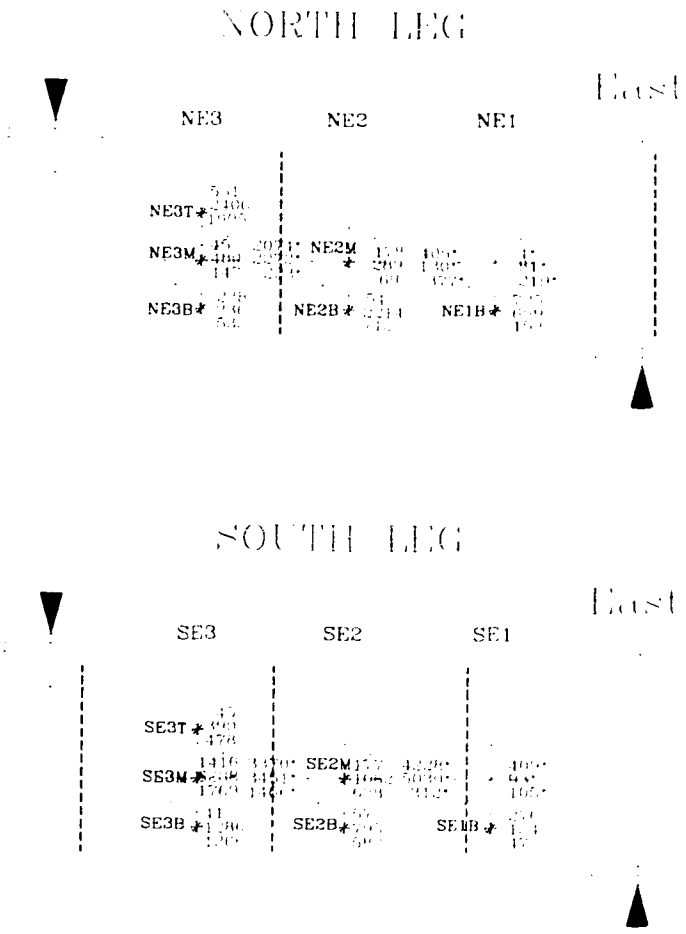

Vertical, horizontal, and diagonal strains are shown

* Starred strains are concrete strains over gauge length shown (200mm)

All other values are strain gauges measurements on CFRP (5mm gauge length)

Figure 4.13 Girder 2, Test 1, East span - Maximum vertical, horizontal and diagonal strains (με)

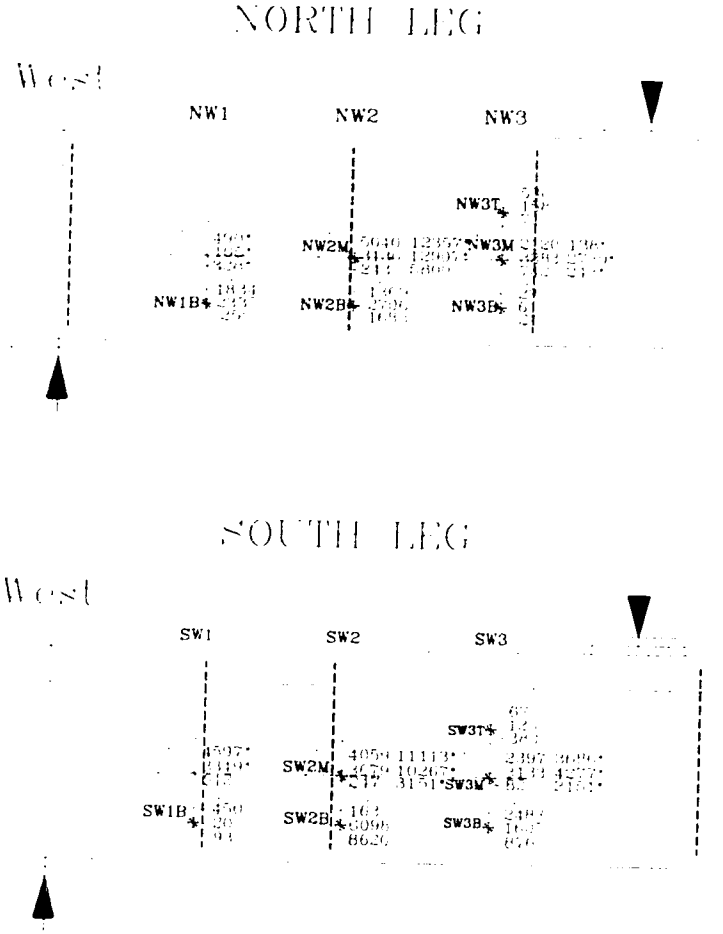

Figure 4.14 Girder 2, Test 2, West span - Maximum vertical, horizontal and diagonal strains (με)

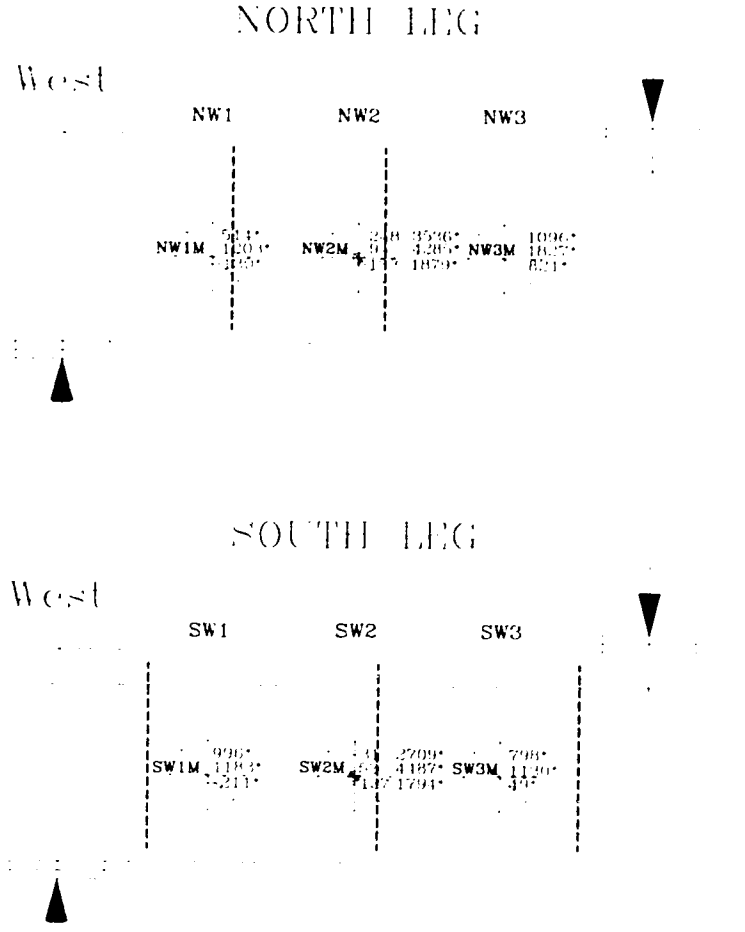

Figure 4.15 Girder 3, Test 1, West span - Maximum vertical, horizontal and diagonal strains (με)

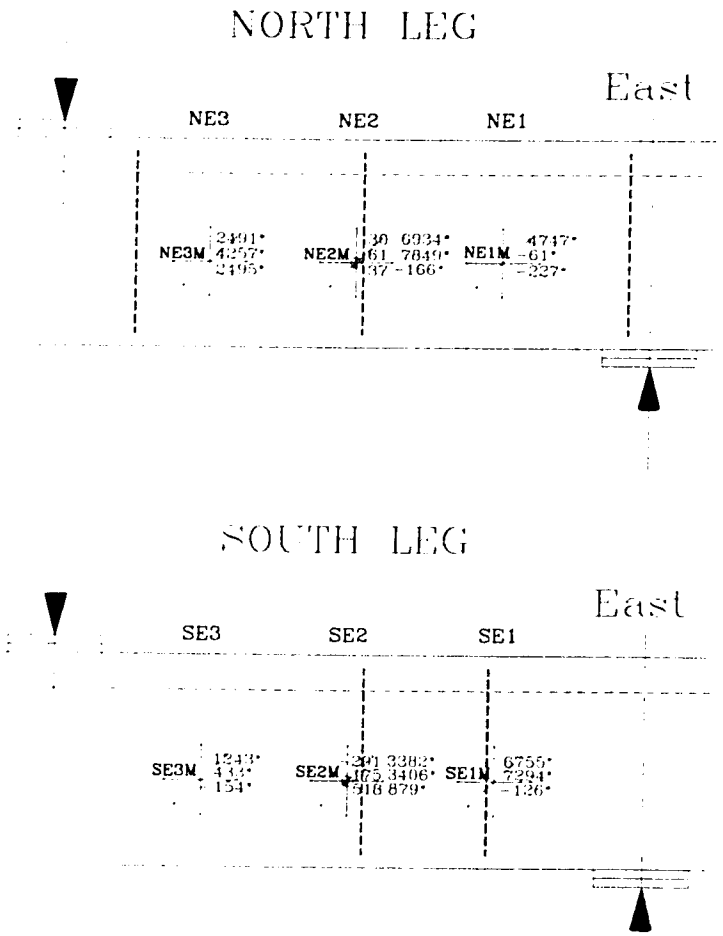

Figure 4.16 Girder 3, Test 1, East span - Maximum vertical, horizontal and diagonal strains (με)

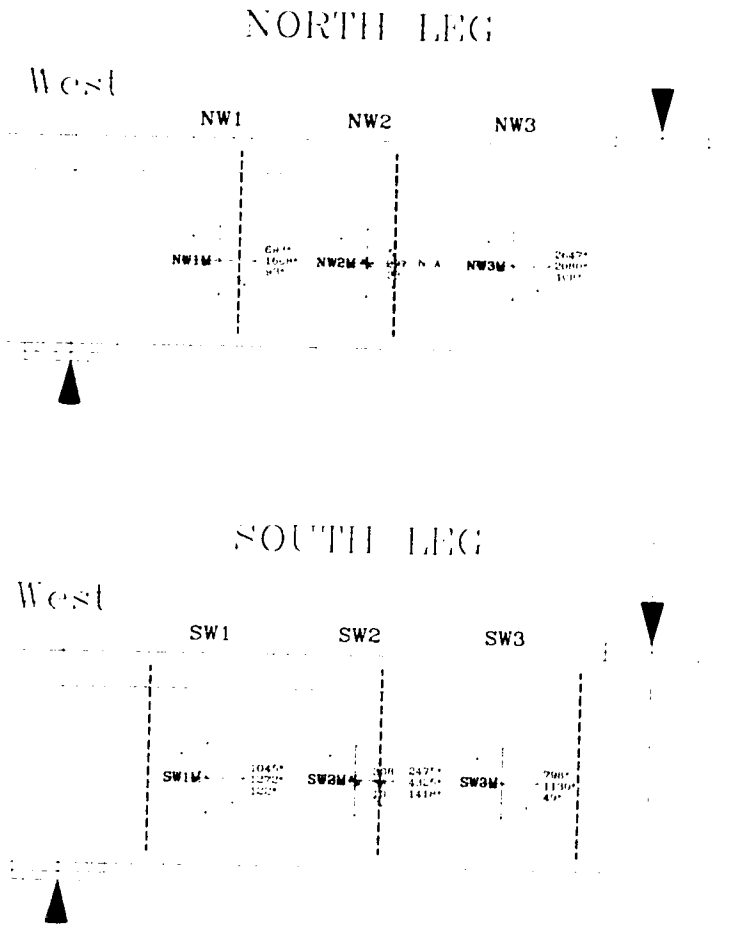

Figure 4.17 Girder 3, Test 2, West span - Maximum vertical, horizontal and diagonal strains (με)

Figure 4.18 Girder 1, Test 1 - South West leg - Interior face of web

Figure 4.19 Girder 2, Test 1 - North East leg - Interior face of web

Figure 4.20 Girder 2, Test 1 - South East leg - Interior face of web

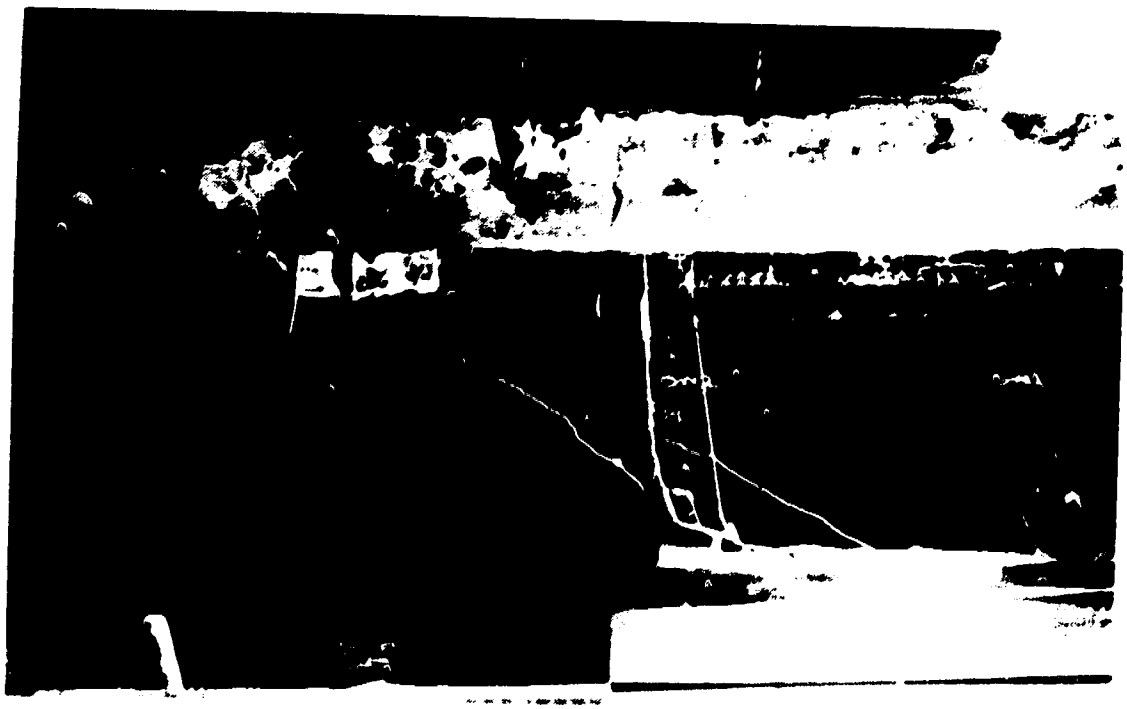

Figure 4.21 Girder 2, Test 2 - South West leg - Interior face of web

Figure 4.22 Girder 2, Test 2 - North West leg - Interior face of web

Figure 4.23 Girder 2, Test 3 - Failure of longitudinally bonded CFRP sheets

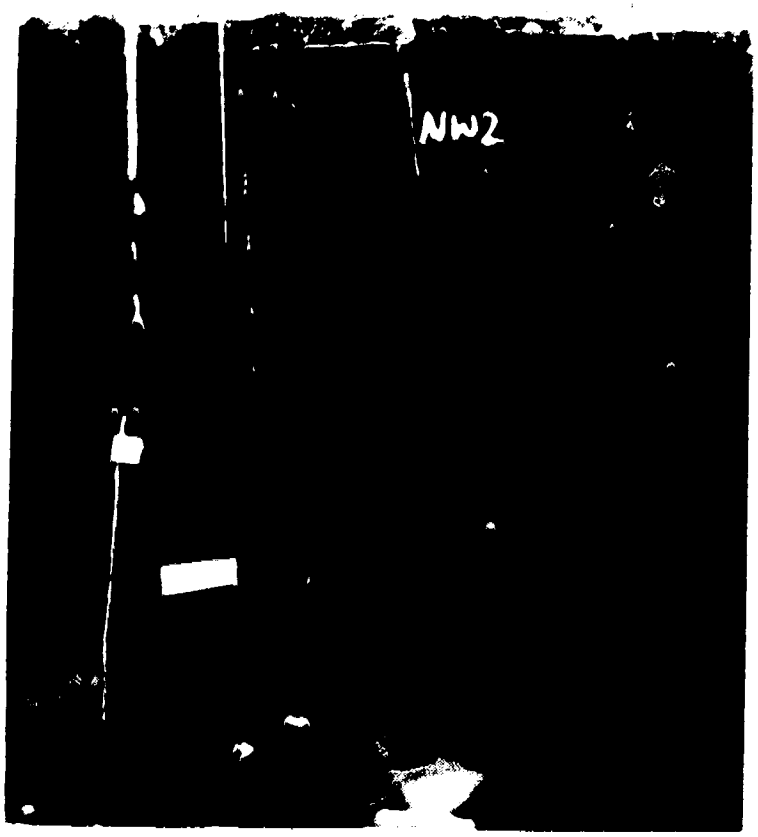

Figure 4.24 Girder 3, Test 1 - North West leg - Exterior face of web

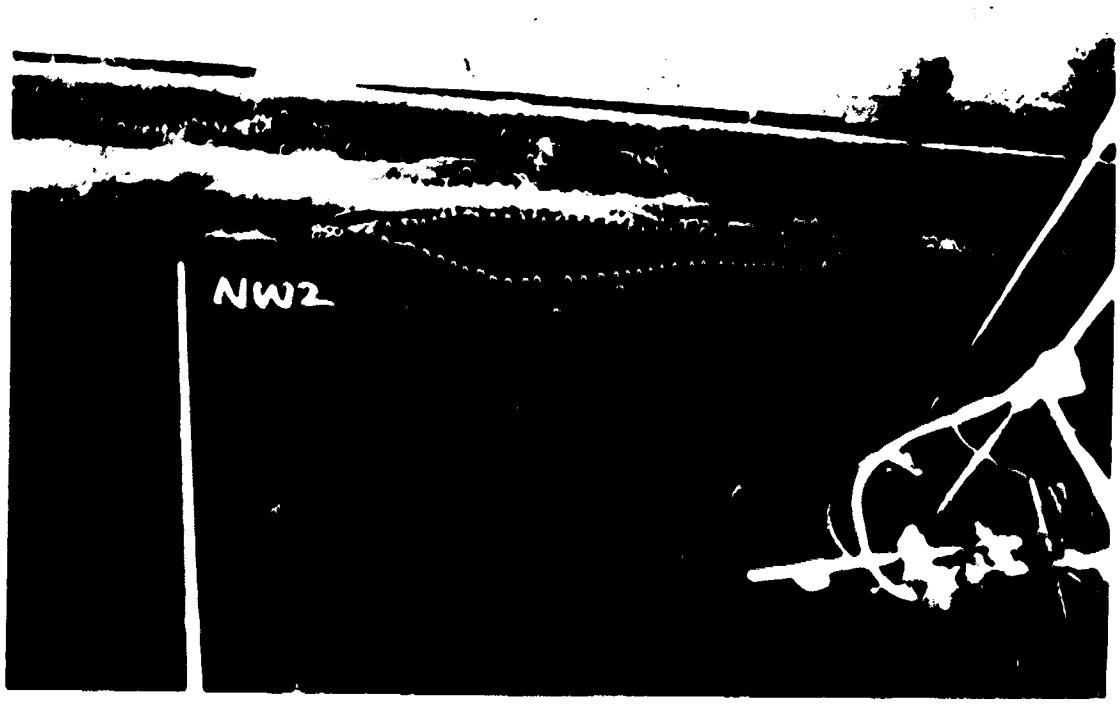

Figure 4.25 Girder 3, Test 1 - North West leg - Interior face of web

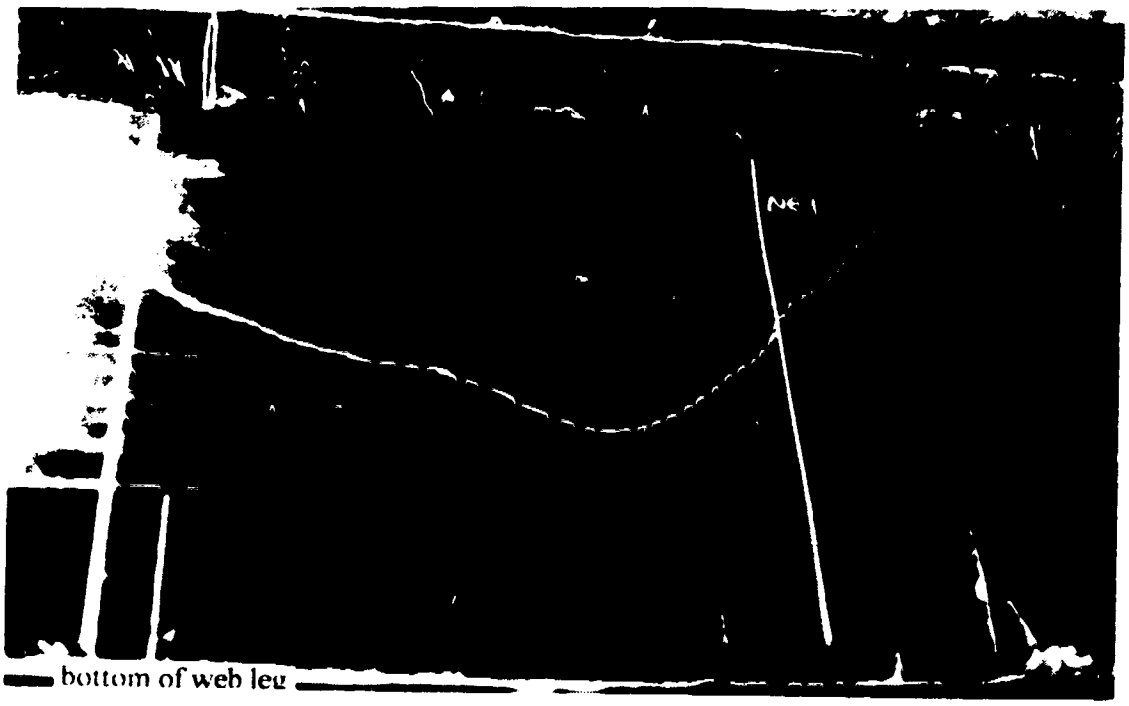

Figure 4.26 Girder 3, Test 1 - North East leg - Interior face of web

Figure 4.27 Girder 3, Test 1 - North East leg - Exterior face of web

Figure 4.28 Girder 3, Test 2 - North West leg - Interior face of web

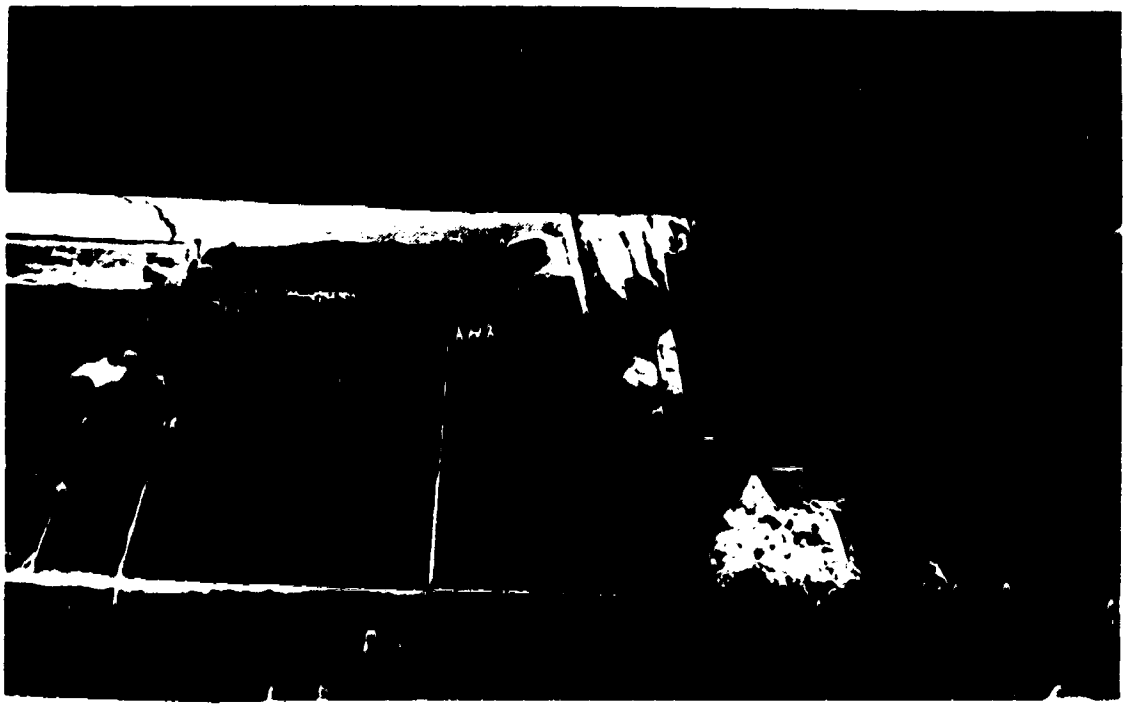

Figure 4.29 Girder 3, Test 2 - South West leg - Interior face of web

Figure 4.30 Girder 3, Test 2 - North West leg - Exterior face of web - Load step #142

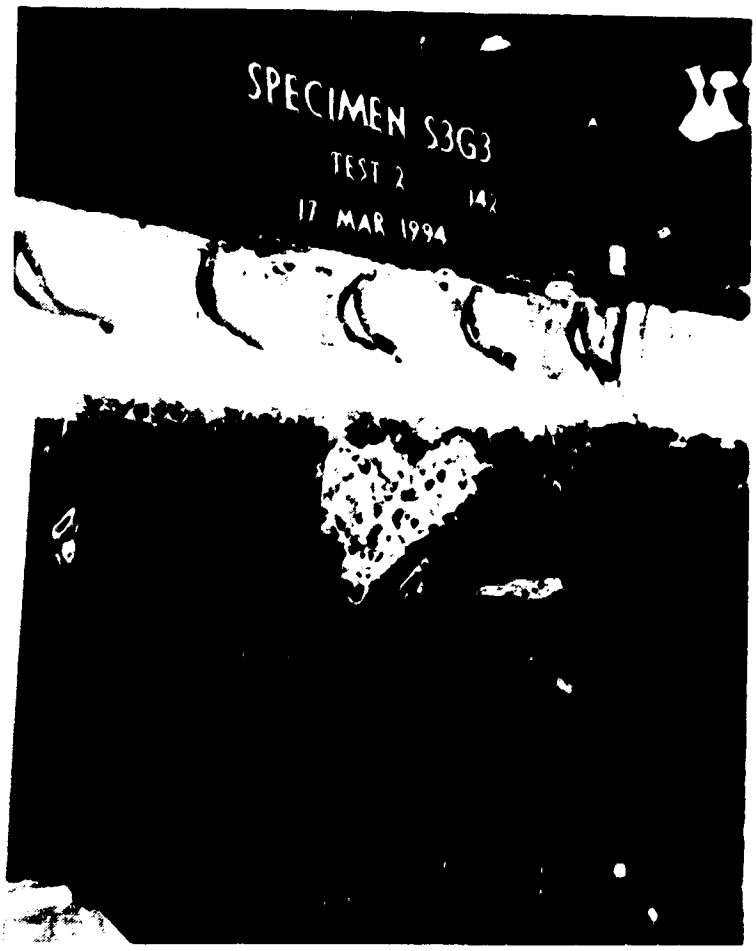

Figure 4.31 Girder 3, Test 2 - South West leg - Exterior face of web - Load step #142

Figure 4.32 Girder 3, Test 2 - South West leg - Exterior face of web

Figure 4.33 Girder 3, Test 3 - Flexural failure

5.0 Discussion of Test Results

5.1 Introduction

This chapter discusses the effect of bonded CFRP sheets on the capacities of the reinforced concrete members. A mechanism is suggested for the contribution of the fibre sheets to the shear capacity of the section, based on test results and observations. Finally, a method is presented for modelling and predicting this shear capacity. Section 5.2 is concerned only with the flexural capacity of the members. Predictions are made for the flexural capacities of both the unstrengthened and flexurally strengthened members. The shear capacity analysis is presented in Section 5.3. The contribution of the CFRP sheets is calculated based on test results, but no predictions are made for estimating it. Section 5.4 discusses how fibre sheets bonded to the webs of concrete members can contribute to shear strength and how they affected the behaviour of the members. A method for predicting the shear contribution of CFRP sheets is presented in Section 5.5 and estimates of capacity are compared to the test results.

5.2 Flexural Strength

The flexural capacity of the unstrengthened Type 'E' girder can be readily predicted by well-known equations for reinforced concrete. The hat-shaped cross-section of the girder is similar to a T-beam in concept, in that the neutral axis may be either in the flange or in the web. The section is shown in Figure 5.1(a). The depth of the equivalent rectangular stress block is first calculated as:

$$a = \frac{A_S f_y}{0.85 f'_c b} \qquad (5.1)$$

where A_S is the cross-sectional area of the tensile steel reinforcement, f_y is the yield strength of the rebar and f'_c is the compressive strength of the concrete. The actual tested material properties were used for f_y and f'_c. Assuming first that the neutral axis is in the top flange, b is the width of the top flange (compression face) of the member. If a is less than h_f (compression flange thickness) then the nominal flexural capacity is calculated as:

$$M_n = A_s f_y (d-a/2) \tag{5.2}$$

where d is the distance from the extreme compression fibre to the centroid of the tensile reinforcement. If a is greater than h_f, then:

$$M_n = (A_s - A_{sf})\, f_y\, (d-a/2) + A_{sf} f_y (d - 0.5\, h_f) \tag{5.3}$$

where:

$$A_{sf} = \frac{.85 f'_c\, (b - b_w) h_f}{f_y} \tag{5.4}$$

and:

$$a = \frac{(A_s - A_{sf}) f_y}{.85 f'_c\, b_w} \tag{5.5}$$

where b_w is the average total width of the two web legs.

The moment capacity calculated using this approach is M_n = 673.7 kNm, which can be compared to the test results from G1-T2:

$$M_{max} = M_{G1T2} + M_{o.w}$$
$$= 676.4 \text{ kNm} + 4.8 \text{ kNm} = 681.2 \text{ kNm}$$

where M_{G1T2} is the maximum moment reached in test G1-T2 and $M_{o.w}$ is the moment due to the girder's own weight. This was determined by the reaction load cells prior to the tests, and excluded from the test results. M_n is within 1% of the test results. The weight of spreader beams and other components of the test setup are included in M_{G1T2}.

Moment prediction for Girders 2 and 3 is complicated by the presence of the CFRP flexural strengthening sheets. Different approaches to this problem have been presented by various researchers (Deblois *et al*, 1992; McKenna, 1993; Sharif *et al*, 1994) and it is not within the scope of this thesis to assess their relative merits or determine an optimum solution. The flexural capacities were estimated herein using strain compatibility and force

equilibrium, with the usual assumption that plane sections remain plane. Two slightly different approaches were tried. First, the maximum strain in the longitudinal CFRP sheets was assumed, based on the maximum strains measured during the flexural tests (G2-T3 and G3-T3). Although this should predict the moment at failure, it cannot predict the ultimate capacity of the strengthened section because both flexural tests failed prematurely. In the second approach, the material properties of CFRP as well as concrete and steel were used to estimate the ultimate capacity of the section. The section used in the analysis and the assumed strain distribution are shown in Figure 5.1. Any possible contribution by the horizontal sheets bonded to the web faces was neglected, as they were not continued through the constant moment region.

For the first method, the assumed maximum strain in the sheets was 6000 με, as determined from the measured strains. Strains measured on the surface of the concrete at the level of the rebar indicated that the steel was strain hardening. Therefore, based on the steel stress-strain curves, 10% strain hardening was assumed as a better estimate of $\sigma_s > \sigma_y$. Table 5.1 summarizes the assumptions and results of the analysis. The actual concrete and steel strengths were used, determined as outlined in Section 3.3. The maximum strains measured on the surface of the CFRP sheet on the bottom tension flange were used. The strains in the concrete and steel were calculated, as was the moment capacity of the strengthened section. The calculated concrete strain was compared to the maximum concrete strain measured on the extreme compression fibre using a Demec gauge. The difference between actual and calculated strains and moments was less than 5%. The steel strains were not similarly compared because it had not been possible to measure ε_s directly.

In the second approach, the allowable stress of the composite was estimated by applying a safety factor of 1.5 to the specified ultimate strength, since the material does not yield. The ultimate flexural capacity thus estimated was about 8% higher than was reached in the test. The plateaus shown in the load vs. deflection curves for G2-T3 and G3-T3 (Figures 4.2 and 4.3) indicate that the ultimate capacity of the girders was almost reached. However, the capacity calculated was limited by the concrete strength used in the analysis, and by ε_c =3000 με, rather than the strength of the CFRP sheets. This was verified in the tests, since concrete crushing was clearly observed in the reduced compression block.

5.3 Shear Strength

The testing arrangement, described in Section 3.5.1, allowed each leg of the girder to be loaded and supported concentrically and so each could be considered independently. Not only did the stirrup locations vary from leg to leg and from shear span to shear span, but readings at the four load cells were not always identical due to non-uniformity of the member, seating etc. Thus, each load cell directly provided the actual shear force in each shear span, for both legs. The shear analysis was based on the effective cross-section of one leg, illustrated in Figure 5.1(b). The total shear capacity is given by:

$$V_n = V_C + V_S + V_{CFRP} \tag{5.6}$$

where V_C, V_S and V_{CFRP} are the shear resistances provided by the concrete, stirrups and fibre sheets, respectively. Note that for the East span of Girder 1, $V_{CFRP} = 0$.

Most commonly, V_S is determined using the truss model analogy. The stirrup spacings in all the girders were so wide that typically in design or analysis it would be assumed that they should be neglected completely, based on the assumption that stirrups must be reasonably closely spaced to be able to provide shear resistance. The S6-88 limit for this spacing is s_{max}= 0.5d. Ignoring all stirrups spaced greater than 0.5d could be overly conservative. The only concern here was to use a method of analysis which accurately quantified the capacity of the section, so that it could be determined how much contribution to attribute to the concrete, the stirrups and the CFRP. Research has also shown that even very widely spaced stirrups can contribute significantly to the shear capacity (ACI-ASCE Committee 426, 1974).

In order to account for the force carried by the stirrups, each leg in each span was considered individually. Observations of the crack patterns and measurement of vertical member deformations indicated if a stirrup was mobilized. Since there was only ever one or two stirrups in the test region, it was relatively straightforward to determine which stirrups were yielding. The stirrup contribution was then calculated as:

$$V_S = A_V f_y \tag{5.7}$$

where A_V is the cross-sectional area of the stirrup(s) and f_y is the yield strength of the stirrup steel.

The 45° truss equation is commonly used to calculate the stirrup contribution:

$$V_S = \frac{A_V f_y d}{s} \tag{5.8}$$

where d is the horizontal projection of the crack, s is the stirrup spacing and d/s is the number of stirrups crossed by the crack. When s=d, Equation 5.8 reduces to Equation 5.7. However, as s becomes larger than d, Equation 5.8 becomes increasingly conservative, not allowing the stirrups any contribution to shear strength. Thus it was considered more realistic to use Equation 5.7 in the analysis.

The control section consisted of the North East and South East legs of Girder 1. Both these regions had one stirrup yielding, and this information was used with Equation 5.7 to calculate the V_S contribution. Since no CFRP sheets were used in the East span, Equation 5.6 could be reduced and rearranged as:

$$V_{C TEST} = V_{TEST} - V_{S TEST} \tag{5.9}$$

where V_{TEST} is the average of the two load cell readings at the North East and South East reactions, including the shear due to the girder's own weight.

Various equations were presented in Section 2.3 for calculating V_c. Each of these methods was used to calculate V_c for Girders 2 and 3, and the results were compared to the benchmark concrete shear capacity from the results of G1-T1, calculated by Equation 5.9. Table 5.2 provides a summary of this comparison. Many assumptions are required in order to apply the Modified Compression Field Theory. To begin with, a specific critical section must be analyzed. Two sections were chosen. The first, 1200 mm from the support, was chosen from crack pattern observations. The second section, 600 mm from the support, was determined by using the average observed angle of the compression strut, Θ, in G1-T1. The critical shear location was taken at the intersection of this diagonal compression strut with the centre of the web, measured from the support. The MCFT analysis based on these two critical sections produced a range of values for V_c of 96.8 kN to 112.7 kN. Based on this comparison, it was decided to use the Zsutty formulation to predict the concrete shear contribution in this analysis.

Table 5.3 summarizes the shear capacity results for each leg of the shear span. V_{TEST} comes directly from the test results and is the maximum shear carried by that leg at failure as measured by the reaction load cell, including the girder's own weight. The concrete contribution was calculated using the Zsutty formulation, Equation 2.12, and the actual material properties. For Girder 2 and 3, the effect of the bonded flexural sheets on ρ_w was not included in the calculations. The shear resistance contributed by the internal stirrups was calculated using Equation 5.8. Since there were only ever one or two stirrups per shear span, in almost all cases it was clear from crack pattern observations and measured vertical strains how many stirrups were yielding. In two cases, observations and measured strains did not warrant neglecting the stirrup completely, yet did not support yielding either. Therefore, an estimate was made of the force in the stirrup, equivalent to half a stirrup (for convenience of the table format).

The shear capacity attributed to the sheets was calculated as:

$$V_{CFRP} = V_{TEST} - V_C - V_S \qquad (5.10)$$

Table 5.3 shows the calculated values for V_C, V_S and V_{CFRP}. The ratio V_{CFRP} / V_{TEST}, which indicates the proportion of the shear capacity of the section which may be attributed to the CFRP sheets, ranged between 17% and 30%. The shear carried by each specimen, V_{TEST}, was compared to the shear carried by the control section, V_{GIT1}, in order to determine the increase in shear strength made possible by the use of the bonded CFRP sheets. Since the control section included only one internal steel stirrup per leg, a direct comparison could only be made to other sections with only one stirrup per leg. If the test section had fewer or greater number of stirrups, the comparison was made possible by adjusting V_{GIT1} appropriately. Hence, for example, for the South East leg of G2-T1, the ratio, V_{TEST} / V_{GIT1} , was calculated as:

$$\frac{V_{TEST}}{V_{GIT1} - \frac{V_S}{2}} = \frac{192\ kN}{169\ kN - \frac{53.5\ kN}{2}}$$

As seen in the Table 5.3, the CFRP strengthened sections showed an improvement of 21% to 55% over the G1-T1. Included in Table 5.3 is the ratio V_{CFRP} / V_{TEST} which

indicates the proportion of the shear capacity attributed to the bonded CFRP sheets. This ratio ranged between 0.17 and 0.30. The degree to which the composite sheets improved the shear capacity did not seem to clearly depend on particular parameters. This was most likely due to the interaction of different conditions, such as strength of concrete (which was not consistent amongst the girders), effectiveness of the internal stirrups and effectiveness of the bonded sheets, and influence of CFRP flexural reinforcement on effective ρ_w (in the cases of Girders 2 and 3).

5.4 Failure Mechanism and Influence of CFRP Sheets

In the previous section, it was demonstrated that the use of CFRP sheets as additional web reinforcement increased the shear capacity of the specimens. The discussion in this section will describe the mechanism of failure observed, and how this was affected by the presence of the bonded sheets.

The overall failure mode of all the shear failures was by diagonal tension failure, as has been described already in detail in Chapter 4. The CFRP sheets did not affect this basic mechanism, nor did they affect the onset of cracking or the angle of the compression diagonal which formed. The overall cracking pattern development, as observed on the outer faces of the girders, was not noticeably altered by the presence of the bonded sheets, but was governed by the distribution of the internal steel stirrups and the concrete strength. The effect of the sheets was noticed once the cracks began to open up, at which time they began to influence the behaviour of the member. This is suggested by the difference between the load-deflection curve of G1-T1 (shear failure of the unstrengthened girder) and the curves for all the other shear failures. The G1-T1 curve began to curve over early on due to shear weakening of the section. The fibre sheets helped postpone this loss of stiffness by helping keep the cracks closed. This would be far more effective if accomplished equally well on both faces of the web. However, as the sheets can only be bonded to one face of each leg of this girder, their contribution cannot ultimately reach its full potential, regardless of how well they perform.

The adequacy of the bond between the CFRP sheets and the substrate is an important concern in assessing the strengthening technique. In order to form the new composite member comprised of the concrete member and the fibre sheets, the requirement of "perfect" bond between the two must be fulfilled. "Perfect" bond is

achieved if failure of the composite member occurs by failure in either the concrete substrate and/or in the fibre material prior to failure in the bondline. The quality of the bond between concrete and sheets was found to be generally excellent, as long as the concrete surface was well-prepared. The only poor bond conditions observed were those along portions of the bottom tensile faces of Girders 2 and 3, between the concrete and the longitudinal sheets. Although this did not cause failure, it was noted afterwards that the rough, uneven surface of the bottom flange prevented proper adhesion. As long as such longitudinal sheets are adequately bonded at their extreme ends, their tensile capacity can still be mobilized throughout their length, as was the case in these tests.

Having satisfied the requirement of good bond, the next critical question is how much anchorage length is required to mobilize the sheets. This is also related to the concept of development length as improved anchorage may decrease the required development length. In the case of the flexural strengthening, the longitudinal sheets were extended past the supports, ensuring adequate bonded length and anchorage, and ensuring they could develop their strength. Anchorage and development length remain serious concerns in the shear strengthening application as the physical limitations of the Type 'E' girder prevented extending the sheets over the full depth of the web. The bonded length was one of the key parameters studied in this test series.

Ideally, the sheets should be extended over the full height of the web. Not only does this allow anchorage into the compression zone in the top flange, it maximizes the development length provided. Proper design and detailing requires internal steel stirrups be extended as close to the compression face as practicable in order to ensure that they can reach yield over most of their depth. This concept can be extended to the FRP sheets. If the fibres are intercepted by a crack near their top edge, there may not be adequate length extending above this point so that the strength can be mobilized over the full length of the sheet.

As described in Chapter 4, failure of the fibre sheets always began at their top free edge, but the severity and progression depended a great deal on the detailing. Figure 5.2 shows the three different details used at the top and how the peeling began and progressed. In (a) the sheet peeled concrete away freely and progressed easily. In (b) and (c) the tension in the sheet straightened the bend that had been forced into it. However, the extra bonded length above the bend, along the chamfer, resulted in a great

improvement in anchorage. Even at failure, the 3 cm length along the underside of the top flange [in (c)], remained secure.

At their lower ends, steel stirrups must be anchored as well, and this is achieved by bearing against the longitudinal reinforcement. This type of anchorage must somehow be provided for the sheets. Ideally, the sheets should be wrapped completely around a member. The optimum situation would be as shown in (a) of Figure 5.3 where the sheets are anchored back onto themselves. Not only does this anchor the sheets, the confinement provided to the concrete enhances its effective compressive strength. Although suitable and attractive for strengthening columns (Ballinger *et al*, 1993), it is not usually a practical method for strengthening beams in situ in a structure. The option shown in (b) is more likely to be encountered but generally there will be some practical limitation to the distance (y). Far less surface is available to work with on the Type 'E' girder (c).

Figure 5.4 shows details at the bottom flange of the girders, and how failure arose. Although (c) behaved better than (b), this was simply due to the extra capacity provided by the outer sheets. The extra anchorage in (b) was sufficient to prevent bottom edge peeling, such as that shown in (a). The benefit gained by wrapping the sheets under the legs was somewhat diminished by the corners which introduced undesirable stress concentrations. In G3-T1 (b), the fibres broke right along the chamfer edge before girder failure, evidently due to the stress concentrations. In G3-T2 (c), fibres broke along the bottom edge at ultimate; this was not only due to the edge stress concentrations but also to the sudden large vertical and horizontal deformations that occurred when the girder failed suddenly and explosively in shear. Although it would be expected that covering both faces of web legs with sheets would considerably improve behaviour, the exterior sheets covered only about 80% of the height available on the inside face. The sheet contribution did increase, but due to the shorter development length, did not double.

In summary, the fibre sheets are most effective when maximum bonded length and/or additional anchorage, such as wrapping around the bottom flange, are provided. The optimum situation for this girder type is a combination of Figure 5.2(c) (for the top) and Figure 5.4(b) (for the bottom); this arrangement had been used in the East span of Girder 3.

Figure 5.5 shows a failure cracks spanned by sheets. The vertical hatching indicates fibres and concrete still intact. The diagonal hatching indicates where the sheets have peeled away the concrete. If the anchorage provided was not adequate, failure progressed as shown in Figure 5.5(a); the first signs of distress were at the top or bottom edges of the sheets and typically this did not occur until the higher load levels (about 90% of Pu). Once the sheets began peeling away the concrete at the top and bottom (Points A and B), failure continued progressively towards the crack line. The peeling began once the bonded length L1 and/or L2 became small enough. During the observed tests, this seemed to occur when L1 or L2 approached about 75 mm. If the anchorage is good enough at top and bottom, then the progression of failure will be more like Figure 5.5(b); the sheets were not peeling away the concrete layer but were bulging away from the substrate. As long as the sheets remain anchored, the tensile strength of the sheet can be developed, despite the bulging, and they can continue to carry load.

As mentioned, the strength of the CFRP sheets never governed failure. In no case did the fibres fail in tension, although they did break at stress concentrations, such as at corners. Thus, since the ultimate strength of the material was not reached, one layer of CFRP would be adequate to achieve the required shear strength. The second layer of horizontally oriented sheets did not appear to be as effective, although it should still contribute to crack control. It would also be possible to reduce the fibre content of the sheets used, or apply discrete strips with gaps between rather than a continuous sheet.

5.5 Model of CFRP Sheet Shear Resistance

It is proposed that the CFRP sheets bonded to the webs of the members contribute to the shear strength of the section by the interaction of two separate mechanisms. The first mechanism is one of crack control, in which the sheets act as 'bandages' to prevent or limit cracking. In the second mechanism, the fibres may be modelled as a series of 'stirrups', and then analyzed in a manner analogous to that used for the analysis of sections reinforced with internal steel stirrups. Both of these two models will be discussed in further detail, and predictions of CFRP contribution to shear strength will be calculated based on the second model.

When glued to the surface of concrete members, FRP sheets can be effective in providing crack control. Fibres oriented in any direction can contribute to this mechanism,

although they will be most efficient when oriented perpendicular to the crack line. If cracks are pre-existing, CFRP sheets may easily be applied in the optimum orientation for repair purposes, and would be even more effective if the member is first jacked so as to close the cracks before the sheets are applied. By holding the cracked surfaces together, the CFRP sheets can help increase the effective shear strength contribution of the concrete by maintaining or improving interface shear transfer. This effect may significantly improve the shear strength of the section. The improvement would be optimized if the sheets were bonded to both faces of the web legs, which generally is not feasible with the Type 'E' girder.

In the second mechanism, the CFRP sheets are modelled as a series of discrete 'stirrups'. If the validity of this assumption is accepted, then the contribution of the sheets may be determined by existing methods of analysis used for steel stirrups, such as the truss model equation. As is the case for internal steel stirrups, the CFRP sheets may be oriented either vertically or inclined to the vertical. For simplicity of design, to deal with stress reversals, and to avoid errors in construction, vertically oriented stirrups are preferable. As this was also the only situation investigated in the experimental program, the discussion will be limited to the vertical 'stirrups'. During testing, the vertical fibres spanned over bulging sections, as long as anchorage at the top and bottom was sufficient, and so continued to carry load over their length for as long as they remained in this condition.

In these tests, the CFRP sheets were applied continuously throughout each shear span, and thus provided uniformly distributed vertical tensile forces. The shear capacity contributed may then be expressed as:

$$V_{CFRP} = t_{CFRP}\,\sigma_{eff}\,l_{eff} \qquad (5.11)$$

where t_{CFRP} is the thickness of the CFRP sheets, σ_{eff} is the design stress level used, and l_{eff} is the effective length of the sheets. If the continuous vertical fibres are modelled as a series of discrete stirrups, then the cross-sectional area of one of these fictitious "stirrups" may be defined as:

$$A_{CFRP} = t_{CFRP}{*}s \qquad (5.12)$$

where s is the spacing and tributary width of the 'stirrup'. In this case, Equation (5.11) may be written as:

$$V_{CFRP} = \frac{A_{CFRP}\,\sigma_{eff}\,l_{eff}}{s} \qquad (5.13)$$

The terms in this equation are defined graphically in Figure 5.6. In this form, the equation is expressed identically to the convential truss analogy equation for shear strength provided by internal steel stirrups. This is the form which is most familiar to engineers and which is used in design codes. It is most likely that in practical applications, the CFRP sheets will not be applied continuously, but in discrete strips, with gaps in between. In this case, the following definition may be used:

$$A_{CFRP} = w * t_{CFRP} \qquad (5.14)$$

where w is the width of a strip of CFRP material.

In the following analysis of the girders tested in this test series, the continuous sheets were modelled as discrete stirrups by assuming a tributary width of s = 100 mm. The stress level, σ_{eff}, is not the specified ultimate strength of the CFRP material, but some reduced value based on the results of the CFRP material testing described in Section 3. In order to check the reasonableness of this value, at least for the particular application herein, estimated and measured strains were compared. Using the test results for σ_{eff} (625 MPa) and modulus of elasticity (E=114 GPa) (see Chapter 3), a maximum strain of ε = 5482 $\mu\varepsilon$ was obtained. The highest strain measured in the direction of the vertically oriented fibres was 5084 $\mu\varepsilon$ (see Appendix B). This indicated that the stress level used was reasonable.

The final parameter, l_{eff}, is the effective length of the fibre sheets. The length, l, is the overall length of the vertically oriented sheets. If the sheet was wrapped around the bottom of the leg (e.g., cases (c) and (d)), l was reduced by l_{bf}, the length of the non-vertical fibres. The sheets are not effective over their full length, but require some minimum length with which they can be adequately anchored. This was described in more detail in Section 5.4, where it was shown that if the crackline intercepted the sheets too close to the edge, the sheets will begin to peel away the concrete, leading to failure. This

effect must somehow be incorporated in the evaluation of l_{eff}. For the cases considered in this testing program, the effective lengths are defined as shown in Figure 5.7. The anchorage length required, l_a, was estimated based on test observations of the minimum length required beyond a crack to avoid peeling. If adequate means of anchorage is provided at the top and/or bottom, it may not be necessary to reduce the length by l_a, e.g. at the bottom of the legs in cases (c) and (d).

The contribution of the sheets to the shear strength of the section (V_{CFRP}) was calculated using Equation 5.11 and the results are summarized in Table 5.4. The concrete and steel stirrup contributions (as calculated in Section 5.3) were added to the predicted V_{CFRP} values in order to obtain a total predicted shear capacity, V_{PRED}. When this value was compared to V_{TEST}, the agreement was quite reasonable, except for the West span of Girder 3, which had CFRP sheets bonded to both faces of the web legs. The larger discrepancy may be due to the fact that the l_a used may not have been as appropriate.

Although the results of the analysis seem to predict well the test results, it is important to note that the validity of the approach may not hold when extended to other types of members. The analysis was based on a very particular type of member and must be verified more rigorously for the more general case.

Table 5.1 Summary of moment capacity analysis

	Specimen:	Girder 2	Girder 3
Measured			
f'_c	(MPa)	27.7	28.5
f_y	(MPa)	337.8	245.9
ε_{CFRP}	($\mu\varepsilon$)	5983	5727
Calculated			
ε_s	($\mu\varepsilon$)	5033	4767
ε_c	($\mu\varepsilon$)	1152	1094
M_{PRED}	(kNm)	793	794
Actual			
ε_c	($\mu\varepsilon$)	1115	1068
Mu	(kNm)	799.6	794.6
$\frac{MPRED}{Mu}$		0.99	0.999

Table 5.2 Theoretical concrete shear strength contribution comparisons

Method	Vc (kN)	V / Vtest
Test Vc	115.7	--
S6-88	109.6	0.95
A23.3	114.1	0.99
Zsutty	117.4	1.01
ACI/326	100.4	0.87
MCFT		
[600 mm]*	112.7	1.11
[1200 mm]*	96.8	0.93

* Critical section, from support

Table 5.3 Shear capacity results of girder tests

Test	Failure Mode	Critical leg	No. of Stirrups Crossed	V_{TEST} (kN)	V_c (kN)	V_s (kN)	V_{CFRP} (kN)	$\frac{V_{CFRP}}{V_{TEST}}$	$\frac{V_{TEST}}{V_{GIT1}}$
Girder 1									
Test 1 (Control)	diagonal shear	South East*	1	168	115.7	53.8	--	--	--
		North East*	1	171	115.7	53.8	--	--	--
Test 2	flexure	South West	0.5	184	115.7	26.9	41.4	0.23	1.29
		North West	1	205	115.7	53.8	35.5	0.17	1.21
Girder 2									
Test 1	diagonal shear	South East	0.5	192	125.2	26.75	40.1	0.21	1.35
		North East*	0.5	198	125.2	26.75	46.1	0.23	1.39
Test 2	diagonal shear	South West*	1	229	125.2	53.5	50.3	0.22	1.35
		North West*	1.5	263	125.2	80.3	57.5	0.22	1.34
Girder 3									
Test 1	diagonal shear	South East	1	237	126.4	54.8	55.8	0.24	1.40
		North East*	1	235	126.4	54.8	53.8	0.23	1.39
Test 2	diagonal shear	South West*	1	239	126.4	54.8	57.8	0.24	1.41
		North West*	1	263	126.4	54.8	81.8	0.31	1.55

* Critical leg(s)

Note: G3-West had 'double' the CFRP

Table 5.4 CFRP shear contribution predictions

Shear Span	Leg	Sheet Pattern	l_{eff} (mm)	Predicted V_{CFRP} (kN)	Vc (kN)	Vs (kN)	V_{PRED} = V_{CFRP} + Vc+Vs	V(test) (kN)	$\frac{V_{TEST}}{V_{PRED}}$
G1-West	South	(a)	280	35.0	115.7	26.9	177.6	184.0	1.04
	North				115.7	53.8	204.5	205.0	1.00
G2-East	South	(a)	280	35.0	125.2	26.75	187.0	192.0	1.03
	North				125.2	26.75	187.0	198.0	1.06
G2-West	South	(b)	354	44.2	125.2	53.5	222.9	229.0	1.03
	North				125.2	80.3	249.7	263.0	1.05
G3-East	South	(c)	455	57.3	126.4	54.8	238.5	237.0	0.99
	North				126.4	54.8	238.5	235.0	0.99
G3-West	South	(d)	786*	97.9	126.4	54.8	279.1	239.0	0.86
	North				126.4	54.8	279.1	263.0	0.94

* Includes both faces of webs

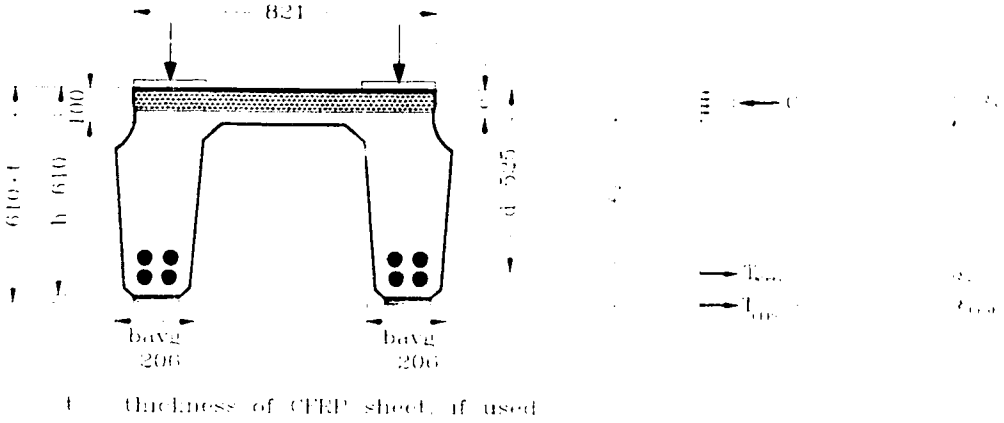

(a)

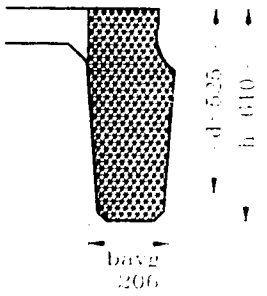

(b)

Figure 5.1 Cross-sections used for flexure and shear calculations

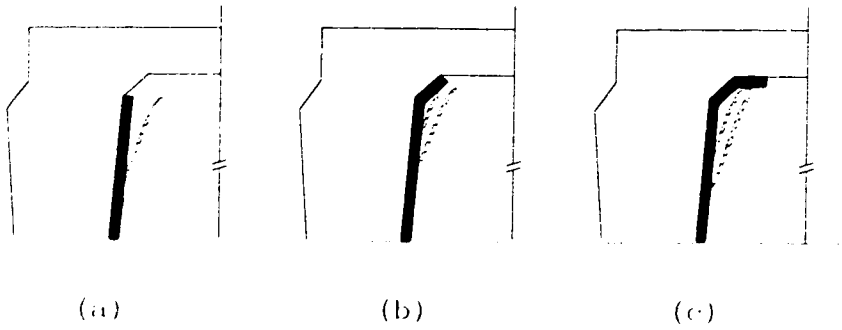

Figure 5.2 CFRP sheet details at top edge at failure

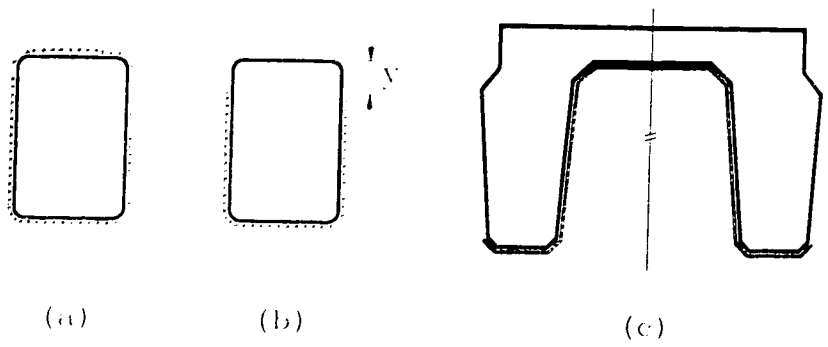

Figure 5.3 CFRP sheet application

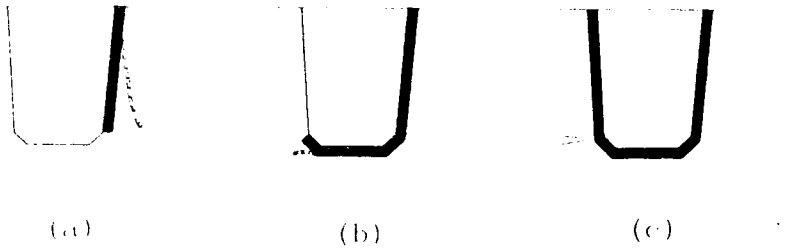

Figure 5.4 CFRP sheet details at bottom edge at failure

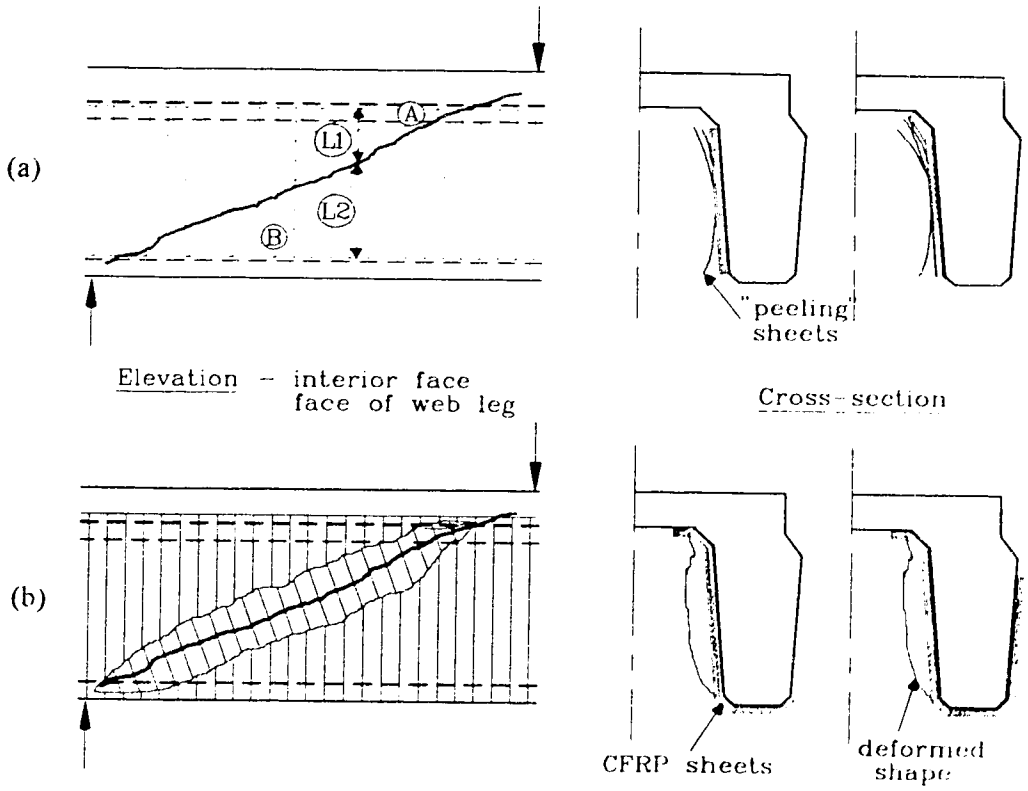

Figure 5.5 Progression of failure of cracked section

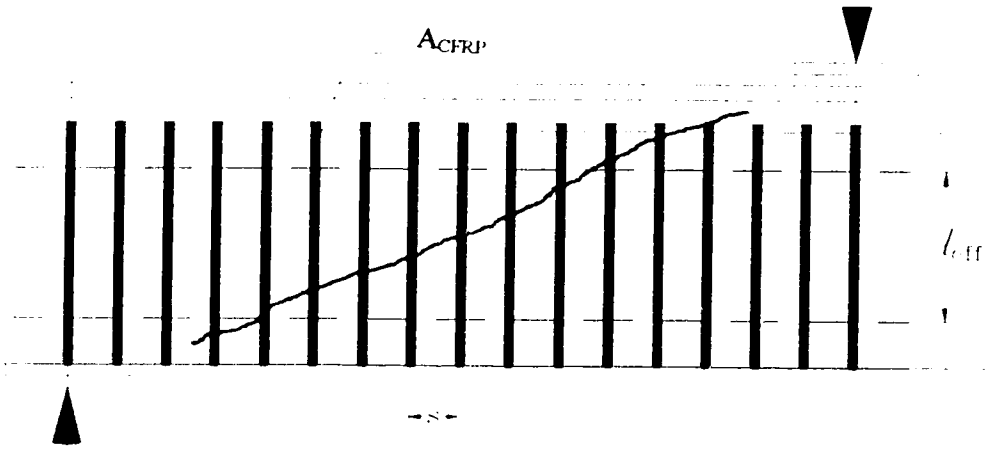

Figure 5.6 Truss equation definitions

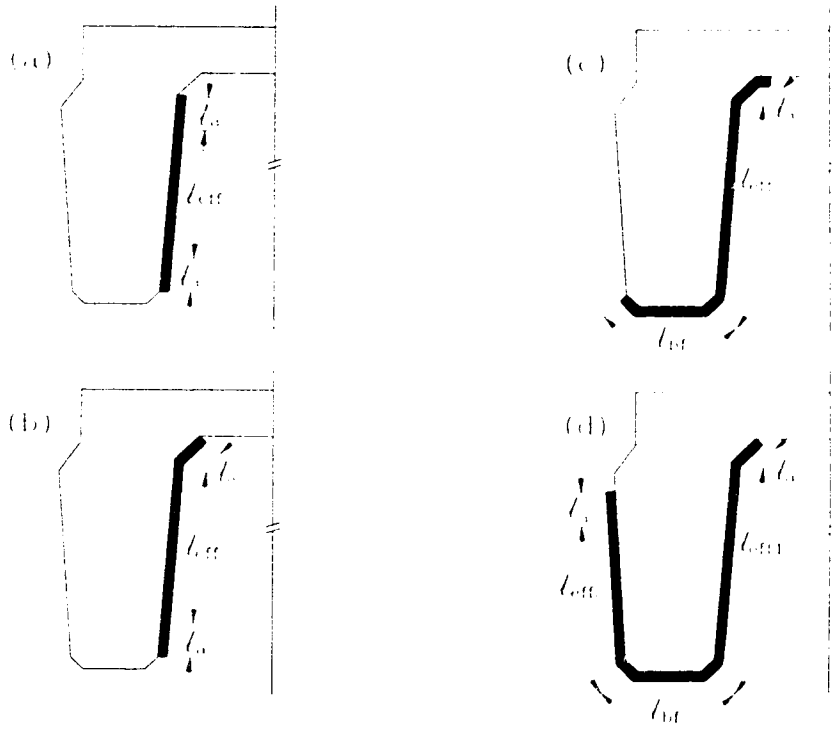

Section	Diagram	l (mm)	l_a (mm)	l_{a2} (mm)	l_{eff} (mm)
Girder 1, East	(a)	430	75 + 75		280
Girder 2, East	(a)	430	75 + 75		280
Girder 2, West	(b)	504	75 + 75		354
Girder 3, East	(c)	700	75	170	455
Girder 3, West	(d)	1070	75 + 75	134	786

Figure 5.7 Effective lengths of bonded CFRP sheets

6.0 Summary, Conclusions and Recommendations

6.1 Summary

The behaviour of concrete girders strengthened for shear with externally-bonded carbon fibre reinforced plastic (CFRP) sheets was investigated.

The experimental program included the testing of full-scale hat-shaped pre-cast reinforced concrete bridge girders which had been salvaged from a demolished highway bridge. This type of girder had been found to be shear deficient due to insufficient transverse steel. The bonded CFRP sheets were used to increase the shear capacity of the girders. A total of eight tests were carried out on three members, five shear tests and three flexural tests. By post-strengthening the member after failing the first shear span, it was possible to perform more than one test on each girder.

The CFRP sheets were bonded to the vertical faces of the webs in four different patterns. Either one or two layers of CFRP sheets were used, oriented vertically and/or horizontally. The main parameter studied was the length of sheets used, and the degree of anchorage provided. The influence of the bonded CFRP sheets on the ultimate shear strength, stiffness, ductility and cracking of the strengthened girders was investigated.

The analytical work included determining the capacity of the unstrengthened girder and the contribution of the CFRP sheets to the shear capacity of the section. Mechanisms were described by which the bonded sheets acted to provide additional strength. A design approach was proposed to predict the capacity of the girders strengthened with bonded CFRP sheets.

6.2 Conclusions

Despite the limitations inherent in using pre-existing specimens, and the limited number of tests that were carried out, several conclusions can be drawn from the results of this investigation:

(1) The CFRP sheets bonded to the web faces of the girders increased the shear capacity of the members by 21% to 55% over the control section. These results were

obtained empirically based on test results by calculating the amount of shear carried by both the concrete and the internal steel stirrups and attributing the remainder of the shear carried by a section to the bonded sheets. The bonded CFRP sheets provided a shear resistance contribution amounting to 17% to 31% of the shear capacity of the section

(2) The failures of the specimens were ultimately governed by the strength of the concrete, rather than by the strength of the bonded sheets. The bonded sheets did not change the fundamental shear failure mode of the specimens, which was always by diagonal tension. They did not postpone the onset of first diagonal cracking. However, they did help keep the cracked section together once cracks began to develop. At the highest load levels reached, concrete crushing could be clearly seen in the web as well as in the flexural compression zone. The bond between the CFRP sheets and the concrete substrate was generally excellent, provided the concrete surface was adequately prepared. Failure never was precipitated by failure in the bondline. The progression of failure of the sheets invariably began at the edges of the sheets, where the shear stresses are highest. Under increasing load, and depending on the bonded length and degree of anchorage provided, the sheets began to peel away a layer of concrete. This suggests that a lower fibre content would provide adequate strength.

(3) The small block tests did not test the breaking strength of the CFRP sheets, but rather the strength of the composite CFRP/concrete system. The stress reached, only about 25% of the specified CFRP material strength, reflects the effect of concrete strength and possible existing stress raisers at edges of the blocks etc. This type of test may be a more realistic manner by which to determine the strength of materials in bonding applications as it more closely represents the actual situation.

(4) Based on test observations, the bonded CFRP sheets can contribute to the shear capacity of the members by two possible mechanisms. First, the bonded sheets can help keep cracks small, thus increasing the shear friction component of the concrete contribution to shear strength. Second, the vertical bonded sheets may act as a series of small stirrups.

(5) The vertical length of the bonded sheet and anchorage of the sheets were important parameters. The longer the bonded length provided, the better the performance of the strengthened member. Anchorage may be improved if longer bonded lengths are

provided or if means of anchorage is provided, preferably not within a zone of high shearing stresses.

(6) The existing truss equation used for determining the shear capacity of a reinforced concrete member was modified in order that it could be used to predict the capacity of a CFRP strengthened concrete section. The parameters used were developed based on the particular members tested in the experimental program. The effective stress used was based on the block tests which are an indication of concrete/CFRP composite behaviour rather than CFRP material strength. The modified equation reasonably predicted the shear resistance provided by the sheets, though its validity must still be confirmed for other more general cases

(7) The contribution of the horizontal sheets to shear capacity of the section was not as evident as was the contribution of the vertical sheets. Specimens strengthened with only the one layer of vertical CFRP performed as well as the specimens also strengthened with a second layer of horizontal CFRP. However, because the horizontal sheets can also contribute to crack control, it is expected that if a single layer of horizontal sheet was used without vertical sheets, the strength of the section would still increase due to an increase in the shear friction term.

(8) The flexural failures of Girders 2 and 3 were precipitated by the sudden breaking of the longitudinal CFRP sheets due to localized pressure applied either by the external steel stirrups, or by overlying sheets. This demonstrates the sensitivity of this CFRP material to transverse pressure; irregularities in the concrete surface, for example ridges caused by formwork, may cause premature failure. This problem must either be designed for or alleviated somehow.

6.3 Recommendations for Further Study

(1) A more rigorous and controlled experimental program should be carried out with appropriately designed laboratory specimens. This would allow a parametric study to be carried out and the results could be extended to a general cross-section. The validity of the proposed truss equation for calculation of CFRP contribution to shear strength must be verified for the general case.

(2) Means of mechanically anchoring the sheets to the substrate should be investigated to prevent or postpone peeling from the edge. This is particularly important when it is not possible to bond the sheets over the full depth of the member. Alternatively, it may be possible to apply the strengthening sheets in such a manner that would help offset the effect of the high shear stresses at the ends of the sheets.

(3) Tests should be carried out on specimens which have only horizontal sheets bonded to the webs to investigate the effect of this strengthening detail on shear strength. This will also contribute to flexural capacity to some extent, which may or may not be desirable. Also of interest is the behaviour of members strengthened for shear using fibres oriented at ±45° which may be preferable in some situations.

(4) The testing program described in this thesis was limited to the use of one particular type of carbon FRP. There are numerous products, utilizing various types of fibres, which may be used. A testing program comparing different materials for a particular kind of application, for example bridge retrofitting, would provide valuable information.

(5) Many non-strength questions concerning FRP's remain to be answered. Testing should be carried out to investigate the behaviour of FRP strengthened beams under the influence of fatigue loading, extreme low temperatures, cyclic temperature, creep, moisture, and durability under various environmental conditions.

(6) Information gained from use of FRP's in real structures is limited. It would be extremely valuable to implement the shear strengthening technique on a real structure and monitor its performance over an extended period, under realistic environmental conditions.

References

AASHO. 1957. Standard specifications for highway bridges, 7th ed. American Association of State Highway Officials, Washington, D.C.

AASHTO. 1989. Standard specifications for highway bridges. 14th ed. American Association of State Highway and Transportation Officials, Washington, D.C.

ACI-ASCE Committee 426. 1974. The shear strength of reinforced concrete members. American Society of Civil Engineers.

ASTM Standard C 42-90. 1990. Standard test method for obtaining and testing drilled cores and sawed beams of concrete. American Society for Testing Materials, pp. 27-30.

ASTM Standard C 617-87. 1987. Standard practice for capping cylindrical concrete specimens. American Society for Testing Materials, pp. 306-309.

ASTM Standard D 3039-76. 1976. Standard test method for tensile properties of fiber-resin composites. American Society for Testing Materials, pp. 118-148.

Alberta Transportation and Utilities. 1993. Standard Alberta truck loads. Personal communications, June 1993.

An, W., Saadatmanesh, H., and Ehsani, M.R. November 1991. R/C beams strengthened with FRP plates. II: Analysis and parametric study. ASCE Journal of Structural Engineering, Vol. 117, No. 11, pp. 3434-3455.

Andrews, G., and Sharma, A.K. 1990. Repaired reinforced concrete beams failing in shear. Concrete International, March, pp. 53-57.

Ballinger, C.A. 1992. Development of fibre-reinforced plastic products for the construction market - How has and can it be done? Proceedings of the First International Conference on Advanced Composite Materials in Bridges and Structures, Sherbrooke, Que., pp. 3-13.

Bartlett, F.M. and MacGregor, J.G. 1994. Prediction of in situ concrete strength from a core test. Structural Engineering Report No. 198, Department of Civil Engineering, University of Alberta, Edmonton, Alta.

Bickley, J.A., Neale, K.W., and Fabbruzzo, G. 1992. Market potential and identification of suppliers of advanced industrial materials for construction of bridges and other structures. Report by John A. Bickley Associates Ltd., Consulting Engineers, Toronto, Ont.

Bresson, J. 1972. Renforcement par collage d'armatures du passage inferieur du CD 126 sous l'autoroute du Sud. Annales de l'Institut Technique du Batiment et des Travaux Publics, No. 297, September, pp. 3-30. (In French)

Bruce, R. 1990. Fiber reinforced plastic bridges in Chongqing. IABSE Symposium: Mixed Structures, including New Materials, Brussels, Belgium, pp. 581-586.

CAN/CSA-A23.2-9C. 1990. Compressive strength of cylindrical concrete specimens. Canadian Standard Association, Rexdale, Ont., March 1990, pp. 230-236.

CAN/CSA-A23.2-13C. 1990. Splitting tensile strength of cylindrical concrete specimens. Canadian Standard Association, Rexdale, Ont., March 1990, pp. 242-246.

CAN/CSA-A23.3-M84. 1984. Design of concrete structures. Canadian Standard Association, Rexdale, Ont.

CAN/CSA-S6-M88. 1988. Design of highway bridges. Canadian Standards Association, Rexdale, Ont.

Calder, A.J.J. 1988. Exposure tests on externally reinforced concrete beams -- Performance after 10 years. Research Report 129, Transport and Road Research Laboratory, Department of Transport, Crowthorne, U.K., p.1-10.

Calder, A.J.J. 1989. Exposure tests on 3.5 m externally reinforced concrete beams -- the first eight years. Research Report 191, Transport and Road Research Laboratory, Department of Transport, Crowthorne, U.K., p.1-16.

Deblois, M., Picard, A., and Beaulieu, D. 1992. Renforcement de poutres en beton arme a l'aide de materiaux composites : Etudes theorique et experimentale. Proceedings of the First International Conference on Advanced Composite Materials in Bridges and Structures, Sherbrooke, Que., pp. 265-275. (In French)

Dussek, I.J. 1980. Strengthening of bridge beams and similar structures by means of epoxy-resin-bonded external reinforcement. Transportation Research Record 785, Transportation Research Board, Crowthorne, U.K., pp. 21-24.

Dutta, F.K. 1989. Fiber composite materials in an arctic environment. Proceedings of the Sessions Related to Structural Materials at Structures Congress 1989 (ASCE), San Francisco, Cal., pp. 216-225.

Eberline, D.K., Klaiber, F.W., and Dunker, K. Bridge strengthening with epoxy-bonded steel plates. Transportation Research Record 1180, Transportation Research Board, National Research Council, Washington, D.C., pp. 7-11.

Engineering News Record. 1993. Swiss bridges get fiber fix. ENR, Vol. 230, No. 6, p. 21.

Erki, M. A., and Rizkalla, S.H. 1993. FRP reinforcement for concrete structures. Concrete International, June, pp. 48-53.

Fleming, C. J., and King, G.E.M. 1967. The development of structural adhesives for three original uses in South Africa. Bulletin Rilem, No. 37 (December), pp. 244-251.

Head, P.R. 1992. Design methods and bridge forms for the cost effective use of advanced composites in bridges. Proceedings of the First International Conference on Advanced Composite Materials in Bridges and Structures, Sherbrooke, Que., pp. 15-31.

Hilado, C.J., editor. 1979. Carbon reinforced epoxy systems, Part V. Materials Technology Series, Vol. 13. Technomic, Lancaster, Penn.

Holloway, L.C., editor. 1990. Polymers and polymer composites in construction. Thomas Telford, London, U.K.

Holloway, L. 1993. Polymer composites for civil and structural engineering. Chapman & Hall, London, U.K.

Hugenschmidt, F. 1976. Epoxy adhesives for concrete and steel. Proceedings of the First International Congress on Polymer Concrete, London, U.K., pp. 195-209.

Ichimazu, H., Maruyama, M., Watanabe, H., and Hirose, T. 1993a. RC slabs strengthened by bonded carbon FRP plates: Part I - Laboratory study. Fiber-Reinforced-Plastic Reinforcement for Concrete Structures - International Symposium, ACI SP-138, Vancouver, B.C., pp. 933-955.

Ichimazu, H., Maruyama, M., Watanabe, H., and Hirose, T. 1993b. RC slabs strengthened by bonded carbon FRP plates: Part II - Application. Fiber-Reinforced-Plastic Reinforcement for Concrete Structures - International Symposium, ACI SP-138, Vancouver, B.C., pp. 957-965.

Iyer, S.L., Sivaramakrishnan, C., and Atmaram, S. 1989. Testing of reinforced concrete bridges for external reinforcement. Proceedings of the Sessions Related to Structural Materials at the (ASCE) Structures Congress '89, San Francisco, Cal., pp. 116-122.

Johnson, R. P., and Tait, C.J. 1981. The strength in combined bending and tension of concrete beams with externally bonded reinforcing plates. Building and Environment, Vol. 16, No. 4, pp. 287-299.

Jones, R., Swamy, R.N., and Bloxham, J. 1987. Crack control of reinforced concrete beams through epoxy bonded steel plates. Proceedings of the International Conference on Adhesion between Polymers and Concrete, Aix-en-Provence, France, pp. 542-555.

Jones, R., Swamy, R.N., Bloxham, J., and Bouderbalah, A. 1980. Composite behaviour of concrete beams with epoxy-bonded external reinforcement. International Journal of Cement Composites and Lightweight Concrete, Vol. 2, No. 2, pp. 91-107.

Jones, R., Swamy, R.N., and Charif, A. 1988. Plate separation and anchorage of reinforced concrete beams strengthened by epoxy-bonded steel plates. The Structural Engineer, Vol. 66, No. 11, pp. 85-94.

Jones, R., Swamy, R.N., and Salman, F.A.R. 1985. Structural implications of repairing by epoxy-bonded steel plates. Proceedings of the Second International Conference on Structural Faults and Repair, London, U.K., pp. 75-80.

Kaiser, Hanspeter. 1989. Bewehren von Stahlbeton mit kohlenstoffaserverstarkten Epoxidharzen. Ph.D. Dissertation ETH Nr. 8918, Zurich, ETH. (In German)

Karam, G.N. 1992. Optimal design for prestressing with FRP sheets in structural members. Proceedings of the First International Conference on Advanced Composite Materials in Bridges and Structures, Sherbrooke, Que., pp. 277-285.

Khalifa, M. A., Kuska, S.S.B., and Krieger, J. 1993. Bridges constructed using fiber reinforced plastics. Concrete International, June, pp. 43-47.

Klaiber, F.W., Dunker, K.F., Wipf, T.J., and Sanders, W.W. 1987. Methods of strengthening existing highway bridges. NCHRP Research Report No. 293 (September), Transportation Research Board, Crowthorne, U.K.

Klein, G. J., and Popovic, P.L. 1985. Shear strength evaluation of existing concrete bridges. Strength Evaluation of Existing Concrete Bridges, ACI SP-88, pp. 199-224.

Ladner, M. 1983. Reinforced concrete members with subsequently bonded steel plates. Proceedings of the International Association for Bridge and Structural Engineering Symposium, Vol. 46: Strengthening of Building Structures - Diagnosis and Therapy, Venice, Italy, pp. 203-211.

Leonhardt, F., and Walther, R. 1964. The Stuttgart shear tests, 1961. Cement and Concrete Association, London, U.K.

Lloyd, G.O., and Calder, A.J. 1982. The microstructure of epoxy bonded steel-to-concrete plates. Report SR 705, Transport and Road Research Laboratory, Crowthorne, U.K.

Lowe, P.G. 1991. Externally reinforced concrete - A new structural material and repair medium. Proceedings of the Innovation and Economics in Building Conference, Brisbane, Australia, pp. 14-17.

Macdonald, M.D. 1978. The flexural behaviour of concrete beams with bonded external reinforcement. Report SR 415, Transport and Road Research Laboratory, Crowthorne, U.K.

Macdonald, M.D. 1982. The flexural performance of 3.5m concrete beams with various bonded external reinforcement. Report SR 728, Transport and Road Research Laboratory, Crowthorne, U.K.,

MacGregor, J.G. 1992. Reinforced concrete - Mechanics and design. Prentice Hall, Englewood Cliffs, N.J.

McKenna, J.K., 1993. Post strengthening of reinforced concrete members using fibre composite materials. M.Eng. Thesis, Royal Military College of Canada.

McKenna, J., and Erki, M.A. 1994. Strengthening of reinforced concrete flexural members using externally applied steel plates and fibre composite sheets -- a survey. Canadian Journal of Civil Engineering, Vol. 21, No. 1, pp. 16-24.

Mays, G.C., and Hutchinson, A.R. 1992. Adhesives in civil engineering. Cambridge University Press, Cambridge, U.K.

Mays, G., and Calder, A. 1988. External plates extend reinforcement's reach. Concrete (London), Vol. 22, November, pp. 25-28.

Meier, U., Deuring, M., Meier, H., and Schwegler, G. 1992. Strengthening of structures with CFRP laminates : Research and applications in Switzerland. Proceedings of the First International Conference on Advanced Composite Materials in Bridges and Structures, Sherbrooke, Que., pp. 243-251.

Meier, U., and Kaiser, H. 1991. Strengthening of structures with CFRP laminates. Proceedings of the ASCE Specialty Conference: Advanced Composite Materials in Civil Engineering Structures, Las Vegas, Nev., pp. 224-233.

Miesseler, H.J., and Wolff, R. 1991. Experience with fiber composite materials and monitoring with optical fiber sensors. Advanced Composites Materials in Civil Engineering Structures, Las Vegas, Nevada, pp. 167-181.

Mufti, A.A., Erki, M.A., and Jaeger, L.G., editors. 1991. Advanced composite materials with applications to bridges. Canadian Society for Civil Engineering, Montreal, Que.

Mufti, A.A., Erki, M., and Jaeger, L.G. 1992. Advanced composite materials in bridges and structures in Japan. Canadian Society for Civil Engineering, Montreal, Que.

Oehlers, D. J. 1992. Reinforced concrete beams with plates glued to their soffits. ASCE Journal of Structural Engineering, Vol. 118, No. 8, pp. 2023-2038.

Oehlers, D.J. 1990. Strengthening reinforced concrete beams by bonding steel plates to their soffits. Proceedings of the Second Annual Structural Engineering Conference of the Institution of Engineers of Australia, Adelaide, Australia, pp. 346-350.

Pakvor, A. 1991. Rehabilitation and reconstruction of concrete structures. Evaluation and Rehabilitation of Concrete Structures and Innovations in Design - Proceedings of the ACI International Conference, (SP-128), Hong Kong, pp. 1407-1422.

Park, R., and Paulay, T. 1975. Reinforced concrete structures. John Wiley & Sons, New York, N.Y.

Parkinson, J. 1978. Glue solves a sticky problem for Gestetner. New Civil Engineer, Vol. 310, September 14th, pp. 26-27.

Plevris, N., and Triantafillou, T.C. 1994. Time-dependent behavior of RC members strengthened with FRP laminates. ASCE Journal of Structural Engineering, Vol. 120, No. 3, pp. 1016-1037.

Raithby, K.D. 1980. External strengthening of concrete bridges with bonded steel plates. Report SR 612, Transport and Road Research Laboratory, Crowthorne, U.K.

Ramsay, B. 1990. Evaluation and strengthening of concrete T-girder bridges for shear. Developments in Short and Medium Span Bridge Engineering, Toronto, Ont., pp. 381-391.

Regan, P. E. 1993. Research on shear: a benefit to humanity or a waste of time? The Structural Engineer, Vol. 71, No. 19, pp. 337-347.

Ritchie, P. A., Thomas, D.A., Lu, L., and Connelly, G.M. 1991. External reinforcement of concrete beams using fiber reinforced plastics. ACI Structural Journal, Vol. 88, No. 4, pp. 490-500.

Rostasy, F.S., Hankers, C., and Ranisch. E.-H. 1992. Strengthening of R/C- and P/C-structures with bonded FRP plates. Proceedings of the First International Conference on Advanced Composite Materials in Bridges and Structures, Sherbrooke, Que., pp. 253-263.

Saadatmanesh, H., and Ehsani, M.R. 1990. Fiber composite plates can strengthen beams. Concrete International, No. March, pp. 65-70.

Saadatmanesh, H., and Ehsani, M. 1989. Application of fiber-composites in civil engineering. Proceedings of the Sessions Related to Structural Materials at Structure's Congress 1989, San Francisco, Cal., pp. 526-535.

Saadatmanesh, H., and Ehsani, M.R. 1991. RC beams strengthened with GFRP plates. I: Experimental study. ASCE Journal of Structural Engineering, Vol. 117, No. 11, pp. 3417-3433.

Sharif, A., Al-Sulaimani, G.J., Basunbul, I.A., Baluch, M.H., and Ghaleb, B.N. 1994. Strengthening of initially loaded reinforced concrete beams using FRP plates. ACI Structural Journal, Vol. 91, No. 2, pp. 160-168.

Swamy, R. N., Jones, R., and Charif, A. 1989. The effect of external plate reinforcement on the strengthening of structurally damaged RC beams. The Structural Engineer, Vol. 67, No. 3, pp. 46-56.

Swamy, R.N., and Jones, R. 1991. Plate bonding technology - The painless technique of structural rehabilitation. Proceedings of the ACI International Conference, Evaluation and Rehabilitation of Concrete Structures and Innovations in Design, Hong Kong, ACI SP-128, pp. 1385-1405.

Swamy, R. N., Jones, R., and Bloxham, J.W. 1987. Structural behaviour of reinforced concrete beams strengthened by epoxy-bonded steel plates. The Structural Engineer, Vol. 65A, No. 2, pp. 59-68.

Tankut, A.T., and Ersoy, U. 1991. Behaviour of repaired/strengthened reinforced concrete structural members. Proceedings of the ACI International Conference, Evaluation and Rehabilitation of Concrete Structures and Innovations in Design, Hong Kong, ACI SP-128, pp. 1257-1276.

Taylor, D. C., and Dykes, J. 1992. Plate bonding - a Scottish case study. Highways and Tranportation, Vol. 39, No. 7.

Theillout, J. N. 1986. Repair and strengthening of bridges by means of bonded plates. ISAP, pp. 601-621.

Toensmeyer, M. R., and Cook, J.P. 1981. Repair of torsionally inadequate concrete beams by use of adhesively bonded plates. Transportation Research Record, Vol. 821, pp. 79-81.

Triantafillou, T. C., and Deskovic, N. July 1991. Innovative prestressing with FRP sheets: Mechanics of short-term behavior. ASCE Journal of Engineering Mechanics, Vol. 117, No. 7, pp. 1652-1672.

Triantafillou, T. C., and Deskovic, N. 1992a. Prestressed FRP sheets as external reinforcement of wood members. ASCE Journal of Structural Engineering, Vol. 118, No. 5, pp. 1270-1284.

Triantafillou, T.C., and Meier, U. 1992b. Innovative design of FRP combined with concrete. Proceedings of the First International Conference on Advanced Composite Materials in Bridges and Structures, Sherbrooke, Que., pp. 491-500.

Triantafillou, T. C., Deskovic, N., and Deuring, M. 1992c. Strengthening of concrete structures with prestressed fiber reinforced plastic sheets. ACI Structural Journal, Vol. 89, No. 3, pp. 235-244.

Triantafillou, T., and Plevris, N. 1991. Post-strengthening of R/C beams with epoxy-bonded fiber composite materials. Advanced Composites Materials in Civil Engineering Structures, Las Vegas, Nevada, pp. 245-256.

Van Ge[illegible]n D.A. 1982. Repairing of concrete structures by externally bonded steel plates. Proceedings of the ICP/RILEM/IBK International Symposium on Plastics in Material and Structural Engineering, Prague, Czechoslovakia, pp. 519-526.

Van Gemert, D.A., and Vanden Bosch, M.C.J. 1985. Repair and strengthening of reinforced concrete structures by means of epoxy bonded steel plates. Proceedings of the International Conference on Deterioration, Bahrain, pp. 181-193.

Wyett, G.W. 1990. Steel plate bonding - Recent Australian examples. Second National Structural Engineering Conference, Adelaide, Australia, pp. 341-343.

Zsutty, T. C. 1968. Beam shear strength prediction by analysis of existing data. ACI Journal, Proceedings, Vol. 65, No. 11, pp. 943-951.

Appendix A
Preliminary Tests at CFER

A.1 Summary

This appendix summarizes the CFER (Centre for Frontier Engineering Research) testing program, designed by the Bridge Engineering Branch of Alberta Transportation and Utilities and carried out six months prior to the experimental work presented in the main body of this thesis. A total of four Type 'E' precast hat-shaped girders, removed from the same bridge, was tested. The girders were identical in design to those that were tested as part of the main experimental program, described in Chapters 3 through 5, although they were removed from a different bridge. The Type 'E' girder has been described in detail in Chapter 3 of the main body of this thesis. The elevation and cross-section of the Type 'E' girder are shown in Figures 3.2 and 3.3. The main objective of the CFER testing program was to determined the shear capacity of the Type 'E' girder prior to strengthening in order to compare to analyses that had been carried out which indicated that the Type 'E' girder was shear deficient. The ductility of the member and the post-cracking behaviour were also of interest.

Three tests were carried out in total. The first two were of single 9.14 m and 12.2 m girders, respectively. The third test involved two 9.14 m girders grouted together longitudinally to model the condition in which they form the superstructure of the bridge. The intent was to fail all the specimens in shear; hence, an unsymmetrical load arrangement was chosen, with a single load point and two unequal shear spans, chosen such that failure would occur in a localized region.

The test set-up and instrumentation used is described in Section A.2. The results of the tests, ultimate loads and behaviour, are described in Section A.3. This includes a description of the progression of failure, and some of the measurements made. The analysis and predictions made are included in Section A.4, while Section A.5 summarizes the results of an evaluation of the Type 'E' girder bridge.

A.2 Test Set-up and Instrumentation

The loading consisted of a single concentrated load at the section that was expected to be most critical in shear. This critical section occurred where the stirrup spacing

increased significantly, in the region where the stirrups began to alternate from leg to leg. Generally, this meant that the load was placed about a quarter of the span length from one support. Figure A.1 shows load and span layouts for all three tests, while Figure A.2 shows the load positions of the loading pads.

In Test A1, a single 9.14 m girder was loaded at 3.15 m from one end and supported over a 8.89 m simple span. Figure A.1 shows the load arrangement. The single load was distributed equally to the two legs of the web using two loading pads. Test A2 was performed on a 12.2 m girder loaded at approximately the fifth point. Since Test A1 ended with a flexural failure, the shear span was decreased for Test A2 (i.e., the shear to moment ratio was increased) in order to force a shear failure. As in Test A1, the load was distributed equally to both legs of the section. In Test A3, two 9.14 m girders were grouted together longitudinally and tested as a unit. The objective was to determine the behaviour of the grouted shear key and the extent to which the load was transferred from the interior legs to the exterior legs. In this case, the two loading pads rested on the interior (grouted) legs; both girders were therefore unsymmetrically loaded.

Loads and reactions were determined by two load cells (i.e., under each leg of the web) both at the load point and at the support at the shear span end of the girder. Vertical displacements were measured using 25 mm LVDT's at load points and at supports. Displacements at supports were measured because of the deflection of the neoprene pads under the supports

Longitudinal strains were measured near the load point, both at the top concrete fibre and at the location of the centroid of the longitudinal steel, on both sides of the channel (i.e., both legs of the web). These strains were measured using 200 mm Demec gauges, one reading taken at each load step.

Strains in the web were obtained at four locations longitudinally along the beam. These concrete strains were measured on both outer faces of the web legs using 200 mm Demec gauges. The Demec targets at each location were arranged to form a three-arm rosette with readings vertically, horizontally and at 45 degrees. Therefore, there was a total of eight rosettes, at four locations longitudinally. They were mounted centred at about 150 mm from the tension flange in order to be clear of the longitudinal reinforcing steel. The 200 mm gauge length was chosen in order to obtain an average strain over a

reasonable length. Figure A.3, A.5 and A.7 show the locations of the Demec and LVDT layouts.

In Tests A1 and A2, similar 200 mm rosettes using 2.5 mm LVDT's were installed on the inside face of the web legs at two locations along the beam corresponding to Demec rosette locations. This was done in order to compare web concrete strains across the cross-section in order to judge whether the rosettes on the outside face of one web leg gave a reasonable indication of the strain on the other face or in the other leg. This was important because when the girders were later grouted together (Test A3), it was no longer possible to install Demec rosettes on the outside faces of the each web. In Test A3, all six LVDT's were used at one location, forming a rosette on each interior web leg face.

A.3 Summary of tests and results

Table A.1 and A.2 contain, respectively, the results of the concrete core and steel reinforcement bar material tests. The concrete strength was found to vary significantly from girder to girder and to be 33% to 93% higher than the specified strength of f'_c of 27.6 MPa. Although concrete does gain strength with age, such increases seem excessive, even for 35 year old concrete. More likely, much higher strength concrete was originally provided. The steel strengths also varied considerably and were well above the specified strength of 276 MPa. Ductile failures were observed when these reinforcement specimens were tested in uniaxial tension.

A summary of the results of the girder tests is presented in Table A.3. Figure A.9 shows the load vs. deflection curves for all three tests.

A.3.1 Test A1 -- Single 9.14 m girder

The long shear span in Test A1 produced a condition of high moment to shear in the section, resulting in a flexural failure. Although shear cracks did develop and grow, the flexural cracking soon began to dominate around the loadpoint. Strains measured at strain rosettes are shown in Figure A.4 at two of the more highly stressed locations. Many cracks were already present in the web of the girder prior to loading. Generally this was flexural cracking in the central portion of the girder, but there were some inclined shear cracks near the supports, particularly at the west end (unloaded end). Vertical flexural

cracks began to appear at various locations along the girder at loads as low as P=80 kN. At about P=260 kN load, steep (~45 degrees) shear cracks began to appear about one metre from the support, i.e., around the point where the stirrups change from double to single. Around the load point, cracks originated within about 500 mm of the load and headed steeply up towards it. The cracks developing in these two regions eventually led to failure, widening more dramatically at about P=340 kN.

A.3.2 Test A2 -- Single 12.2 m girder

Although the 12.2 m girder, Test A2, had heavier flexural reinforcement than the 9.14 m girders, the shear reinforcement was the same, by design. That is, a greater proportion of the length of the girder has single stirrups spaced at the maximum. The weak section for shear was expected to be at the location where this maximum spacing began. In order to ensure failure was primarily by shear, the supports were moved inward to decrease the span length. The adjustment resulted in a shear failure.

Many cracks were present in the girder before testing, most of which were flexural. As the test began, flexural cracking began to appear at relatively low loads, about P=120 kN. Although this continued throughout the test, the flexural cracks did not propagate the way the shear cracks did. The shear cracks which eventually led to failure first appeared at a load of about P=420 kN and extended from the support to the load point. On the south face (south web leg) one such crack formation dominated. The average angle of this crack was about 30 degrees, although within about 600 mm of the load the crack travelled horizontally through the top flange. Two stirrups were crossed over the extent of the crack and as such contributed to the load carrying capacity. A second crack pattern at a slightly steeper angle (about 40 degrees) began between the first crack pattern and the load point. This did not grow as rapidly as the first pattern until the end of the testing and did not govern the failure. On the north face (north web leg), two prominent crack formations contributed to the failure. The one closer to the support travelled at an average angle of about 22 degrees. The one closer to the load was steeper (about 35 degrees) and, at its lower end, travelled horizontally near the level of the bottom steel towards the support.

The average angle of the principal strains as measured by the LVDT's at Location B was about 40 degrees. The Demec rosette on the opposite face of the same leg at this

location indicated an average principal strain angle which varied from about 20 degrees to about 45 degrees. At the same location on the opposite outer face of the web, Demecs at location F indicated an average strain angle of about 30-35 degrees. The Demec rosettes at locations A and E showed principal strain angles of about 35 and 30 degrees, respectively. The actual failure cracks were located between rosette locations A/E and B/F and the average angle of these cracks was about 20 degrees. Inspection of local cracking near the rosettes shows cracks progressing at much steeper angles than 20 degrees, at times as high as 45 degrees. The failure cracks passed quite close to this rosette location. The load-deflection diagram shows almost no ductility in the behaviour of this girder. However, from the time of diagonal cracking, it was possible to increase the load by 20%, allowing some advance warning before shear failure. Figure A.6 shows strain measurements at two of the strain rosettes.

A.3.3 Test A3 -- Double 9.14 m girders

The double girder arrangement in Test A3 made it more difficult to observe the progression of failure since most of the action occurred in the two adjacent inner legs, which were directly loaded. Cracks did not appear on the outer faces of outside legs until the higher load increments. On the north exterior face of the north specimen, cracks began to appear at about P=520 kN. On the south exterior face of the south specimen, cracks began to appear at about P=600 kN. Up until this time, cracks formed primarily on the inside legs, and these were the ones that eventually widened significantly, leading to failure. The shear cracking on the outside legs at higher loads indicates that these legs eventually picked up some of the load as the inside legs become overloaded and shed some of the load. Therefore, there was some load transfer from inner legs to outer with shear flow across the top flange.

At about P=600 kN, longitudinal cracking along the grout key (at the south grout/concrete interface) began to appear, eventually extending right to the east edge of the beam so that the two beams separated slightly. Failure occurred at about P=760 kN though the beams did carry some load beyond this. The cracks on the interior legs widened a great deal, as did the longitudinal crack along the shear key. There was also a punching failure around the load and interior legs.

In Test A3, the load was placed over the interior legs (Figure A.2). Therefore, both girders were loaded unsymmetrically. In this case, it was interesting to see how the load was transferred from interior legs to exterior legs of the web. In this test, an LVDT rosette was mounted directly on the other face of the same leg at the same location as Demec G. Unfortunately, the LVDT readings for the horizontal and diagonal arms of the rosette diverged almost immediately. Inspection of the interior of the webs after failure did not reveal any cracks passing through these arms that could have caused such extreme strain measurements. Therefore, it must be concluded that these two LVDT's failed to operate. The vertical LVDT matched the Demec G readings quite well for the first few load steps, then it too diverged wildly. Interestingly, the strains from the interior LVDT matched the strains measured from both Demecs C and G. This indicates that the strains were similar across the double girder cross-section, and that the two worked compositely. The strains measured by Demecs and LVDT's are compared in the shear vs. strain diagrams in Figure A.8.

Load cells were used only under the four legs at the support at the shear span end. These measured reactions can be used to estimate the fraction of the load which was transferred from the inner (loaded) legs to the outer (unloaded legs). Up until this cracking load, 80% or more of the total reaction was felt on the outside legs. Beyond this load, the proportion carried by the outer legs of the webs decreased steadily. At about P=700 kN, the load vs. deflection curve indicates another change in the way the reactions were distributed. In the south girder, the proportion of the reaction which was transferred to the outer leg continued to decrease. However, in the north girder, the proportion of the reaction transferred to the outer leg began to increase. On the load-deflection curve, P=700 kN is the point where the load began to level off. Failure eventually was triggered primarily in the south girder, as was confirmed by inspecting the crack formations on the inside of the webs after the test was completed . This was also indicated by the dropping of the south girder at the final load step. At the higher load increments, a longitudinal crack began to appear along the edge of the grout shear key on the south girder side. Evidently this contributed to the failure mode. The primary crack formation which led to this shear failure occurred on the inside leg of the south girder, at an angle of almost 30 degrees. This crack pattern travelled from the load point (centred near a stirrup) to the bottom of the next stirrup in that leg of the web. The other (outer) leg of this web did have a stirrup between these, but this stirrup was not intercepted by cracks which appeared on the inside face of this outer leg. These cracks were also at about 30 to 35

degrees. This behaviour indicated that the two legs of the web acted together even though the stirrups were not present at the same locations in both. Other shear cracks on the inner leg formed at even lower angles, as low as 20 degrees. Longitudinal cracking progressed along the flange/web interface, parallel to the shear key line.

A.4 Analysis and predictions

Using the actual material properties and several different methods of analysis, predictions of shear capacity were made. Figures A.10 and A.11 show the shear strength predictions by the S6-88 code, ACI code, the MCFT and Zsutty equation for Tests A2 and A3. Test A1 is not included as that girder failed by flexure. These methods are described in detail in Section 2.3. The analysis is complicated by the randomness of the widely spaced stirrups. The codes tend to neglect stirrups that are spaced too widely. However, even extremely widely spaced stirrups, if they happen to be in the right location in the span, can contribute significantly to the shear strength of the section.

The estimates provided by the different methods were not dramatically different, implying that equally reasonable estimates would be obtained by any of these means. It is more important and useful to know the material strengths of the specimens. The concrete strength determined from cores from the four girders described in this appendix were up to twice the specified strength. However, the concrete strengths determined from coring the girders of the main (CFRP strengthened) test series, were all quite similar and essentially identical to the specified strength (within 3%). Since the stirrup spacings also varied greatly from girder to girder (this applies to girder in both test series), it is difficult to decide what parameters should be used in the evaluation of such members. It may be most advisable to use the specified concrete strengths and stirrups spacings. Such an analysis is presented in the next section for the evaluation of Type 'E' girders.

A.5 Analysis and predictions

The evaluation of the Type 'E' girder bridges was carried out in accordance with Clause 12 of S6-88. The shear and flexural capacities were determined in accordance with

bridge was much lower, barely meeting the specified compressive strength. Unless a substantial coring program can be carried out, one cannot know what strength is available. Although the Clause 12 ratings indicate shear deficiencies, the ratios are still relatively high. It is likely that for some bridges it may be possible to increase this rating if, for example, coring showed that the concrete strength was substantially higher than specified.

Table A.1 Concrete core results (CFER tests)

Specimen	Number of Samples	f'_c (MPa)	σ (MPa)
Girder 1	5	45.2	2.67
Girder 2	5	53.1	2.05
Girder 3	5	36.9	2.10
Girder 4	4	52.0	1.71

σ: standard deviation

Table A.2 Steel coupon results (CFER tests)

Specimen	Number of Samples	f_y (MPa)	σ (MPa)
Longitudinal bars			
Girder 1	1	412.1	--
Girder 2	2	341.2	4.05
Girder 3	2	443.6	15.60
Girder 4	1	316.1	--
Stirrups			
Girder 1	2	397.8	14.95
Girder 2	2	398.1	3.45
Girder 3	2	387.2	6.50
Girder 4	2	398.4	6.50

σ: standard deviation

Table A.3 Summary of tests results of girder tests

Test	Length (m)	MTS Load (kN)	Shear (kN)	Moment (kNm)	Type of Failure
A1	9.14	340	219	692	Flexure
A2	12.2	540	428	941	Shear
A3	2 @ 9.14	760	585	1112	Shear

Note: Effect of own weight not included

Table A.4 Evaluation of Type 'E' girder bridge by Clause 12 of S6 -- Shear

Distance from end of girder (mm)	Factored dead loads V_D (kN)	Factored live loads V_L, for truck loading type: CS1 (kN)	CS2 (kN)	CS3 (kN)	Factored Resistance Vr (kN)	Live load resistance factor LLRF CS1	CS2	CS3
600	43.6	203.3	214.4	193.3	419.3	1.8	1.8	1.9
775	41.7	198.8	208.7	188.1	284.9	1.2	1.2	1.3
1000	39.2	193.1	201.3	181.4	284.9	1.3	1.2	1.4
1470	34.1	181.1	185.8	167.5	238.2	1.1	1.1	1.2
1980	28.5	168.1	169.0	152.3	234.2	1.2	1.2	1.4
2235	26.3	169.1	169.0	152.2	170.0	0.8	0.9	0.9
2910	18.7	151.1	151.0	136.0	170.4	1.0	1.0	1.1
3660	10.3	131.1	130.9	117.9	170.4	1.2	1.2	1.4

Table A.5 Evaluation of Type 'E' girder bridge by Clause 12 of S6 -- Flexure

Distance from end of girder (mm)	Factored dead loads M_D (kN)	Factored live loads M_L, for truck loading type: CS1 (kN)	CS2 (kN)	CS3 (kN)	Factored Resistance Mr (kN)	Live load resistance factor LLRF CS1	CS2	CS3
600	27.4	77.1	84.9	76.5	283.4	3.3	3.0	3.3
775	34.7	97.2	106.1	95.6	283.4	2.6	2.3	2.6
1000	43.5	119.7	131.2	118.2	283.4	2.0	1.8	2.0
1470	60.3	167.1	175.2	157.9	404.4	2.1	2.0	2.2
1980	75.8	207.8	210.3	189.5	522.0	2.1	2.1	2.4
2235	82.6	224.9	224.8	202.4	522.0	2.0	2.0	2.2
2910	97.0	259.4	259.3	233.4	522.0	1.6	1.6	1.8
3660	107.3	280.8	280.6	252.7	522.0	1.5	1.5	1.6

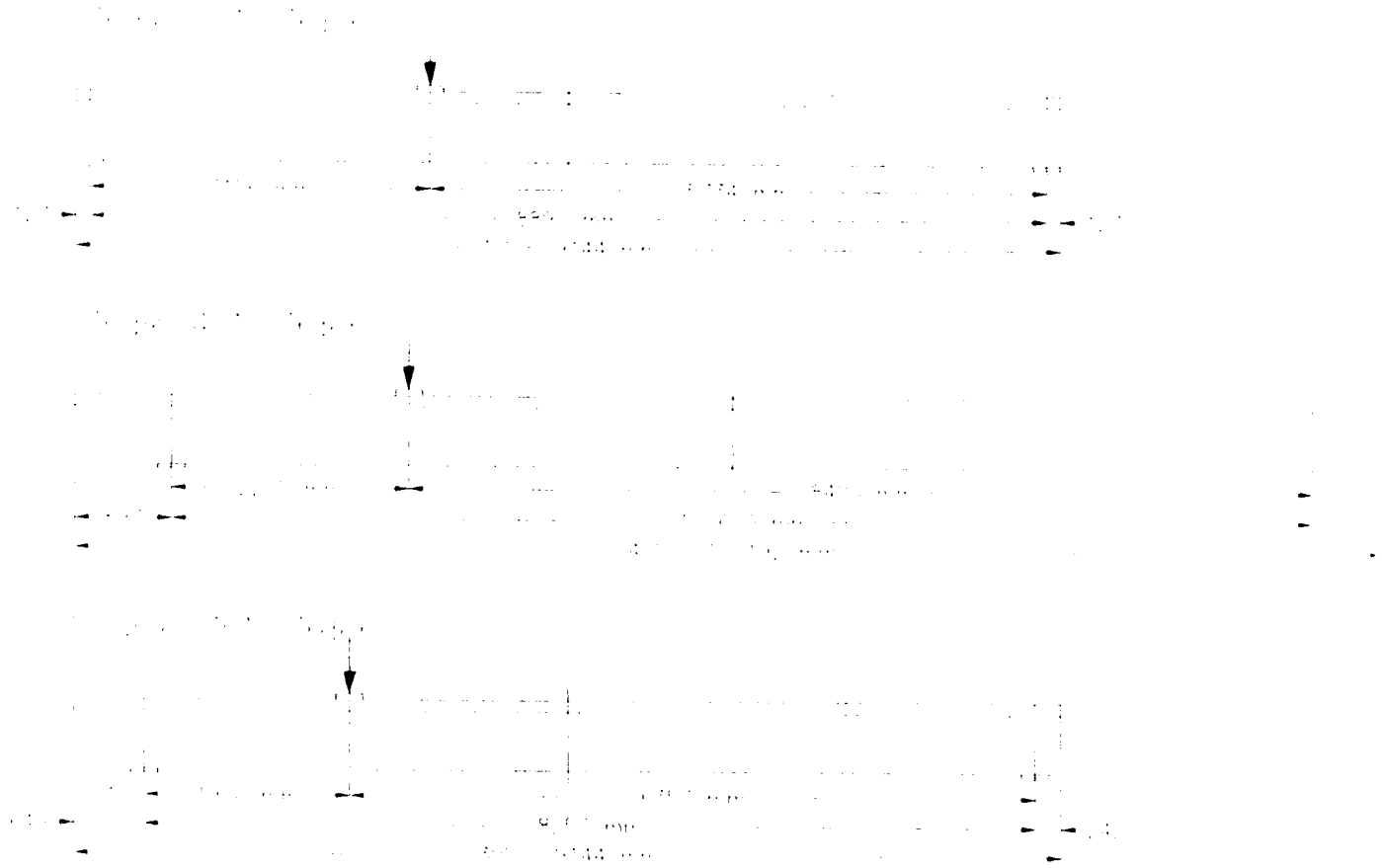

Figure A.1 Test layout for Tests #1, #2 and #3

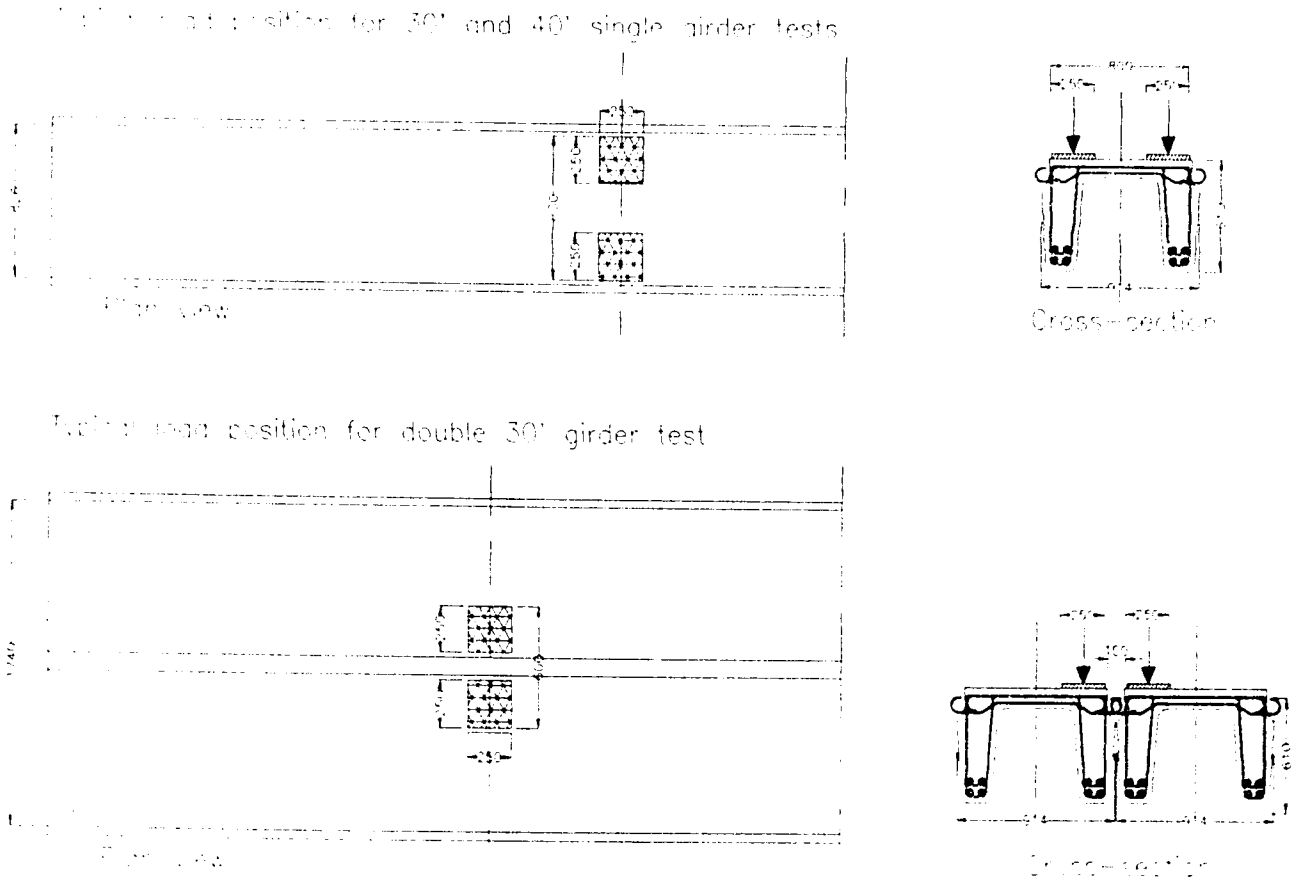

Figure A.2 Load positions for single and double girder tests

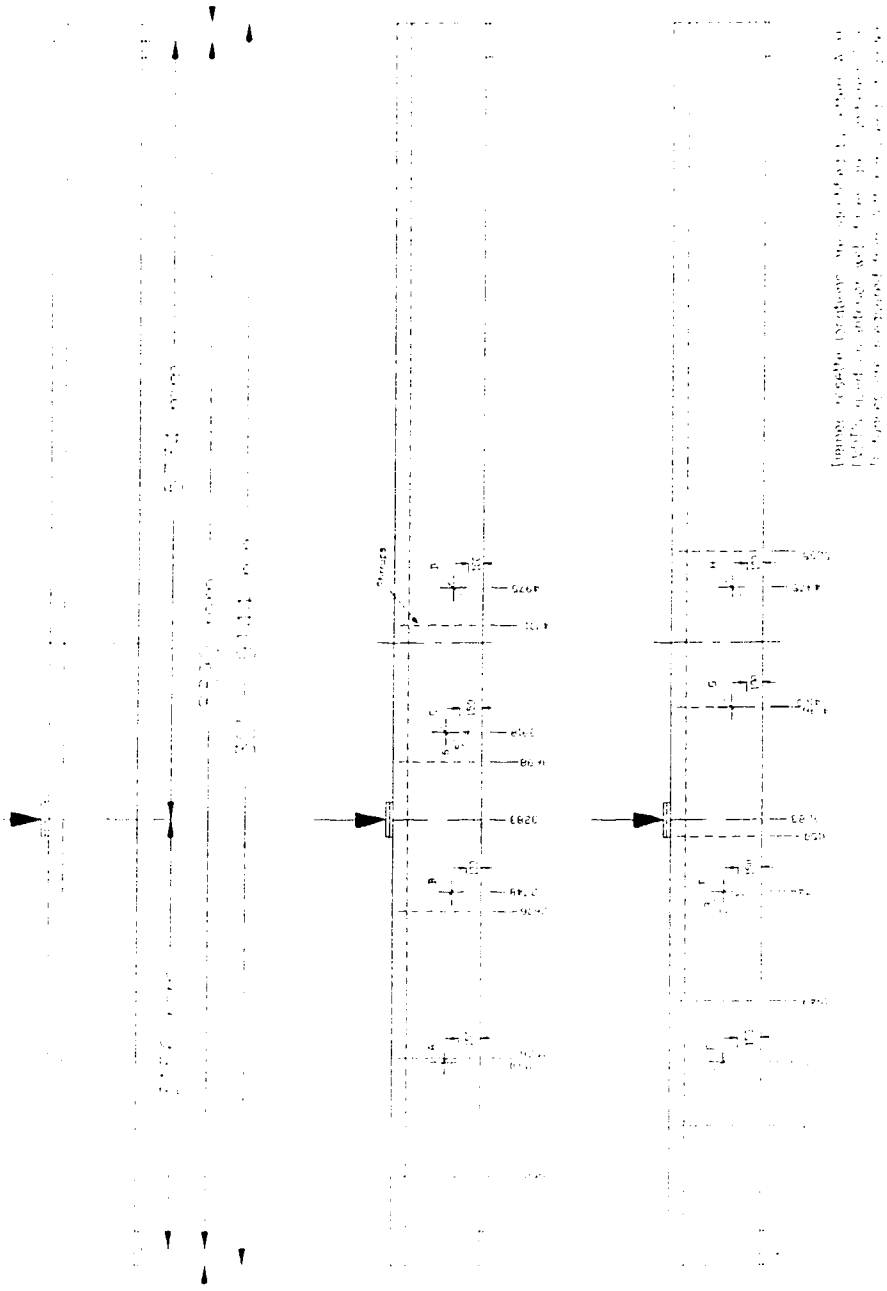

Figure A.3 Test A1 -- Single 9.14 m girder

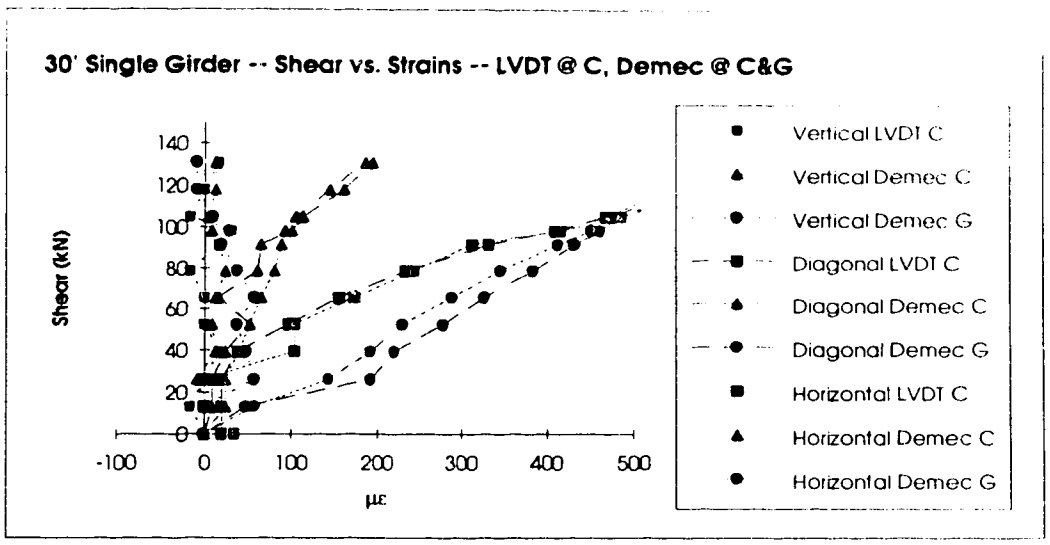

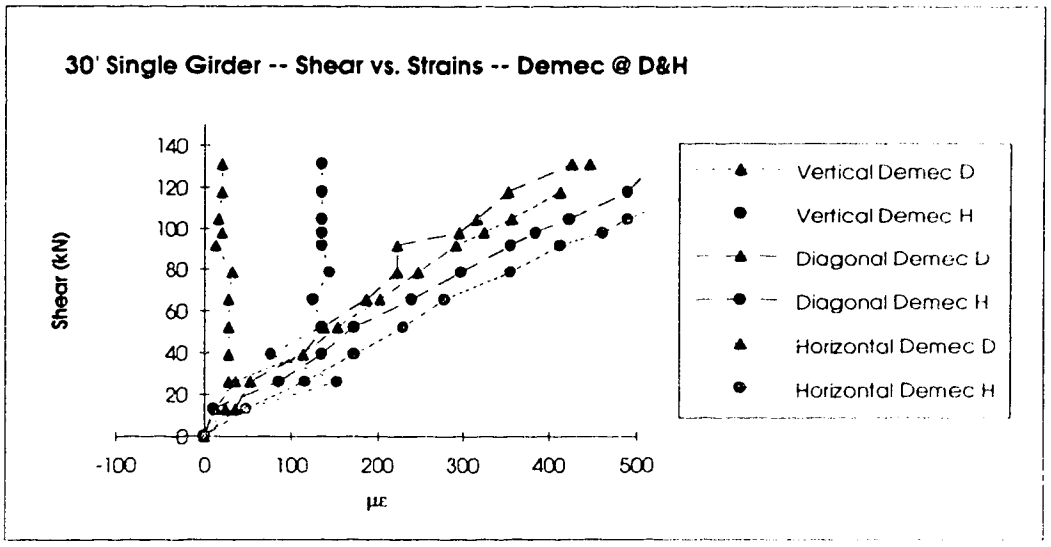

Figure A.4 Test A1 -- Strains vs. shear

Figure A.5 Test A2 -- Single 12.2 m girder

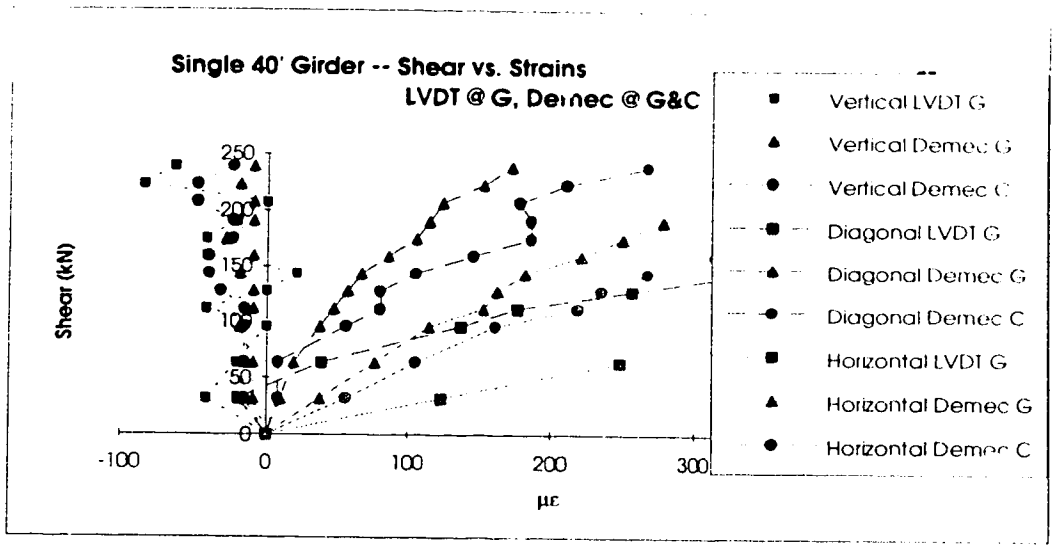

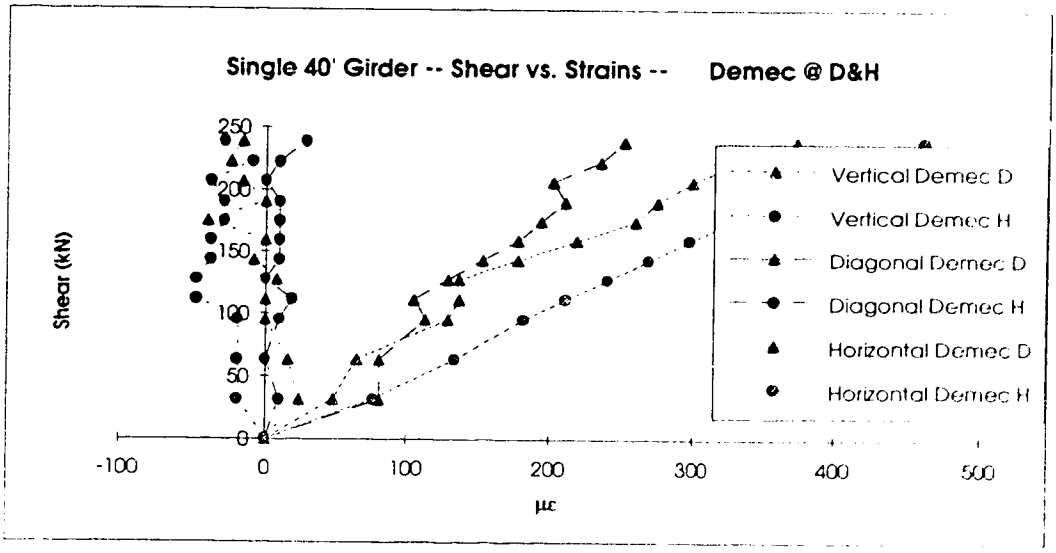

Figure A.6 Test A2 -- Strains vs. shear

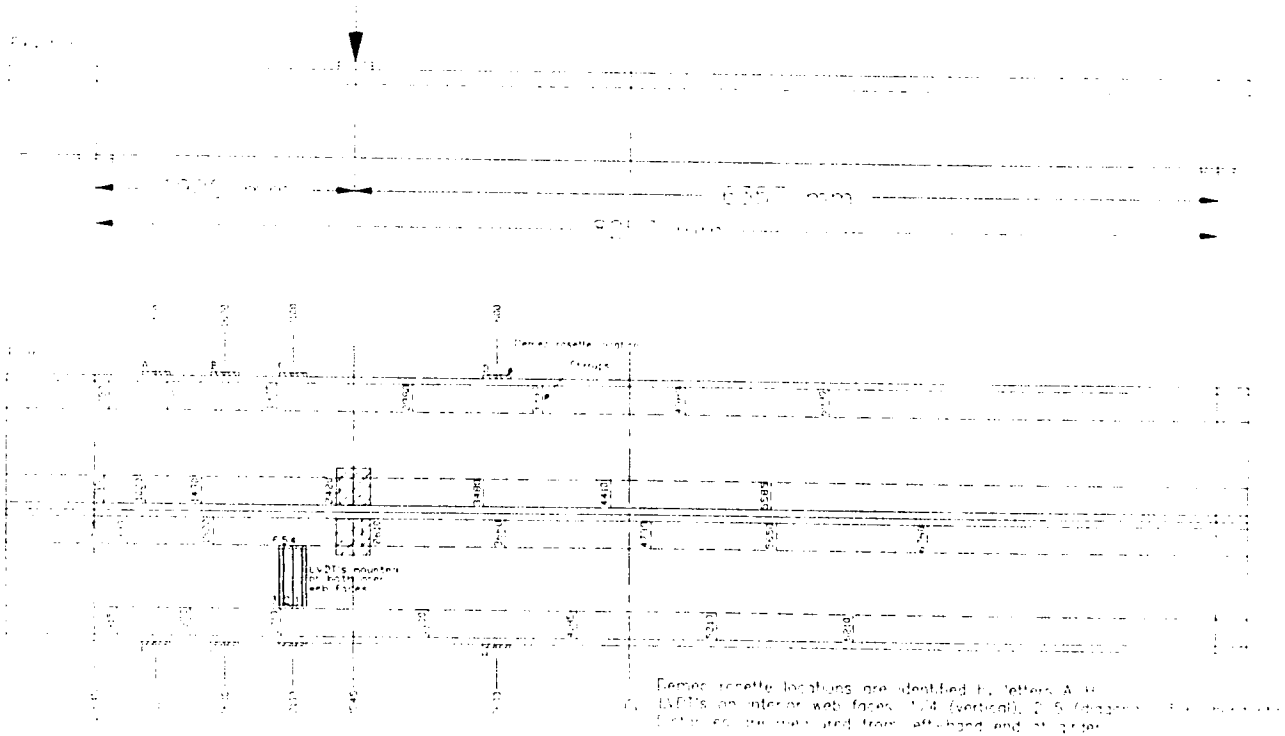

Figure A.7 Test A3 -- Double 9.14 m girders

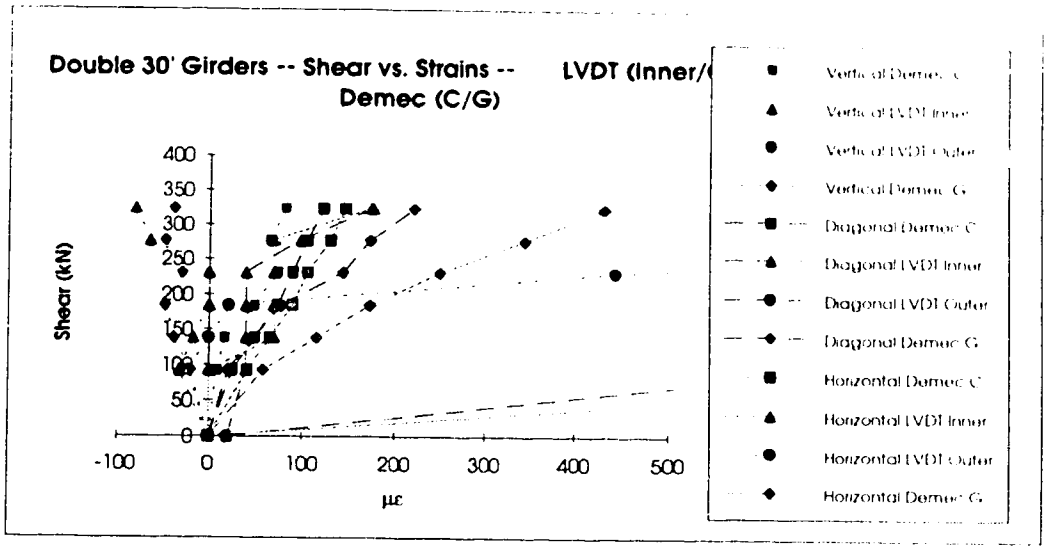

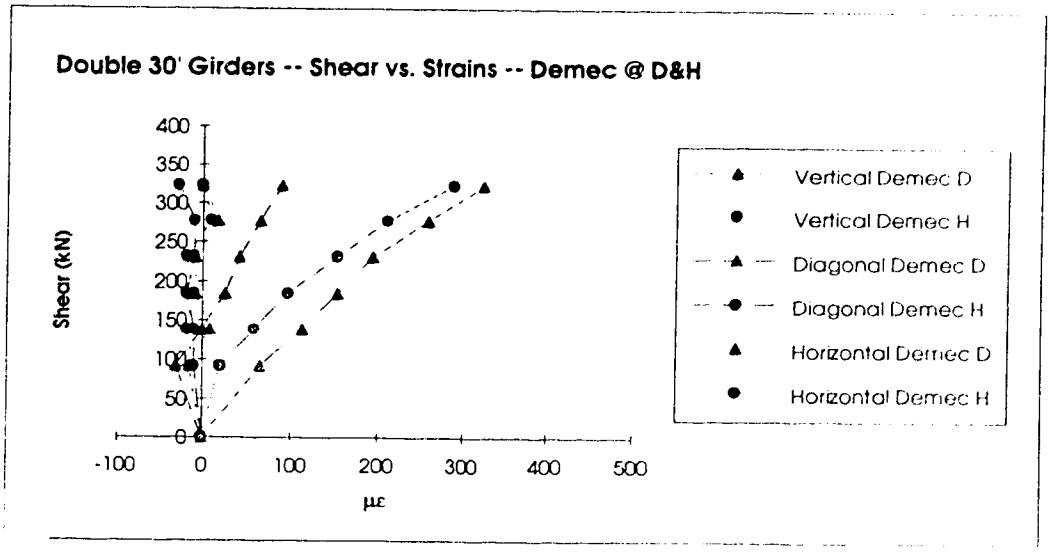

Figure A.8 Test A3 -- Strains vs. shear

Figure A.9 Tests A1, A2 and A3 -- Load vs. deflection curves

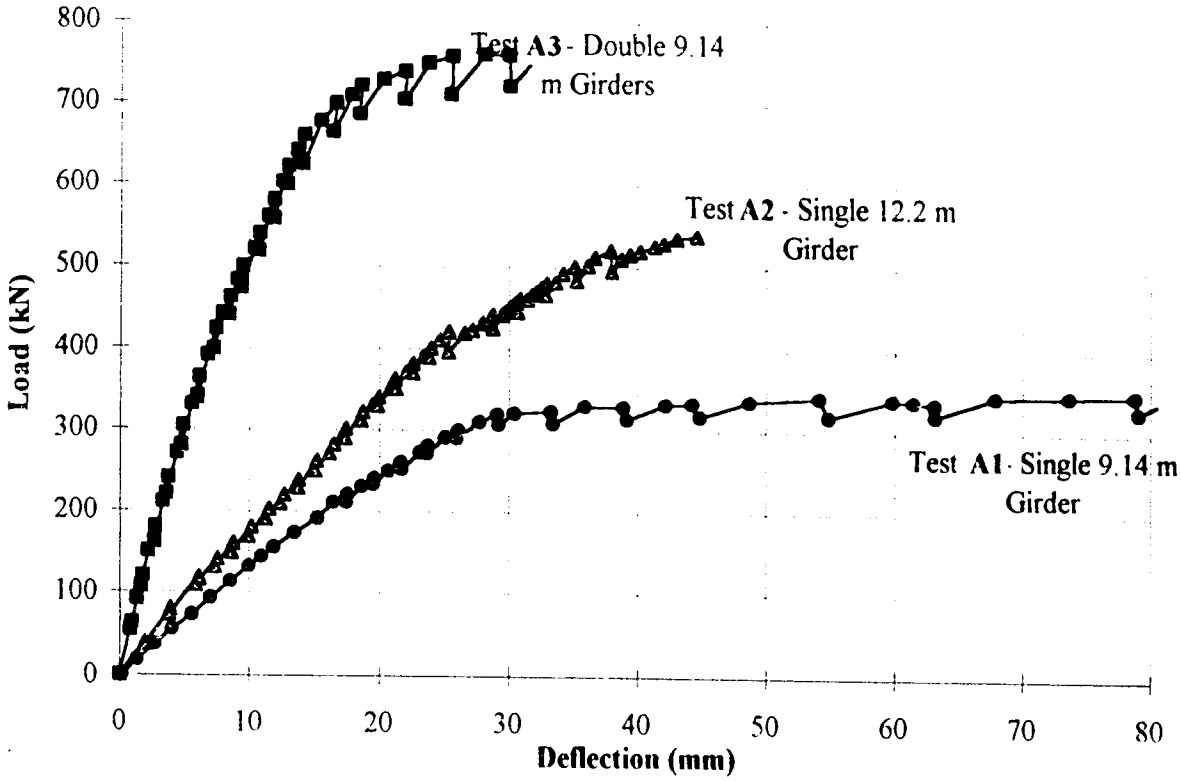

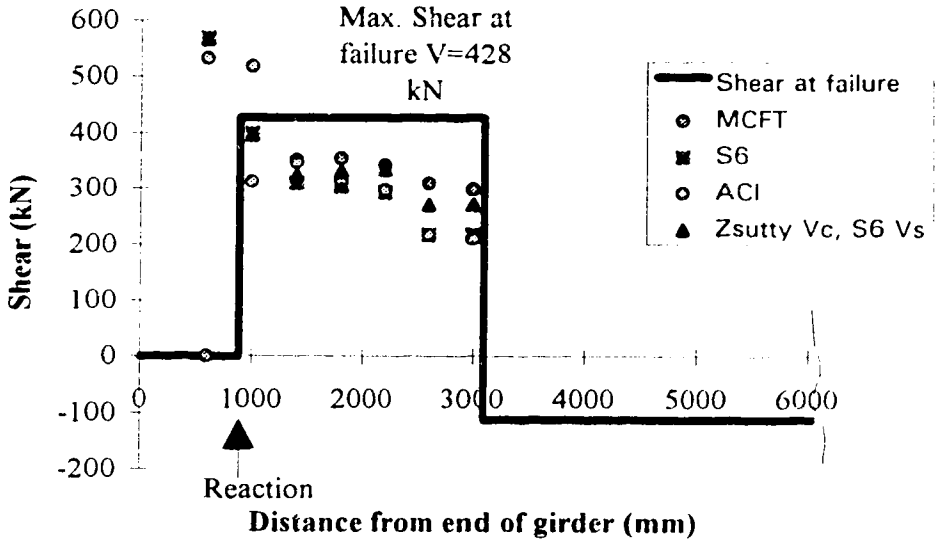

Figure A.10 Test A2 -- Single 12.2 m girder -- Shear capacity

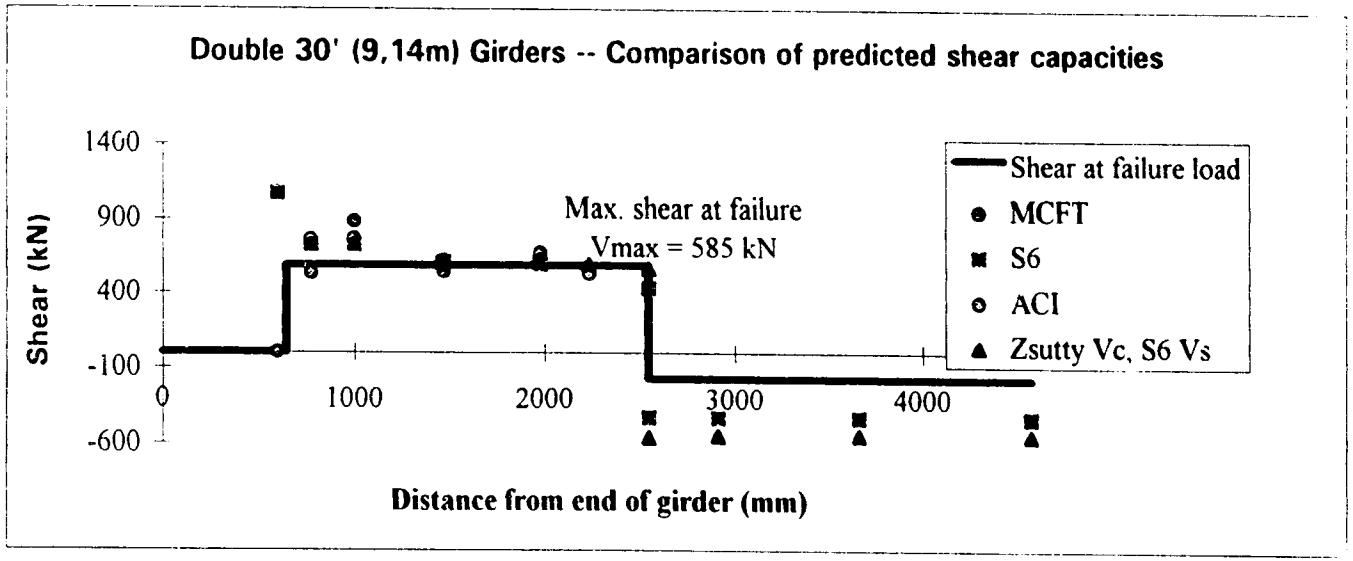

Figure A.11 Test A3 -- Double 9.14 m girders -- Shear capacity

Appendix B
Principal strain measurements for CFRP strengthened Girders 1, 2 and 3

The strain measurements included on the following pages are for Tests 1 and 2 of Girder 1, Tests 1, 2 and 3 of Girder 2 and Tests 1, 2 and 3 of Girder 3.

Each group of three values represents, from top to bottom, the principal tensile strain, principal compressive strain, and angle of inclination of the principal axis. The strains are in units of micro-strain; the angle in degrees.

Locations where measurements were taken (NW1, etc.) are defined in Chapter 3.

GIRDER 1 – TEST 1

P = 400 kN	SOUTH			NORTH		
	Strain Gauges	Demecs	LVDTs	Strain Gauges	Demecs	LVDTs
W 1 TOP	72 -89 44			100 -240 34		
W 1 MID	48 -24 45	43 -19 33		228 -132 12	119 -30 30	
W 1 BTM	53 -67 -33			437 -67 -44		
W 2 TOP	84 -4 -20			84 -380 -25		
W 2 MID	127 -86 37	158 -4 9		1454 -253 22	456 -60 24	
W 2 BTM	97 -40 5			557 -54 -18		
W 3 TOP	70 -81 -37			56 -2 2		
W 3 MID	77 -35 38	234 9 11	275 -322 -45	157 -41 32	73 -20 28	
W 3 BTM	124 -69 23			88 -23 29		
E 3		182 -134 38			304 93 31	
E 2		348 -137 31			274 -64 24	
E 1		117 -68 37			181 -19 38	

GIRDER 1 – TEST 1

P = 605 kN (Ultimate)	SOUTH			NORTH		
	Strain Gauges	Demecs	LVDTs	Strain Gauges	Demecs	LVDTs
W 1 TOP	96 -131 -41			95 -253 32		
W 1 MID	83 -43 -30	41 -146 44		127 -71 20	128 -176 40	
W 1 BTM	282 -236 -43			1276 -551 -39		
W 2 TOP	231 16 40			147 -879 -23		
W 2 MID	432 -245 41	1553 -565 38		1256 -776 37	454 56 -28	
W 2 BTM	479 -275 38			435 315 -32		
W 3 TOP	489 -310 -32			208 -27 13		
W 3 MID	164 -5 17	2608 907 -38	1377 -443 -44	239 -55 22	451 128 -37	
W 3 BTM	188 -104 29			274 -49 29		
E 3		2254 -1233 -35			818 49 -16	
E 2		13272 2401 -20			12892 1421 -20	
E 1		36 -239 -24			135 -191 -17	

GIRDER 1 -- TEST 2

P = 300 kN	SOUTH			NORTH		
	Strain Gauges	Demecs	LVDTs	Strain Gauges	Demecs	LVDTs
W 1 TOP	46			412		
	-69			-49		
	-40			20		
W 1 MID	20	3		76	44	
	-24	-39		-26	-64	
	44	30		30	35	
W 1 BTM	190			623		
	-188			178		
	-44			14		
W 2 TOP	69			39		
	-6			-242		
	-34			-23		
W 2 MID	135	371	303	440	109	
	-79	-233	-7	-251	-61	
	41	42	24	36	44	
W 2 BTM	198			203		
	-89			14		
	37			1		
W 3 TOP	184			64		
	-127			-47		
	-31			37		
W 3 MID	82	750		109	148	157
	-12	303		-29	35	23
	20	43		27	38	-38
W 3 BTM	88			112		
	-40			-30		
	24			27		

GIRDER 1 – TEST 2

P = 500 kN

	SOUTH			NORTH		
	Strain Gauges	Demecs	LVDTs	Strain Gauges	Demecs	LVDTs
W 1 TOP	73			402		
	-98			-39		
	-40			17		
W 1 MID	45	36		115	84	
	-38	-61		-21	-129	
	-43	--		28	38	
W 1 BTM	n/a			1003		
	n/a			220		
	n/a			24		
W 2 TOP	131			64		
	-9			-395		
	-39			-24		
W 2 MID	246	817	561	725	300	
	-126	-444	103	-436	-203	
	41	42	30	37	-44	
W 2 BTM	380			367		
	-184			-9		
	38			11		
W 3 TOP	411			120		
	-202			-91		
	-29			36		
W 3 MID	156	1667		190	263	525
	-2	638		-49	57	-63
	16	-42		27	44	-40
W 3 BTM	147			190		
	-63			-45		
	26			29		

GIRDER 1 -- TEST 2

P = 712 kN (Ultimate)	SOUTH			NORTH		
	Strain Gauges	Demecs	LVDTs	Strain Gauges	Demecs	LVDTs
W 1 TOP	145 -166 -40			500 -102 18		
W 1 MID	98 -88 -38	321 -78 15		2 -172 -12	4117 -1225 -27	
W 1 BTM	n/a n/a n/a			4643 -2484 -42		
W 2 TOP	215 -22 -40			421 -2950 -23		
W 2 MID	282 -188 43	1246 -711 -37	1777 -303 -40	1193 -940 42	200 -265 -24	
W 2 BTM	1118 103 32			1865 -1040 37		
W 3 TOP	7427 -4788 -44			119 -168 41		
W 3 MID	812 139 27	8434 -536 -26		244 -84 33	222 50 -33	2918 558 13
W 3 BTM	223 -64 18			483 -108 32		

GIRDER 2 -- TEST 1

P = 200 kN

	SOUTH			NORTH		
	Strain Gauges	Demecs	LVDTs	Strain Gauges	Demecs	LVDTs
W 1	36 -32 36	60 -113 -20		33 -15 -34	27 -27 -32	
W 2 TOP	157 -71 -39			15 -35 36		
W 2 BTM	1717 -1578 44	89 -36 35		10 1 16	77 -191 -31	11 -48 -29
W 3 TOP	-4 -24 -6			12 -101 -23		
W 3 MID	27 -19 -43	81 40 39		339 -115 -33	174 174 174	
W 3 BTM	29 -5 43			11 -34 12		
E 1	98 -3 24	34 10 30		20 0 4	30 -66 -31	
E 2 TOP	11 2 -32			61 -80 32		
E 2 BTM	61 -7 23	97 -101 43	17 -42 13	544 -329 32	44 -129 -30	
E 3 TOP	0 -56 -10			146 -421 -37		
E 3 MID	603 -560 42	122 -9 -41		95 -1 -2	174 49 -44	
E 3 BTM	713 -241 31			90 -21 -6		

GIRDER 2 -- TEST 1

P = 400 kN

	SOUTH			NORTH		
	Strain Gauges	Demecs	LVDTs	Strain Gauges	Demecs	LVDTs
W 1	71	189		105	228	
	-49	-169		-16	-171	
	39	-33		-24	-33	
W 2 TOP	727			26		
	-402			-51		
	-38			36		
W 2 BTM	3057	279		11	242	87
	-2906	-16		-13	-226	-18
	44	36		-41	-40	-18
W 3 TOP	-9			38		
	-35			-121		
	-36			-39		
W 3 MID	17	381		846	-44	
	-14	40		-297	-44	
	-20	-44		-31	-44	
W 3 BTM	338			7		
	-22			-55		
	23			18		
E 1	188	72		48	58	
	4	13		-3	-70	
	24	31		-3	-40	
E 2 TOP	21			163		
	14			-203		
	29			34		
E 2 BTM	134	191	94	1245	156	
	-12	-114	-147	-854	-152	
	23	38	22	35	-35	
E 3 TOP	1			284		
	-66			-606		
	-15			-41		
E 3 MID	1229	326		313	467	
	-1053	46		24	72	
	40	40		2	42	
E 3 BTM	1246			210		
	-304			-52		
	28			0		

GIRDER 2 – TEST 1

P = 600 kN

	SOUTH			NORTH		
	Strain Gauges	Demecs	LVDTs	Strain Gauges	Demecs	LVDTs
W 1	129	571		391	923	
	-84	-178		-30	-421	
	-41	-17		-19	-29	
W 2 TOP	1594			64		
	-562			2		
	-31			14		
W 2 BTM	252	1009		87	440	47
	-457	275		-10	-278	-25
	29	-34		-11	-20	29
W 3 TOP	-24			243		
	-82			-168		
	-34			-34		
W 3 MID	1531	3993		3811	2484	
	-843	1450		-988	-856	
	-34	-37		-31	-44	
W 3 BTM	935			18		
	-56			-113		
	19			27		
E 1	174	101		1182	-22	
	15	-65		14	-160	
	20	-44		-41	-19	
E 2 TOP	545			329		
	0			-563		
	25			43		
E 2 BTM	234	1226	735	2479	369	
	-22	-1060	-958	-1857	-333	
	24	-43	-45	41	-10	
E 3 TOP	0			894		
	-101			-418		
	-33			41		
E 3 MID	2714	1174		413	1234	
	-2046	348		-256	-396	
	43	-32		38	-28	
E 3 BTM	1202			444		
	-267			-217		
	27			13		

GIRDER 2 -- TEST 1

P = 712 kN (Ultimate)	SOUTH			NORTH		
	Strain Gauges	Demecs	LVDTs	Strain Gauges	Demecs	LVDTs
W 1	267 -145 -33	1361 -174 -14		823 -17 -13		
W 2 TOP	2086 -147 -12			1448 -148 18		
W 2 BTM	211 -412 26	2725 665 -27		723 -216 -36		1281 -963 41
W 3 TOP	22 -136 -26			1532 -159 -18		
W 3 MID	3569 -1432 -27	6041 2092 -32		4108 -1068 -31		
W 3 BTM	1189 -63 19			29 -113 31		
E 1	282 41 9	416 -112 6		800 78 -19	0 -223 -8	
E 2 TOP	1099 -294 36			293 -540 41		
E 2 BTM	862 -223 31	5778 -1861 -27	954 -1257 45	2252 -1594 39	422 -393 -8	
E 3 TOP	530 -98 17			2590 -155 30		
E 3 MID	6241 -3056 44	3822 1013 -24		491 -389 39	2695 -844 -25	
E 3 BTM	1534 -227 23			577 -282 13		

GIRDER 2 – TEST 2

P = 300 kN	SOUTH			NORTH		
	Strain Gauges	Demecs	LVDTs	Strain Gauges	Demecs	LVDTs
W 1	101	364		82	153	
	-58	-145		-14	-72	
	42	-15		-25	-13	
W 2 TOP	573			219		
	-88			-25		
	-19			-4		
W 2 BTM	348	642	226	267	604	
	-264	143	-194	-130	48	
	40	-29	42	-41	-21	
W 3 TOP	-5			198		
	-94			-191		
	-16			-27		
W 3 MID	626	1283		1247	932	
	-181	406		-22	-842	
	-27	-35		-33	-45	
W 3 BTM	213			51		
	7			-21		
	17			19		

GIRDER 2 – TEST 2

P = 600 kN	SOUTH			NORTH		
	Strain Gauges	Demecs	LVDTs	Strain Gauges	Demecs	LVDTs
W 1	221	774		264	409	
	-112	-150		-17	-117	
	-44	-19		-17	-7	
W 2 TOP	1471			726		
	-185			-53		
	-19			0		
W 2 BTM	562	1577	905	719	1585	
	-497	408	-626	-281	250	
	42	-27	39	-40	-22	
W 3 TOP	-4			1622		
	-178			-128		
	-19			-15		
W 3 MID	1925	3372		2698	2616	
	-564	1128		-111	-2357	
	-27	-34		-35	45	
W 3 BTM	741			58		
	-14			-43		
	16			30		

GIRDER 2 -- TEST 2

P = 800 kN	SOUTH			NORTH		
	Strain Gauges	Demecs	LVDTs	Strain Gauges	Demecs	LVDTs
W 1	323	1738		1533	571	
	-209	-37		-217	-183	
	43	-19		-22	1	
W 2 TOP	2633			2309		
	-113			-140		
	-17			1		
W 2 BTM	1042	4824	2782	1641	6173	
	-929	1129	-2217	-279	1413	
	42	-25	-41	-43	-22	
W 3 TOP	-20			507		
	-282			-555		
	-24			-39		
W 3 MID	3478	4474		3564	4706	
	-1073	1402		-376	-4390	
	-28	-31		-36	-45	
W 3 BTM	1997			69		
	142			-58		
	7			38		

GIRDER 2 – TEST 2

P = 900kN	SOUTH			NORTH		
	Strain Gauges	Demecs	LVDTs	Strain Gauges	Demecs	LVDTs
W 1	202	3955		2514	499	
	-375	386		-924	-280	
	27	-20		-27	-1	
W 2 TOP	4294			4623		
	-273			-262		
	-20			-5		
W 2 BTM	13756	12199	5722	2567	11826	
	-2052	2065	-721	232	3292	
	29	-19	-34	42	-24	
W 3 TOP	-42			150		
	-399			-751		
	-18			31		
W 3 MID	3539	4479		3409	3135	
	-1176	1357		-518	-2795	
	-29	-30		-35	-45	
W 3 BTM	2411			65		
	762			-64		
	3			36		

GIRDER 2 – TEST 2

P = 923 kN (Ultimate)	SOUTH			NORTH		
	Strain Gauges	Demecs	LVDTs	Strain Gauges	Demecs	LVDTs
W 1	136	4732		2653	491	
	-493	477		-1069	-329	
	15	-10		-28	-2	
W 2 TOP	3577			5151		
	-129			-341		
	-20			-8		
W 2 BTM	8951	OOR	6424	2717	14119	
	-168	OOR	-327	334	4037	
	11	OOR	-32	41	-25	
W 3 TOP	-38			213		
	-409			-813		
	-16			32		
W 3 MID	3490	4685		3407	2730	
	-1175	1411		-546	-2350	
	-29	-30		-35	44	
W 3 BTM	2486			65		
	872			-68		
	3			35		

GIRDER 3 – TEST 1

P = 200 kN	SOUTH			NORTH		
	Strain Gauges	Demecs	LVDTs	Strain Gauges	Demecs	LVDTs
W 1		57 8 0			91 -30 32	
W 2		99 -131 -40			33 -13 37	
W 3		41 -5 26			120 18 14	8 -37 23
W ext.	30 -11 42			32 11 3		
W int.	21 -25 44			8 -10 -5		
E 1		31 -11 -30			37 4 38	
E 2		131 -33 29			149 -80 38	
E 3		86 -17 39	106 -18 -22		181 -31 -21	
E int.	44 -41 31			4 -11 -39		

GIRDER 3 – TEST 1

P = 400 kN	SOUTH			NORTH		
	Strain Gauges	Demecs	LVDTs	Strain Gauges	Demecs	LVDTs
W 1		107 15 19			208 -82 35	
W 2		224 -118 38			81 -37 -42	
W 3		121 -36 37			256 -13 22	35 -50 37
W ext.	73 -44 43			65 43 -6		
W int.	29 -50 39			13 -27 -13		
E 1		61 -16 43			102 -37 -42	
E 2		265 -63 29			353 -90 35	
E 3		194 -100 39	293 -50 -22		375 -39 -17	
E int.	67 -57 26			24 -33 43		

GIRDER 3 – TEST 1

P = 600 kN	SOUTH			NORTH		
	Strain Gauges	Demecs	LVDTs	Strain Gauges	Demecs	LVDTs
W 1		147 -9 31			312 -203 -44	
W 2		401 -239 40			1214 305 -40	
W 3		358 -168 -39			260 -107 34	43 -148 28
W ext.	121 -84 43			84 20 -19		
W int.	47 -84 -39			38 -75 -9		
E 1		78 -9 -19			178 -49 -28	
E 2		255 -12 -18			782 64 -37	
E 3		2964 -1032 -29	782 -68 -28		2290 -180 33	
E int.	109 -355 -25			9 -37 41		

GIRDER 3 -- TEST 1

P = 800 kN	SOUTH			NORTH		
	Strain Gauges	Demecs	LVDTs	Strain Gauges	Demecs	LVDTs
W 1		1119 -512 -27			1021 -717 -37	
W 2		3910 -30 -40			3663 877 -34	
W 3		918 -299 -30			556 -135 -38	330 -219 -39
W ext.	274 -249 -42			126 -44 -7		
W int.	53 -166 -37			72 -94 -5		
E 1		940 -118 6			4498 -918 21	
E 2		2912 369 -23			7598 -1591 -24	
E 3		7705 -1902 -26	1727 143 -39		4014 647 44	
E int.	257 -616 -37			26 -55 37		

GIRDER 3 – TEST 1

P = 883 kN (Ultimate)	SOUTH			NORTH		
	Strain Gauges	Demecs	LVDTs	Strain Gauges	Demecs	LVDTs
W 1						
W 2						
W 3						2079 -1823 -30
W ext.	218 -192 -42			210 -130 -10		
W int.	52 -205 -36			161 -138 0		
E 1						
E 2						
E 3			2183 -287 -42			
E int.	3624 -3874 42			38 -62 42		

GIRDER 3 -- TEST 2

P = 100 kN	SOUTH			NORTH		
	Strain Gauges	Demecs	LVDTs	Strain Gauges	Demecs	LVDTs
W 1	N/A			N/A		
W 2						
W 3						79 -4 11
W ext.	10 -3 -16			18 -10 -37		
W int.	7 -9 14			-1 -6 31		

GIRDER 3 -- TEST 2

P = 200 kN	SOUTH			NORTH		
	Strain Gauges	Demecs	LVDTs	Strain Gauges	Demecs	LVDTs
W 1	N/A			N/A		
W 2						
W 3						158 -21 -20
W ext.	13 -10 -10			21 -5 -26		
W int.	16 -18 8			9 -21 30		

GIRDER 3 – TEST 2

P = 300 kN	SOUTH			NORTH		
	Strain Gauges	Demecs	LVDTs	Strain Gauges	Demecs	LVDTs
W 1		340			362	
		-146			-233	
		-30			-38	
W 2		889			1036	
		-100			102	
		-38			-34	
W 3		326			451	380
		-79			-1010	-120
		-38			26	-29
W ext.	16			44		
	-23			-20		
	-4			-34		
W int.	23			28		
	-28			-51		
	8			34		

GIRDER 3 – TEST 2

P = 400 kN	SOUTH			NORTH		
	Strain Gauges	Demecs	LVDTs	Strain Gauges	Demecs	LVDTs
W 1		529			506	
		-229			-320	
		-30			-37	
W 2		1334			1499	
		6			158	
		-39			-34	
W 3		504			622	564
		-127			-995	-241
		-37			28	-33
W ext.	19			38		
	-38			-5		
	0			-20		
W int.	35			50		
	-37			-81		
	5			36		

GIRDER 3 – TEST 2

P = 500 kN	SOUTH			NORTH		
	Strain Gauges	Demecs	LVDTs	Strain Gauges	Demecs	LVDTs
W 1		696			652	
		-307			-442	
		-29			-38	
W 2		1786			1958	
		-41			233	
		-39			-33	
W 3		667			54159	766
		-153			-8702	-358
		-35			22	-34
W ext.	23			44		
	-55			0		
	3			0		
W int.	53			73		
	-45			-108		
	3			36		

GIRDER 3 – TEST 2

P = 600 kN	SOUTH			NORTH		
	Strain Gauges	Demecs	LVDTs	Strain Gauges	Demecs	LVDTs
W 1		817			790	
		-340			-507	
		-28			-37	
W 2		2232			2392	
		-17			309	
		-39			-33	
W 3		838			954	1060
		-202			-800	-1131
		-35			32	-31
W ext.	27			53		
	-71			0		
	5			1		
W int.	67			95		
	-51			-131		
	1			36		

GIRDER 3 – TEST 2

P = 800 kN	SOUTH			NORTH		
	Strain Gauges	Demecs	LVDTs	Strain Gauges	Demecs	LVDTs
W 1		1106 -410 -27			1085 -672 -36	
W 2		3135 -45 -39			3451 393 -33	
W 3		1354 -321 -36			1380 -724 35	1777 -1549 -30
W ext.	41 -112 11			90 -19 25		
W int.	112 -69 0			153 -203 37		

GIRDER 3 – TEST 2

P = 850 kN	SOUTH			NORTH		
	Strain Gauges	Demecs	LVDTs	Strain Gauges	Demecs	LVDTs
W 1		N/A			N/A	
W 2						
W 3						2536 -2000 -34
W ext.	47 -127 12			110 -37 30		
W int.	107 -73 4			192 -253 37		

GIRDER 3 – TEST 2

P = 900 kN	SOUTH			NORTH		
	Strain Gauges	Demecs	LVDTs	Strain Gauges	Demecs	LVDTs
W 1		1419			1536	
		-520			-969	
		-27			-36	
W 2		4075			4589	
		-264			-3349	
		-37			41	
W 3		1715			1655	3024
		-350			-659	-2796
		-39			38	-30
W ext.	52			122		
	-150			-42		
	13			30		
W int.	105			266		
	-79			-326		
	6			39		

GIRDER 3 – TEST 2

P = 956 kN (Ultimate)	SOUTH			NORTH		
	Strain Gauges	Demecs	LVDTs	Strain Gauges	Demecs	LVDTs
W 1		1460			1666	
		-536			-1066	
		-27			-37	
W 2		4383			--	
		-491			--	
		-39			--	
W 3		1786			1721	3244
		-357			-603	-2842
		-39			39	-30
W ext.	51			104		
	-265			-32		
	15			29		
W int.	70			300		
	-131			-264		
	24			43		